KOMUNIKÁCIE
COMMUNICATIONS

**5**
Csaba Balázsi – Ferenc Wéber – Zsolt Kasztovszky
**MANUFACTURE AND COMPOSITIONAL ANALYSIS OF SILICON NITRIDE COMPOSITES WITH DIFFERENT CARBON ADDITIONS**

**10**
Grzegorz Kłapyta
**SHAPE MEMORY ALLOY – MODERN SMART MATERIAL FOR VARIOUS APPLICATIONS**

**15**
Wojciech Żórawski – Rafał Chatys
**INFLUENCE OF HEAT TREATMENT ON THE MICROSTRUCTURE AND COMPOSITION OF PLASMA SPRAYED COATINGS**

**19**
Mirosław Wendeker
**ADAPTIVE FUELLING OF THE SI ENGINE**

**26**
Rastislav Isteník - Dalibor Barta - Wladyslaw Mucha
**INFLUENCE OF THE WHEELS ON THE AUTOMOBILE DYNAMICS**

**29**
Peter Choroba
**DYNAMIC AIR TRAFFIC CONTROL WAKE VORTEX SAFETY AND CAPACITY SYSTEM**

**34**
Gergely Biczók – Kristóf Fodor – Balázs Kovács
**HANDOVER LATENCIES IN BCMP NETWORKS**

**38**
Martin Kuchař – Pavel Brandštetter
**DEVELOPMENT AND DSP IMPLEMENTATION OF ANN-BASED VPWM IN A VOLTAGE SOURCE INVERTER**

**42**
Libor Štěpanec – Pavel Brandštetter
**DSP IMPLEMENTATION AND SIMULATION OF IM DRIVE USING FUZZY LOGIC**

**46**
Martina Blašková
**INDIVIDUAL AND SECTIONAL COMMUNICATION SYSTEMS IN MANAGEMENT AND DEVELOPMENT OF HUMAN POTENTIAL**

**50**
Michal Žarnay
**HUMAN FACTOR IN DECISION-MAKING IN SIMULATION MODEL OF TRANSPORTATION SYSTEM AND APPROACHES TO ITS MODELLING**

**54**
Mariana Strenitzerová
**CHANGE MANAGEMENT: THE PEOPLE DIMENSION OF CHANGE**

**58**
Eva Remišová
**THEORY AND MEASUREMENTS OF BITUMEN BINDERS ADHESION TO AGGREGATE**

**64**
Ján Leľak – Dušan Slávik – Martin Mečár
**STATIC AND DYNAMIC TESTS OF THE RAILWAY SUBGRADE CONSTRUCTION MODEL**

**68**
Slávka Tkáčová
**THE EIGENVALUE APPROXIMATIONS OF THE LAPLACE OPERATOR DEFINED ON A DOMAIN WITH STRONGLY DEFORMED BOUNDARY**

**72**
Andrzej Surowiecki – Edward Hutnik
**TESTS OF DEFORMATION AND TENSIONS IN REINFORCED NON-COHESIVE SOIL LAYER**

*Dear reader,*

*the 5th International scientific conference TRANSCOM 2003, organised also as an activity in the framework of the CETRA project (Centre for Transportation Research, University of Žilina, Slovak Republic – Centre of Excellence supported by the European Commission), was held in the University of Žilina, Slovak Republic, in June 2003.*

*The main purpose of the conferences TRANSCOM organised regularly every other year since 1995, is a presentation of scientific works (from the fields of transportation, telecommunications, mechanical, electrical and civil engineering) of young research workers incl. PhD. students up to the age of 35 from universities, scientific institutions and industry.*

*More than 362 contributions were published in seven proceedings of the conference TRANSCOM 2003 (213 contributions were from abroad, Bulgaria, Czech Republic, Yugoslavia, France, Germany, Hungary, Italy, Poland, Romania, Russia, Republic of Belarus, Sweden, Ukraine, 15 were from the universities of the Slovak Republic and 134 contributions were from the University of Žilina).*

*This volume of Communications is devoted to the selected contributions (recommended by scientific committee) of the 5th International scientific conference TRANSCOM 2003, Žilina, Slovak Republic.*

*Otakar Bokůvka*

https://doi.org/10.26552/com.C.2004.1.5-9



Csaba Balázsi – Ferenc Wéber – Zsolt Kasztovszky *

# MANUFACTURE AND COMPOSITIONAL ANALYSIS OF SILICON NITRIDE COMPOSITES WITH DIFFERENT CARBON ADDITIONS

*Carbon black and graphite nano/micrograins and sintering additives ($Al_2O_3$ and $Y_2O_3$) were added to silicon nitride starting powder. These mixtures were mechanochemically activated several hours in a planetary type alumina ball-mill in order to achieve a homogenous mass. As an alternative to nano- and micrograins, carbon fibres were added to carbon free silicon nitride batches. After dry pressing of rectangular bars sinter-HIP was applied. Structural, morphological and compositional analyses were performed on as-prepared samples. Bending strength and elastic modulus were found to be influenced by amount of carbon black and graphite introduced in silicon nitride matrix.*

## 1. Introduction

Ceramics based on silicon nitride are well-known as low density materials with high strength and toughness. With this combination of properties silicon nitride based ceramics are an ideal candidate for several structural applications, even at high temperatures. Lately, by *in-situ* tailoring the microstructure, new observations were performed on structural and morphological development on silicon nitride ceramics in order to understand the governing principles of sintering processes [1, 2]. In this way, through formation of tough interlocking microstructure mechanical properties may be improved. Intensive research work has been done to improve physical and mechanical properties of silicon nitride ceramics through nanocomposite processing [3]. To increase the fracture toughness, incorporation of various energy-dissipating components into ceramic matrices have been performed [4, 5].

These components can be introduced in whisker, platelets, particles or fibre forms. A low cost silicon carbide-silicon nitride nanocomposite processing route has been reported by Hnatko et al [6]. In this case, the formation of bulk silicon nitride based nanocomposite is realized by carbothermal reduction of $SiO_2$ by carbon in the $Y_2O_3$–$SiO_2$ system at the sintering temperature, with SiC nanoparticles as result. Although, the mechanical properties of as-prepared samples should be further optimized, this process seems to be a perspective choice for silicon nitride-silicon carbide nanocomposite production [7]. In this paper silicon nitride based nanocomposites were prepared through carbon black addition by mechanochemical synthesis and hot isostatic pressing (HIP). Results about structural, morphological and compositional measurements are presented.

## 2. Experimental method

Details about sample preparation can be followed in Table 1. The compositions of the starting powder mixtures of the four materials were the same: 90 wt.% $Si_3N_4$ (Ube SN-ESP), 4 wt.% $Al_2O_3$, and 6 wt.% $Y_2O_3$. In addition to batches carbon black (Taurus Carbon black, N330, average particle size between $\sim$ 50–100 nm), graphite (Aldrich, synthetic, average particle size 1–2 $\mu$m) and carbon fibre (Zoltek, PX30FBSWO8) were added. The powder mixtures were milled in ethanol in a planetary type alumina ball mill for 150 hours. The samples were compacted by dry pressing at 220 MPa. Samples from 644 and 645 batches were collected during milling process after several stops. Carbon fibres were added to mixtures only before dry pressing (samples 629 from Table 1.) Samples were passed to FTIR examinations. Infrared absorption spectra were taken by BOMEM MB-102 FTIR spectrophotometer equipped with a deutero-triglicine-sulfate detector, at a resolution of 4 $cm^{-1}$, in the range of 400-4000 $cm^{-1}$; 2 mg/g KBr pellets were used. The materials were sintered at 1700 °C in high purity nitrogen by a two-step sinter-HIP method using BN embedding powder. First, some of the samples were sintered without applying pressure. In second step, the samples from first sintering step (serving as reference samples) were re-introduced in the HIP, together with the rest of examined samples. Then, pressure of 20 bar was applied for one hour.

The dimensions of the as-sintered specimens were approximately 3.5 × 5 × 50 mm.

After sintering the weight-gain values were determined. The density of the as-sintered materials was measured by the Archimedes method. To identify the crystalline phases X-ray diffraction of Cu

* [1]Dr. Csaba Balázsi, [1]Ing. Ferenc Wéber, [2]Dr. Zsolt Kasztovszky
[1]Ceramics and Refractory Metals Laboratory, Research Institute for Technical Physics and Materials Science, Hungarian Academy of Sciences, 1121 Budapest, Konkoly-Thege út 29-33, E-mail: balazsi@mfa.kfki.hu, weber@mfa.kfki.hu.
[2]Department of Nuclear Research, Institute of Isotope and Surface Chemistry, Chemical Research Center, POB 77, H-1525 Budapest, Hungary, E-mail: kzsolt@alpha0.iki.kfki.hu

Kα radiation was applied. Morphology of the solid products was studied by scanning electron microscopy, with a JEOL-25 microscope. The elastic modulus and the four-point bend strength were determined by a bending test with spans of 40 mm and 20 mm. Three-point strength was measured on broken pieces with a span of 20 mm.

The compositional analysis of sintered samples was performed by prompt-gamma activation analysis (PGAA) which is based on the detection of prompt gamma rays originating from (n, γ) reaction, and gives average elemental composition of the total volume of the sample [8].

The composition of starting powder mixtures. Table 1.

| Batch | Composition, wt% | | | Added carbon | | |
|---|---|---|---|---|---|---|
| | $Si_3N_4$ | $Al_2O_3$ | $Y_2O_3$ | carbon black | graphite | carbon fibre |
| | | | | $C/Si_3N_4$ molar ratio | $C/Si_3N_4$ molar ratio | wt% to batch |
| 642 | 90 | 4 | 6 | – | – | – |
| 644 | 90 | 4 | 6 | 3 | – | – |
| 645 | 90 | 4 | 6 | – | 3 | – |
| 629 | 90 | 4 | 6 | – | – | 1 |

## 3. Results and discussion

Infrared spectroscopy measurements are presented in Fig. 1. Samples extracted from 644 batch during long duration milling experiment can be followed in Fig. 1c, Fig. 1d and Fig. 1e. Infrared spectra of yttria and alpha silicon nitride starting powders are presented in Fig. 1a and Fig. 1b. iN yttria powder spectra we can distinguish two characteristic peaks at 606 and 631 $cm^{-1}$. The mixture of powders mechanically activated for 1 hour (Fig. 1c) is characterized mainly by alpha silicon nitride vibration modes (as in Fig. 1b). O-H stretching modes at 3432 $cm^{-1}$ and O-H bending at 1634 $cm^{-1}$ can be found in infrared spectra.

These vibrations are assigned with N-H vibrations in case of inert atmosphere working conditions. At the end of mechanical activation (Fig. 1d) as a result we have a mixture with dominant alpha silicon nitride vibration modes. The vibration modes considered to be Si-N at 600 $cm^{-1}$ and yttria at 640 $cm^{-1}$ appeared. At the end of activation O–H bonds disappeared from spectra. After oxidation at 800° C for 2 hours (Fig. 1e) peaks characteristic to alpha silicon nitride and yttria can be observed on infrared spectra. Alumina which has a broad band at 798 $cm^{-1}$ (not presented in figure) and presents 4 wt% of the mixture can not be seen and has no substantial effect on the spectra of mixtures.

We found the same characteristic vibrations in the case of preparations with graphite (batch 645). After performing the mechanical activation of powder mixtures, rectangular samples were obtained

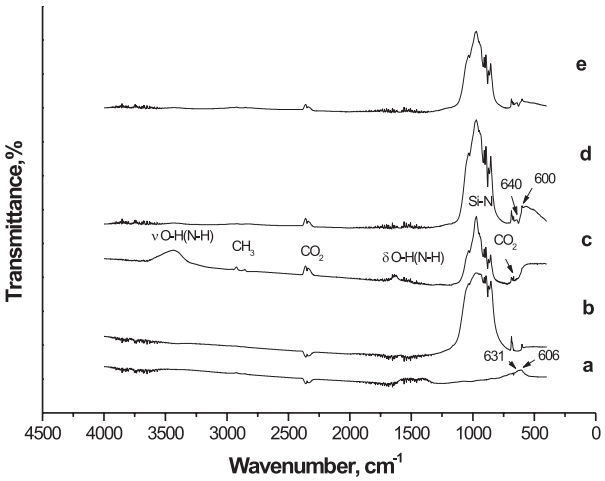


*Fig. 1 FTIR spectra of starting materials and milling products (batch 644); a - $Y_2O_3$ starting sintering additive powder; b - α-$Si_3N_4$ starting powder; c - Resulting mixture after 1h activation; d - Resulting mixture after 150 h activation; e - Resulting mixture after 150 h activation and oxidation at 800 °C for 2 h.*

by dry pressing at 220 MPa. The as-obtained samples were oxidized at different temperatures. Oxidizing at different temperatures resulted in samples with different carbon content as presented in Fig. 2. An interesting remark can be added to observations presented in Fig. 2. The behavior of nanocrystalline carbon black and graphite added to silicon nitride matrix was found to be sharply different regarding the oxidation process.

From 450 °C up to 600 °C the carbon black content has a decreasing tendency, at 600 °C was 0.4 wt%. At this stage, the graphite content is around 10 wt%. From this point the graphite content has also a decreasing tendency with increasing tempera-

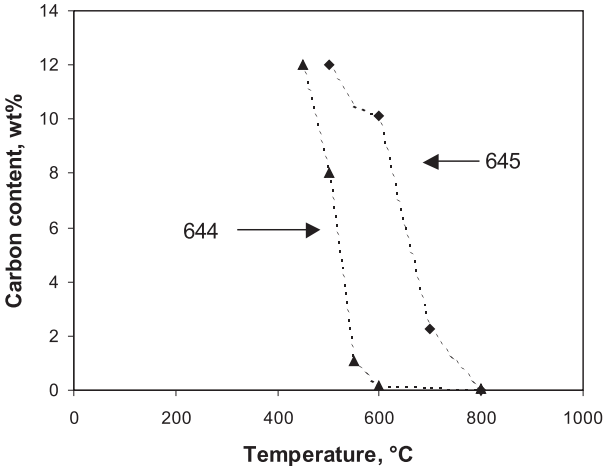


*Fig. 2 Samples with different carbon contents after oxidation in atmosphere. In each point the average value of four samples is presented.*

ture. Continuing the oxidation process above 800 °C, according to weight losses, we obtained a carbon free structure.

Morphological study was performed after two-step sintering by scanning electron microscopy. In Fig. 3a. the microstructure of a reference sample (642) consisting of equiaxial grains can be seen. The structure of the sample characterized by high content of nanocrystalline carbon black is sharply different, the grains are connected through elongated necks (Fig. 3b). Huge sticking grains can be also observed, which developed during a milling process. On the microstructure of sample with no carbon content, derived from oxidation at 800 °C of carbon black containing sample, more developed grains can be observed (Fig. 3c).

Similarly developed grains and sticking tendency can be followed in the case of a sample with high graphite content (Fig. 3d). can be foreseen that the fracture, crack propagation in this sample involves a combination of intra- and intergranular path which needs higher energy demand. As regards the samples from batch 644 however, the sticking grains of 10–30 $\mu$m in size (Fig. 4b, and 4c) act as inclusions in structure and induce intergranular fractures, which requires less energy input.

In Fig. 5a and Fig. 5b carbon fibers pulled out from the matrix and embedded in the matrix can be seen. A deterioration of carbon fibers, cavities developing on the surface of fibers should be noticed.

Relation between apparent density of samples containing carbon (644 and 645) and reference (642) carbon free sample and modulus of elasticity after sintering are presented in Fig. 6.

A higher apparent density and higher modulus than samples with carbon content characterize the 642 reference samples. Samples

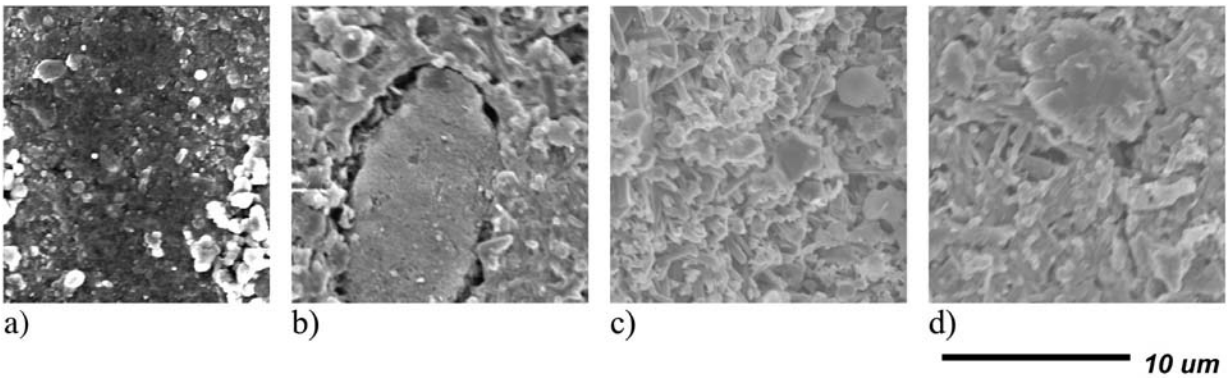


*Fig. 3 Scanning electron micrographs of the surface of the samples after two-step sintering process. a - reference sample (642). b – sample from batch 644, with 11,9 wt% carbon content after oxidation at 450 °C (as in Fig. 2) c – sample from batch 644, with no carbon content after oxidation at 800°C (as in Fig. 2). d – sample from batch 645, with 12 wt% graphite content after oxidation at 500 °C (as in Fig. 2).*

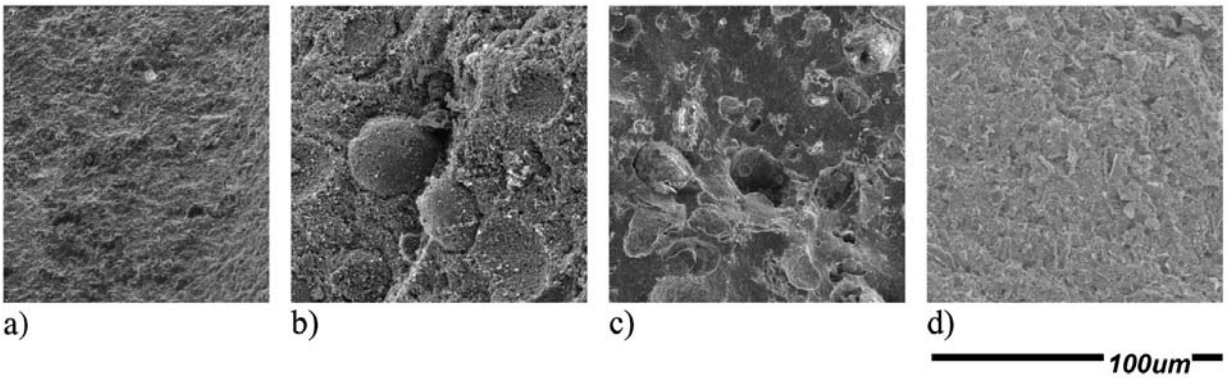


*Fig. 4 Scanning electron micrographs of fracture surface of the samples after two-step sintering process. a – reference sample (642). b – sample from batch 644, with 11,9 wt% carbon content after oxidation at 450 °C (as in Fig. 2) c – sample from batch 644, with no carbon content after oxidation at 800°C (as in Fig. 2). d – sample from batch 645, with 12 wt% graphite content after oxidation at 500 °C (as in Fig. 2).*

A morphological study was made on fractured surfaces as shown in Fig. 4. In Fig. 4a the homogenous microstructure of a reference sample (642) can be seen. From these micrographs 644 (nanocrystalline carbon black) have higher modulus values than samples with graphite (645). Linearly fitted straight line 176 were added to Fig. 6 from Ref. 9.

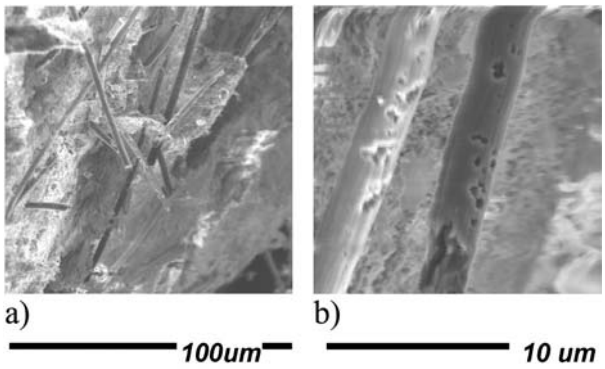


*Fig. 5 Scanning electron micrographs of fracture surface of the carbon fiber containing samples (629) after sintering process. a - fibers pulled out from matrix. b - fibers embedded in matrix, presenting deterioration (holes) on surface.*

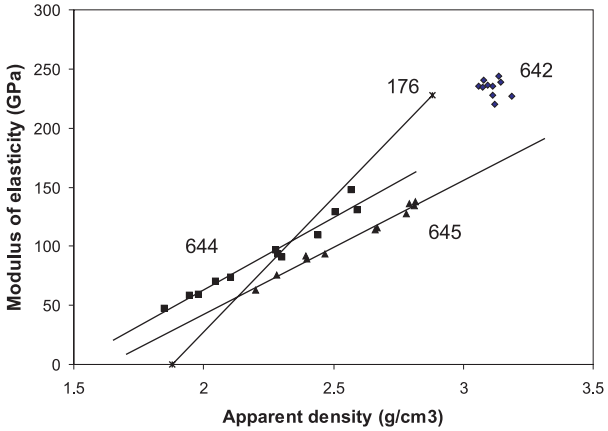


*Fig. 6 Relation between apparent density and modulus of elasticity after sintering. 644 and 645 samples containing carbon, 642 and 176 carbon free samples.*

These lines were produced to study partial and final sintering processes. From Fig. 6 it seems that carbon content variation has the same role as partial sintering. The same curves (regression lines) as in the case of line 176, but different gradients can be observed at samples 644 and 645. The linear regression line 176 has the intersection with *x* axis is at 1.88 value. As conclusion can be drawn that samples 644 at low densities have higher modulus values than the reference samples. This means that at the initial stage of sintering a certain amount of carbon addition has a beneficial role to the modulus of elasticity. This tendency is maintained till 2.338 value obtained from intersection of regression lines 176 and 644. Above this value, although modulus of batches 644 and 645 have an increasing tendency, compared with reference 176 carbon content has a detrimental role to modulus.

In Fig. 7a the x-ray diffractogram of a reference sample can be seen after sintering at 1700 °C, nitrogen atmosphere and without applying pressure. The structure consists of $\beta$-$Si_3N_4$ and $\alpha$-$Si_3N_4$.

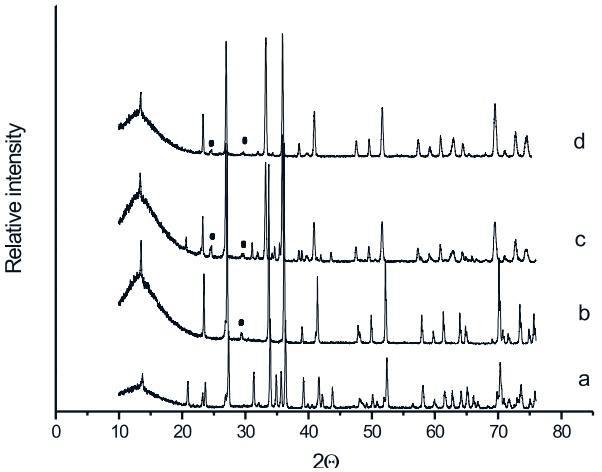


*Fig. 7 X-ray diffractograms of one and two step sintered samples; a - reference sample (642) sintered without pressure; b - reference sample (642) sintered under pressure; c - nanocrystalline carbon added (644) sample first step sintered; d - carbon added sample (644) after two-step sintering. Black points mark the new phase(s).*

After the second sintering step (Fig. 7b) mostly the reflection of $\beta$-$Si_3N_4$ can be recognized. At $d = 0.3041$ nm however, an unidentified peak has appeared. At this stage of study identification of this peak is still uncertain, however this reflection is close to $\delta$-$Y_2Si_2O_7$ reflections. In Fig. 7c the reflections of sample from batch 644 can be seen after first sintering step. The structure consists of $\beta$-$Si_3N_4$, $\alpha$-$Si_3N_4$ and a minor contribution of SiC (JCPDS 31-1231) can be observed. In addition to this reflections at $d = 0.3613$ nm and $d = 0.3041$ nm can be observed, which may be attributed to $\delta$-$Y_2Si_2O_7$ reflections. After the second sintering step the structure is converting to $\beta$-$Si_3N_4$ phase, but retains some of the possible $\delta$-$Y_2Si_2O_7$ reflections ($d = 0.3613$ nm and $d = 0.3041$ nm) and some of the $\alpha$-$Si_3N_4$ reflections ($d = 0.2259$ nm, 0.2619 nm and 0.280 nm).

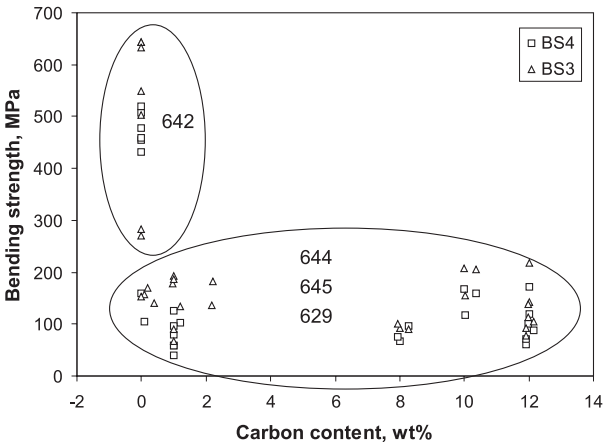


*Fig. 8 Relation between carbon content and four point bending strength (BS4) and three point bending strength (BS3). Carbon contents for samples 644 and 645 resulted from oxidation process as in Fig. 3. Samples 629 are characterized by 1 wt% carbon content as in Table 1.*

A comprehensive view about the carbon content effect to strength can be seen in Fig. 8. Samples with added carbon (629, 644, 645) present lower values for strength as compared with 642 reference samples.

vibration modes. Carbon addition has the same role as partial sintering. In the initial stage of sintering the carbon addition has a beneficial role to the modulus of elasticity. Above a certain value however, carbon content has a detrimental role to the modulus. The

The composition of sintered samples Table 2

| Reference sample from batch 642 | | | | | | Carbon black-silicon nitride composite | | | | | |
|---|---|---|---|---|---|---|---|---|---|---|---|
| Z | El | M | atomic % | **wt%** | rel. unc % | Z | El | M | atomic % | **wt%** | rel. unc % |
| 1 | H | 1.01 | 0 | **< 0.001** | | 1 | H | 1.01 | 0.438 | **0.023** | 7.9 |
| 5 | B | 10.8 | 0.036 | **0.019** | 0.9 | 5 | B | 10.8 | 0.13 | **0.073** | 0.9 |
| 7 | N | 14 | 56.05 | **37.62** | 1.9 | 6 | C | 12 | 23.33 | **14.677** | 12.8 |
| 13 | Al | 27 | 1.588 | **2.053** | 2.9 | 7 | N | 14 | 38.21 | **28.028** | 2.3 |
| 14 | Si | 28.1 | 41.16 | **55.38** | 2.3 | 13 | Al | 27 | 12.03 | **16.995** | 2.3 |
| 39 | Y | 889 | 1.154 | **4.915** | 1.9 | 14 | Si | 28.1 | 25.15 | **36.998** | 2.6 |
| | | | | | | 39 | Y | 889 | 0.678 | **3.156** | 2.4 |
| Si/N = 1.47 ± 0.04 | | | | | | Si/N = 1.32 ± 0.04 | | | | | |

The compositions of sintered samples were determined by prompt-gamma activation analyses. Comparing the Si/N mass fractions of the reference sample and the composite sample (sample from batch 644, with 11.9 wt% carbon content after oxidation at 450 °C) the effect of carbon content on the complex sintering process is observed, namely in the presence of carbon, the Si/N mass fraction has decreased. Because of high relative uncertainty the amount of oxygen was neglected.

## 4. Conclusion

Preparation of C/Si3N4 nanocomposites was performed. The milling product of added carbon black and graphite could be characterized by the same structural characteristics, nearly by the same morphological studies showed the sticking tendency of powders. Carbon added samples are characterized by lower bending strengths than reference monolithic samples. During a pressureless sintering step the structure retains the $\alpha$-$Si_3N_4$ phase, after the second sintering step the alpha silicon nitride to beta silicon nitride phase transformation was completed. The Si/N fraction decreased during sintering process because of the presence of carbon.

## 5. Acknowledgements

Csaba Balázsi thanks for OTKA Postdoctoral Research Grant (D38478), János Bolyai Research Grant and Hungarian State Eötvös Fellowhsip. Support from OTKA T043704 is greatly acknowledged.

## References:

[1] SHEN, Z., ZHAO, Z., PENG, H., NYGREN, M.: *Nature*, Vol. 417, 16 May 2002, 266.
[2] THOMPSON, D. P.: *Nature*, Vol. 417, 16 May 2002, 237.
[3] BHADURI, S., BHADURI, S. B.: *JOM*, January (1998) 44-50.
[4] STERNITZKE, M.: *Journal of European Ceramic Society*, 17 (1997) 1061-1082.
[5] DJURICIC, B., LACOM, W., KRUMPEL, G., BRABETZ, M.: *Nano-Science*, It's time 02/02, 1-8.
[6] HNATKO, M., SAJGALIK, P., LENCES, Z., MONTEVERDE, F., DUSZA, J., WARBICHLER, P., HOFER, F.: *Key Eng. Mat.* Vols 206-213 (2002) 1061.
[7] BALÁZSI, CS., WÉBER, F., ARATÓ, P.: *Mat.-wiss. u. Werkstofftech,* 34 (2003) 332-337.
[8] KASZTOVSZKY, ZS., RÉVAY, ZS., BELGYA, T., FAZEKAS, B., ÖSTÖR, J., MOLNÁR, G. L., MOLNÁR, G., BOROSSAY, J.: J. *Anal. At. Spectrom.*, 14 (1999) 593-596.
[9] ARATÓ, P., BESENYEI, E., KELE, A., WÉBER, F.: *J. Mat. Sci.* 30 (1995) 1863.

https://doi.org/10.26552/com.C.2004.1.10-14

komunikácie
COMMUNICATIONS

Grzegorz Kłapyta *

# SHAPE MEMORY ALLOY – MODERN SMART MATERIAL FOR VARIOUS APPLICATIONS

*The article deals with modern materials - Shape Memory Alloys. The author presents short history of its discovery and its particular properties. One-way and two-way shape memory effects are illustrated and explained. Advantages and disadvantages of SMA are listed and possibilities of usage are discussed. There are also given some interesting applications in various fields of life illustrated by pictures and photos gathered from Internet sites.*

## 1. Introduction

Shape Memory Alloys (SMA) are new very specific materials with unique properties. It has an ability to perform physical work under temperature rise or fall. This feature is due to two different internal structures that depend on the range of temperature. The goal of this paper is to characterise shape memory alloys and present some recent interesting applications.

## 2. History

In 1932 a Swedish researcher Arne Ölander observed the shape recovery abilities of a gold-cadmium alloy (Au-Cd). He gave this phenomenon the name: Shape Memory Effect (SME). Later, the same effect was observed in many other alloys like Fe-Pt, In-Tl, Ni-Al, Cu-Zn, Cu-Al, Cu-Sn, Cu-Zn-X (where X=Al, Si, Ga, Sn, Ni), Cu-Al-X (where X=Ni, Fe, Be, Mn), Ni-Ti-Cu etc.

In 1950 C. Chang and T.A. Read at Columbia University in New York used X-rays to test an alloy Au-Cd and in 1958 they showed that this material can be used in mechanical systems for performing physical work.

In 1962 William J. Buehler at the U.S. Naval Ordnance Laboratory (NOL) investigated the shape memory effect in an alloy of nickel and titanium. He named this alloy briefly "NiTiNOL" (NIckel – TItanium – Naval Ordnance Laboratory) and patented its technology. This was a starting point for a great material revolution.

In 1989 Dr. Darel E. Hodgson at Shape Memory Applications, Inc., after years of experiences, began to produce high quality SMA wires that are named Flexinol.

## 3. What is The Shape Memory Effect?

The shape memory effect is caused by temperature and stress dependent shift in the material's crystalline structure changing between two different phases called martensite and austenite. Martensite, the low temperature phase, is relatively soft whereas austenite, the high temperature phase, is relatively hard. The change of state follows as a result of the heating or cooling of the alloy. During state change the phenomenon of the temperature hysteresis appears. Hysteresis width (T1 in Fig. 1) is defined as the difference between the temperatures at which the material is 50 % transformed to austenite upon heating and 50 % transformed to martensite upon cooling. This difference of temperatures can reach 20–30 °C.

If any NiTiNOL part (Fig. 2a) is annealed at 540 °C and is allowed to cool below the phase transition temperature (Mf), the crystalline structure will change to martensite (Fig. 2b) without shape change. Now, if the part is plastically deformed (Fig. 2c), for example by bending, and then reheated above the phase transition temperature (Af), it returns to its original shape. This phenomenon is material property and is called one-way shape memory effect (Fig. 2.).

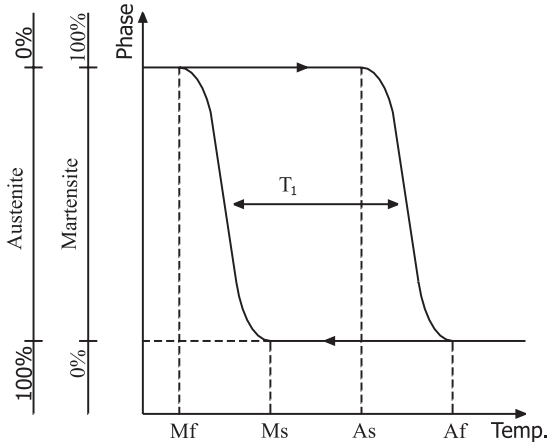


*Fig. 1 Hysteresis of SME*

* **MSc Grzegorz Kłapyta**
Silesian University of Technology, Electrical Faculty, Institute of Theoretical and Industrial Electrotechnical, Division of Mechatronics, Ul. Akademicka 10a, 44-100 Gliwice, Poland, Tel.: (+48 32) 237-28-03, Fax: (+48 32) 237-12-58, E-mail: KAPI@POLSL.GLIWICE.PL

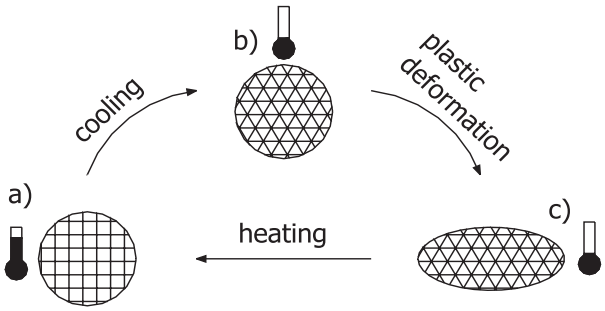


*Fig. 2 One-way shape memory effect*

There is also a phenomenon called two-way shape memory effect (Fig. 3.). Its main feature is that during a change of crystalline structure from austenite to martensite (during cooling) a sample of material also changes its shape. The material is as if it had remembered two shapes and becomes transformed between them without part of external stresses but only due to a change of temperature. However, the two way shape memory effect is no longer material property, but is acquired in technological process, which is called training. It consists of serial repetition of the following procedure:

- Max. 3% bending in martensite;
- Heating over austenite transformation temperature (material recovers its primary shape);
- Cooling to martensite.

After many repetitions, finally we get shape memory alloy capable of recovering a pre-set shape upon heating above its transformation temperatures and returning to an alternate shape upon cooling.

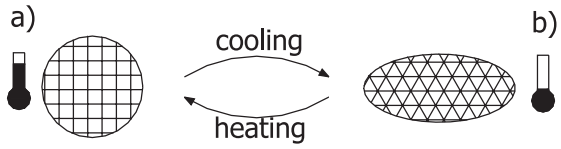


*Fig. 3. Two-way shape memory effect*

## 4. Basic Properties

In industrial applications only AlCuZn and NiTi alloys are being used. The latter known as NiTiNOL (or Flexinol) is used most often. Beside the above-mentioned effect it has several additional properties as e. g.:

*Superelasticity* – in some temperature range ($Ms < T < As$) NiTiNOL shows its unusual elasticity and as soon as the stress is removed it returns to its original shape. The reason for this is that in this temperature range the material is over its normal martensite temperature.

*Relatively constant force* during decompressing in quite wide range of deformation (few %).

*Biomechanical and biological compatibility* – unlike steel or Titan, NiTiNOL has non-linear mechanical characteristics like natural tissues: hair, bone or tendon. This causes that NiTiNOL is ideal prosthetics material. Even though it includes more Nickel (considered as toxic) than steel it is safe because in NiTi alloy intermolecular bonds are stronger and the alloy is covered with a layer of $TiO_2$ so less Nickel is released. Experiments confirm that NiTiNOL is chemically more stable and more resistant to stain than stainless steel.

*Magnetic properties* – NiTiNOL is non-ferromagnetic with a lower magnetic susceptibility than stainless steel.

The following tables present basic physical and chemical parameters of NiTiNOL (Tab. 1.) and Flexinol wires (Tab. 2.)

Elementary properties of NiTiNOL Tab. 1

| | |
|---|---|
| Activation start temperature | 68 °C |
| Activation finish temperature | 78 °C |
| Effective transition temperature | 70 °C |
| Relaxation start temperature | 52 °C |
| Relaxation finish temperature | 42 °C |
| Annealing temperature | 540 °C |
| Melting temperature | 1300 °C |
| Heat capacity | 0.322 J/g °C |
| Density | 6.45 g/cm$^3$ |
| Energy conversion efficiency | 5 % |
| Max. deformation ratio | 8 % |
| Recommended deformation ratio | 3 – 5 % |
| Young's Modulus | 28 GPa |

## 5. Possibility of usage

Possible applications are based on basic properties of shape memory alloys. They are most frequently used as temperature-controlled actuators. Such actuator has various advantages:

- It has a very simple structure - it is small and safe,
- It offers linear movement without any transmission needed in rotary machines,
- The stroke and force can be easily modified by the selection of the SMA element,
- It works clean, silently, makes no vibrations, no dust (there is no friction), no sparks - it does not need high voltage,
- It can be safely used in very flammable environments,
- SMA element can be easily controlled in range of small movements and accelerations,
- These elements offer very high power to weight (power to volume) ratio. They can lift about thousand more than their own mass.

All this means that shape memory alloys are extremely attractive in microactuator technology. But, of course, there are some disadvantages of SMA actuators:

Elementary properties of Flexinol for different wire diameters Tab.2

| Wire diameter ((m) | 25 | 37 | 50 | 100 | 150 | 250 |
|---|---|---|---|---|---|---|
| Min bend radius (mm) | 1.3 | 1.8 | 2.5 | 5.0 | 7.5 | 12.5 |
| Linear resistance (Ohm/m) | 1770 | 860 | 510 | 150 | 50 | 20 |
| Recommended current (mA) [1] | 20 | 30 | 50 | 180 | 400 | 1000 |
| Recommended power (W/m) [1] | 0.71 | 0.77 | 1.28 | 4.86 | 8.00 | 20.0 |
| Max. recovery force (N) [2] | 0.284 | 0.645 | 1.147 | 4.599 | 10.356 | 28.763 |
| Rec. recovery force (N) [3] | 0.069 | 0.204 | 0.343 | 1.471 | 3.236 | 9.12 |
| Rec. deformation force (N) [4] | 0.020 | 0.039 | 0.078 | 0.275 | 0.608 | 1.687 |
| Min. contraction time (s) | 0.1 | 0.1 | 0.1 | 0.1 | 0.1 | 0.1 |
| Relaxation time (s) | 0.1 | 0.2 | 0.3 | 0.8 | 2.0 | 5.5 |
| Typical cycle rate. (cycles/min) | 55 | 52 | 46 | 33 | 20 | 9 |

[1] In still air at 20 °C
[2] Wire stress 600 MPa
[3] Wire stress 190 MPa
[4] Wire stress 35 MPa

*Low energy efficiency* – the maximum theoretical efficiency of a Carnot cycle between the temperature at which a shape memory alloy finishes transforming to austenite upon heating and the temperature at which a shape memory alloy finishes transforming to martensite upon cooling is about 10 %. In reality, that efficiency is at least one order smaller than the theoretical Carnot value.

*Limited bandwidth due to heating and cooling restrictions* – shape memory actuators can be heated in different ways, radiation or conduction (thermal actuators) and by inductive or resistive heating (electrical actuators), and this is generally fast. The response speed is mainly limited by the cooling capacities.

*Degradation and fatigue* – the reliability of shape memory devices depends on its global lifetime performance. Parameters having strong influence on the lifetime are: time, temperature, stress value, deformation value, number of cycles, the alloy system, composition, the heat treatment, and the processing technology.

The table (Tab. 3.), presented by D. Stöckel in 1992, shows maximum values of stress and strain according to number of cycles for standard binary Ni-Ti alloys.

Maximum values of strain and stress for assumed number of cycles Tab. 3.

| Cycles | Max. strain | Max. stress |
|---|---|---|
| 1 | 8 % | 500 MPa_ |
| 100 | 4 % | 275 MPa_ |
| 10000 | 2 % | 140 MPa_ |
| 100000+ | 1 % | 70 MPa_ |

*Complex control* – shape memory alloys show complex three-dimensional thermomechanical behaviour with hysteresis. Moreover, this behaviour is influenced by a large number of parameters. It follows that there are, in general, no direct and simple relations between the temperature and the position or force. Therefore, accurate position or force control by SMA actuators requires the use of powerful controllers and the experimental determination of complex data. Many mathematical models are being developed nowadays by different research groups to overcome this important limitation.

In spite of these limitations, SMA has a lot of advantages and this is why shape memory alloy actuators are widely used in many fields of life.

## 6. Interesting applications

Nowadays shape memory alloys are no longer eccentrics but they have widely entered our environment. We can meet them in everyday life and we often do not even know about their existence. The number of known applications exceeds several thousands. Shape Memory Alloys are most often used as thermostats, grippers, valves, catheters, actuators or connectors. Let's take a look at some interesting applications.

Figure 4 shows the idea of SMA usage to control position of steering flaps on aircraft's wing instead of heavy and complicated hydraulic systems. System using SMA wires is lighter and more reliable.

A submarine presented in Fig.5 is propelled, like natural fish, by moves of its body. SMA wires and bias springs are used to contract submarine sides alternately. They are supplied with a battery and controlled by a computer stored in the nose. This kind of propulsion is very silent and such a submarine is difficult to be detected by sonar. One-meter long prototype has been already built.

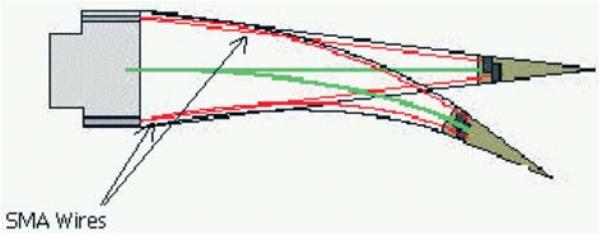


*Fig. 4. SMA wires (instead of hydraulic system) manipulate a flap on the end of airplane's wing. (http://database.cs.ualberta.ca/MEMS/sma_mems/sma.html)*

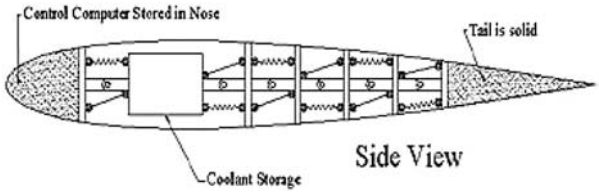


*Fig. 5. Submarine propelled by SMA wires. (http://www.spacedaily.com/news)*

In medicine Shape Memory Alloys are widely used for different kinds of prostheses because of their biocompatibility. But there are also other applications. Figure 6 shows surgical tools that can be easily deformed to a required shape and during sterilization process they come back to their original form. Orthodontic archwires presented in figure 7 have great advantage – they need not be regulated so often. When teeth straighten up the wires still press them in quite a wide range.

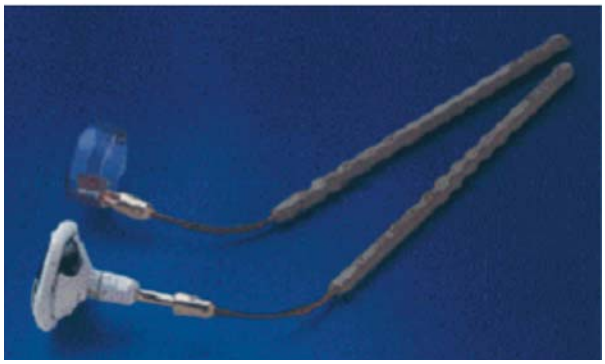

*Fig. 6. Surgical tools (http://www.sma-inc.com/StJude.html)*

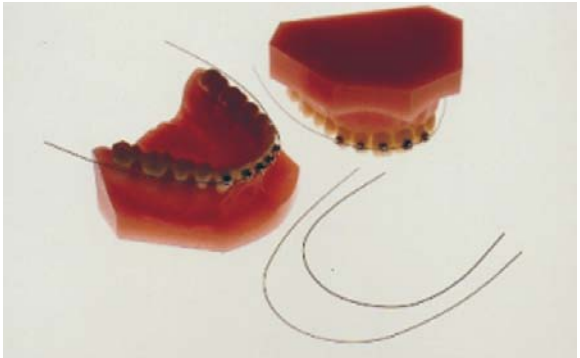

*Fig.7. Orthodontic archwires (http://www.nitinol.com/4applications.htm)*

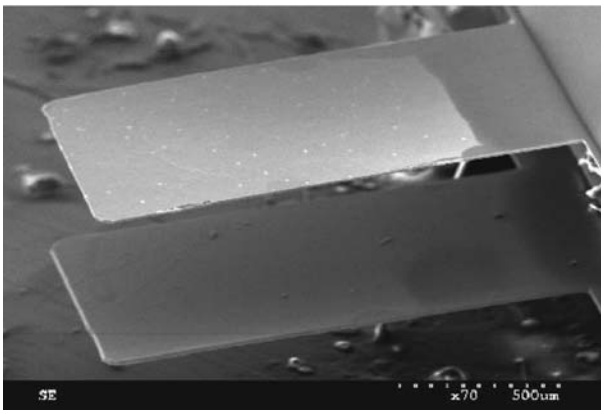


*Fig. 8. Microgripper http://www.ntu.edu.sg/mpe/Research/Programmes/MEMS/Project/weimin1.html#publication*

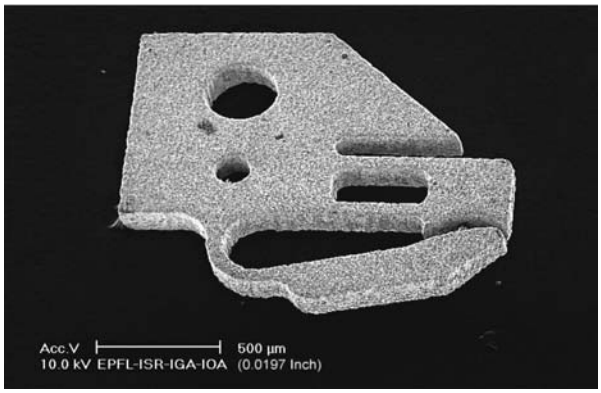


*Fig. 9. Microgripper www.epfl.ch/isr/hpr*

Miniature grippers can be used in medicine as well as in nanotechnology. The microgrippers presented in figures 8 and 9 are smaller than 2 millimetres.

SMA materials are very often used as thermostats in various devices – cars, coffeepots, fire systems, ventilation systems and many others. Figure 10 presents an automatic ventilation system with a thermostat using Shape Memory Alloys.

Robotics is a modern field of science and it makes use of modern technologies and materials. In robot dynamics it is very important to move quickly and precisely. It is easier to move and control a smaller mass, so SMA actuators are willingly used in robotics because of their weight to force ratio. Figures 11 and 12 present the usage of SMA wires for actuating the whole robot (Fig. 11.) or its particular parts (Fig. 12.).

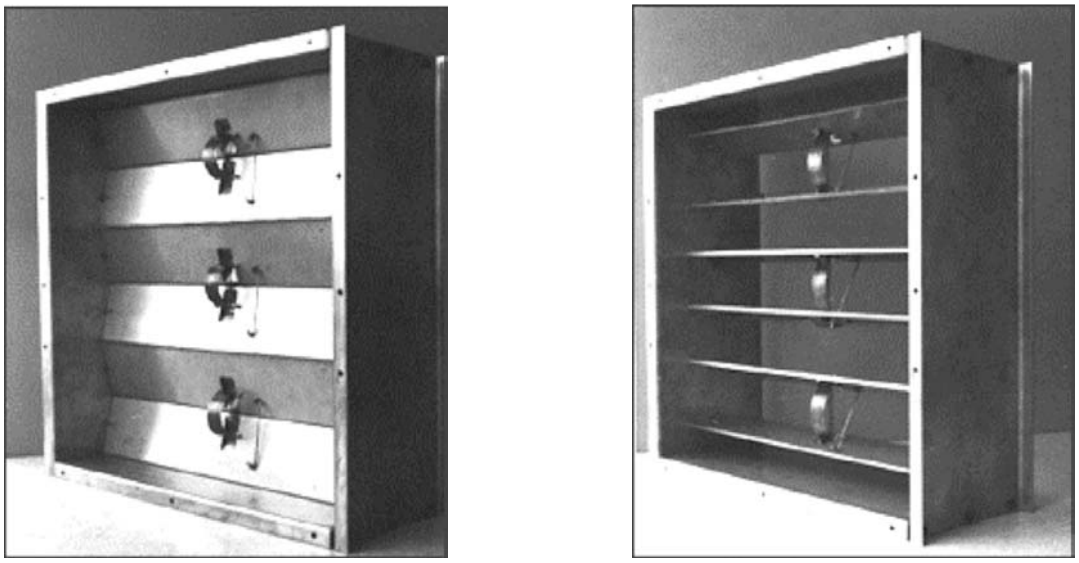

*Fig.10. Self-accommodating ventilation system, closed(on the left), opened (on the right).*
*(http://www.amtbe.com/general4.html#app13)*

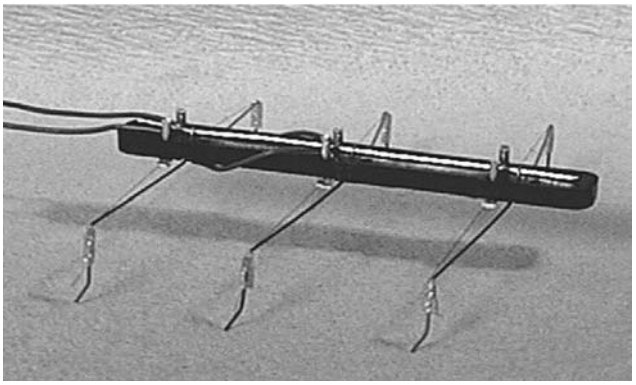

*Fig. 11. Walking robot - Stiquito*
*www.stiquito.com*

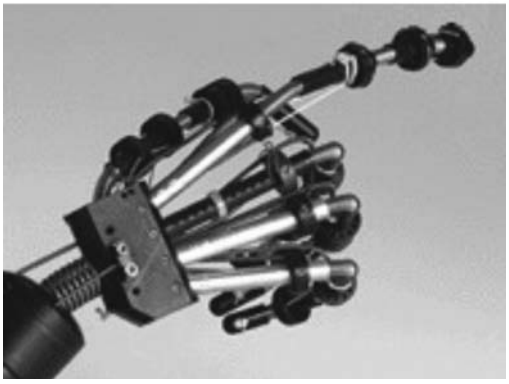

*Fig. 12. Robot's hand*
*(http://database.cs.ualberta.ca/MEMS)*

**References:**

[1] G. KŁAPYTA: *Shape Memory Alloy Actuators In Mechatronics,* Seminar on Electrical Engineering BSE '2002, 8–11 December 2002, Istebna-Zaolzie, Poland.
[2] G. KŁAPYTA: *Shape Memory Alloy - Revolutionary Material For Mechatronics Applications,* Transcom '2003, 23–25 June 2003, Žilina, Slovak Republic.
[3] http://www.nitinol.com/4applications.htm.
[4] http://www.totse.com/en/technology/science_technology/mslwire.html.
[5] http://www.stiquito.com.
[6] http://www.epfl.ch/isr/hpr.
[7] http://www-civ.eng.cam.ac.uk/dsl/sma/smasite.html.
[8] http://database.cs.ualberta.ca/MEMS/sma_mems/sma.html.
[9] http://www.amtbe.com.
[10] http://www.ntu.edu.sg/mpe/Research/Programmes/MEMS.
[11] http://www.sma-inc.com.
[12] http://www.dynalloy.com.

https://doi.org/10.26552/com.C.2004.1.15-18



Wojciech Żórawski – Rafał Chatys *

# INFLUENCE OF HEAT TREATMENT ON THE MICROSTRUCTURE AND COMPOSITION OF PLASMA SPRAYED COATINGS

*Plasma sprayed coatings have been used in various industries for a number of purposes. To increase their mechanical properties, different methods of thermal treatment are being applied. This work is concerned with composite coatings obtained by plasma spraying of the $Al_2O_3 3TiO_2$ and NiO powders (50 % and 50 % by weight), which were then reduced at an atmosphere of dissociated ammonia. Their chemical composition and morphology were determined by means of the EDS microprobe and the Joel 5400 scanning microscope respectively. It has been reported that the process of reduction contributes to the homogeneity of the coating, and that the modified structure contains $Al_2O_3$ and Ni.*

***Key words:*** *plasma spraying, composite coating, reduction*

## 1. Introduction

Composite ceramic coatings produced by plasma spraying have a great number of applications. The desired properties such as resistance to wear, erosion, or corrosion, as well as thermal insulation are obtained by means of various methods of plasma spraying, various techniques of powder feed, as well as various compositions of the coating material [1, 2]. Although it is possible to modify the composition and morphology, the high temperature of the plasma stream reaching 15,000 K causes that the chemical and phase composition of the coatings is different from that of the solid material. Moreover, a number of defects (i.e. porosity, microcracks, non-molten powder grains, poor cohesion between lamellae) are observed in the microstructure, all having a negative influence on the mechanical properties. Undesirable changes in the coating composition can be reduced if plasma spraying is performed in a special chamber with a regulated atmosphere, the process being extremely costly, though [3]. Another method allowing changes in the structure of coatings is thermal treatment. Numerous works, see Refs. [4, 5, 6, 7], present and discuss the results of the research into the influence of carburizing, nitriding, and laser or electron beam treatment on the properties of plasma sprayed coatings. It is possible to obtain a coating with a homogeneous structure characterised by better properties and better adhesion to the substrate. It has not yet been explained, however, what impact the process of reduction has on such structures. The investigations described in this paper aimed at determining the influence of the reduction process on the structure of plasma sprayed $Al_2O_3$-NiO coatings.

## 2. Experiment

### 2a. Material

The material used for the coating was a mixture of powders, the proportion by weight being 50 % $Al_2O_3 3TiO_2$ (Metco 101NS) and 50 % NiO. The two materials were mixed in a V type blender for 1 hour. Their morphology is shown in Fig. 1a, b. The sharp edges of the $Al_2O_3 3TiO_2$ grains prove that the powder was ground. The other component of the composite, the NiO powder, is a chemical reagent.

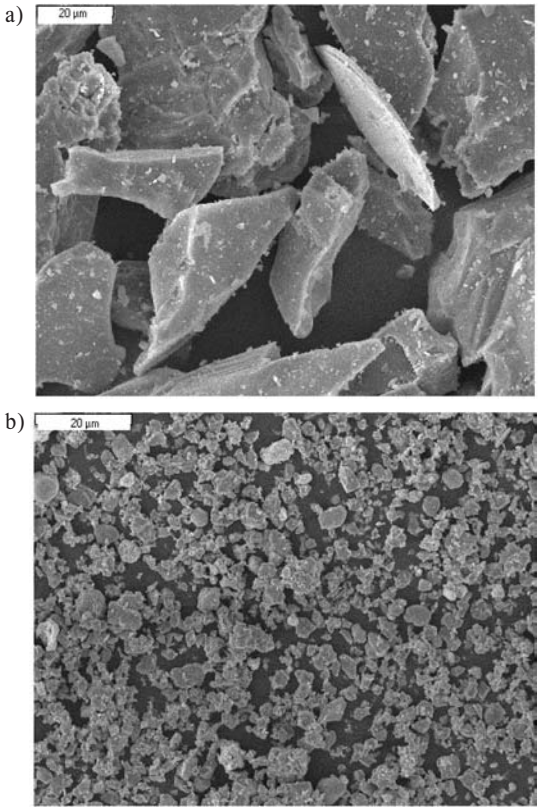


*Fig. 1. Grains of the a) $Al_2O_3 3TiO_2$ and b) NiO powders*

* **Wojciech Żórawski, M.Sc.Eng, Rafał Chatys, DrSc.**
Technical University of Kielce, Al. 1000-lecia P.P. 7, 25-314 Kielce Poland Tel. (41)3424513, 34245027, Fax: (41)3424519, 3424515,
E-mail: ktrwz@eden.tu.kielce.pl, chatys@tu.kielce.pl

The distribution of grains was determined using the Helos (Sympatec GmbH) laser particle size analyser. The range of grain size for $Al_2O_3$ and NiO was $-45 + 11$ $\mu$m and $-20 + 5$ $\mu$m respectively.

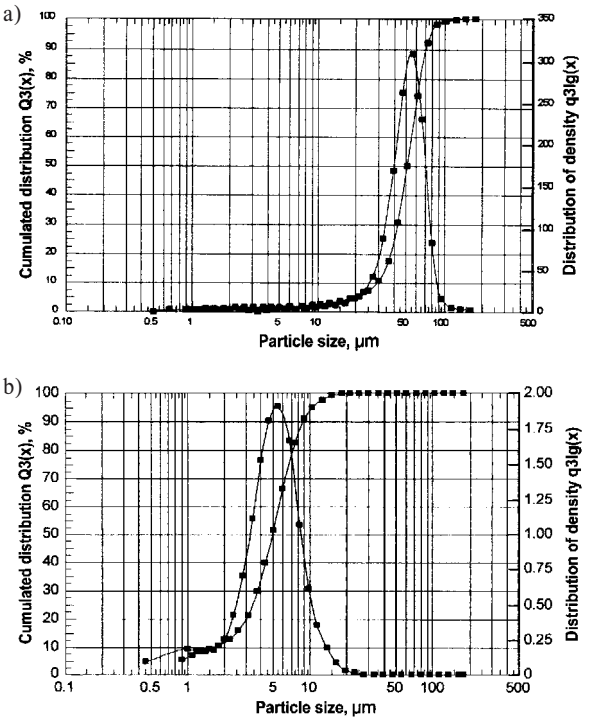


*Fig. 2. Grain size distribution and relative density of the a) $Al_2O_3 3TiO_2$ and b) NiO powders*

## 2b. Plasma spraying

Plasma spraying belongs to semi-molten state surface coating techniques and basically consists of the injection of selected powders into a direct current plasma jet, where they are molten, accelerated and directed onto the substrate surface. The coatings are actually splats of molten droplets instantly solidified on the substrate surface because of its lower temperature. The principles of plasma spraying are shown in Fig 3.

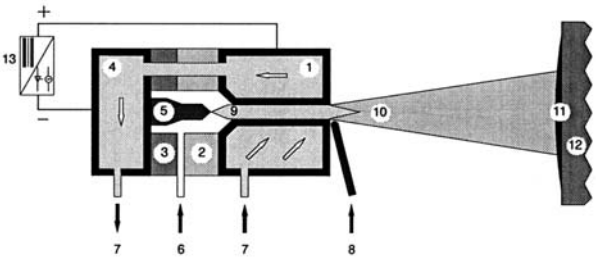


*Fig. 3. Plasma spraying principles: 1 - nozzle (anode), 2 - insulation, 3 - center section, 4 - rear section, 5 - electrode (cathode), 6 - plasma gas, 7 - water cooling, 8 - powder, 9 - electrical arc, 10 - plasma jet, 11 - coating, 12 - workpiece, 13 - generator*

In the experiment the composite coatings were sprayed on 3 mm thick low-carbon steel samples. Before the spraying, the samples were blasted using alundum EB 12 with a grain size of 1.5−2 mm at a pressure of 0.5 MPa. The plasma spraying was performed by means of the PLANCER set equipped with the PN 120 gun and the Thermal Miller 1264 powder feeder. Argon plasma with 7% hydrogen was used for the process. The plasma spraying parameters are given in Table1.

Plasma spraying parameters — Table 1.

| Voltage (V) | Current (A) | Spraying distance (mm) | Powder feed rate (g/min) |
|---|---|---|---|
| 60 | 550 | 100 | 8 |

## 2c. Heat treatment

The process of reduction involves a reaction during which the metal valency drops to zero. The material being surrounded by a protective gas does not oxidize. The pressure of oxygen particles is smaller than the pressure of the pairs of oxides dissociating in the material at the reduction temperatures. The atmosphere of pure hydrogen is one of the most common atmospheres of sintering. Dissociated ammonia can substitute hydrogen, though it is equally costly. Ammonia is dissociated ($2NH_3 = N_2 + 3H_2$) at a temperature ranging between 600 and 950 °C. The protective atmosphere is selected depending on the chemical composition of the sintered material, the furnace type and economic factors. It is quite difficult to prevent oxidization when the materials contain oxides that are hard to reduce (Cr, Ti, Al).

For reduction purposes the plasma sprayed coatings were placed in a pipe furnace with a reducing atmosphere. The process of reduction was carried out for an hour at a temperature of 900 °C and an atmosphere of dissociated ammonia. Hydrogen being the result of the dissociation of ammonia joined the oxygen originating from the oxides reducing them to a pure metal and producing vapour.

## 2d. Methodology

The microstructure of the sprayed composite coatings before and after the thermal treatment was analysed by means of the Jeol JSM-5400 scanning microscope. To study their chemical composition, and perform a point or linear analysis we used the ISIS 300 Oxford Instruments microprobe. The distribution of elements, on the other hand, was determined by applying the EDS method.

## 3. Results and discussion

### 3a. Structure and composition of the coating after spraying

Some lateral microsections of the sprayed coatings were analysed for morphology (Fig. 4a,b,c) and it was reported that the structures consist of deformed particles well-adjacent to each other.

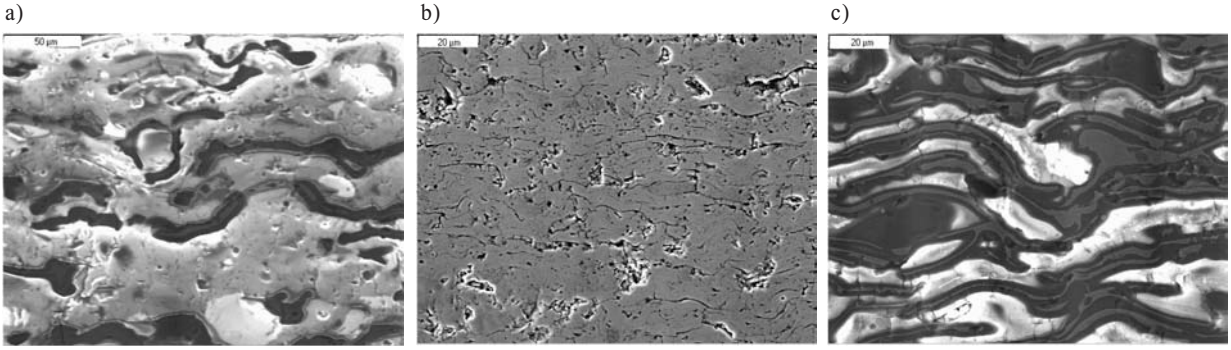


*Fig.4. Microstructure of coating a) $Al_2O_33TiO_2$ b) NiO c) $Al_2O_33TiO_2$/NiO*

This testifies to good remelting of the powder grains. The number of pores is small, which is characteristic of the plasma spraying technology.

In the structure of the $Al_2O_33TiO_2$ coating we distinguish between three phases: the white one, the grey one, and the dark one. In the predominant white phase, there are bands of the dark phase containing bands of the grey phase (Fig. 4a). The test results concerning the chemical composition of the phases based on the point analysis are presented in Table 2. As can be seen from the table, $Al_2O_3$ with minute quantities of $TiO_2$ constitutes the white phase. Then, $TiO_2$ with a considerable amount of $Al_2O_3$ and minute quantities of other oxides is the predominant component of the grey phase. The analysis of the dark phase in three points shows that the proportions of the main components vary, but all of them contain a considerable amount of $ZrO_2$ and that the chemical composition specified by the producer is quite different. The linear analysis (Fig. 5) confirmed the lamellar system of each component.

Chemical composition of the Al2O33TiO2 coating (EDS). Table 2

| Compound [%wt.] / Phase | $Al_2O_3$ | $TiO_2$ | MgO | $SiO_2$ | CaO | $ZrO_2$ |
|---|---|---|---|---|---|---|
| white | 98.71 | 1.25 | – | – | – | – |
| grey | 17.86 | 77.28 | 1.44 | 0.49 | 0.99 | 1.95 |
| dark 1 | 74.49 | 12.11 | 1.76 | 8.11 | 2.42 | 1.11 |
| dark 2 | 52.76 | 24.56 | 4.11 | 3.07 | 1.01 | 14.49 |
| dark 3 | 40.63 | 31.99 | 3.91 | 2.56 | 0.99 | 19.92 |

As far as the NiO coating structure is concerned, we observe some lateral microcracks in the adjacent lamellae. By contrast, the $Al_2O_3$ coating structure exhibits no such cracks. They occur either in a single lamella or go through several lamellae. The same parameters were applied for the NiO and $Al_2O_33TiO_2$ powders. As a result, there was an excessive increase in the melting temperature of the grains of the finer NiO powder. Its melting point being 1984 °C was lower than that of $Al_2O_3$. Hence, some local stresses occured, which caused microcracks in the coating. The analysis of the chemical composition of the NiO coating showed some minute quantities of CoO and MgO. The composite coating obtained by spraying a mixture of the above-mentioned components is characterised by a homogeneous lamellar microstructure. The considerable difference in the size of grains of both components and more than half as great density of NiO did not cause any separation of the components during their feeding into the plasma gun or in the plasma stream. Great extension of the grey phase, i.e. nickel oxide, was observed.

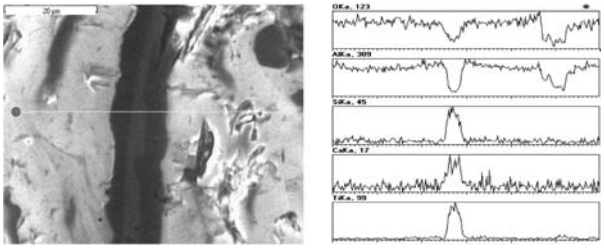

*Fig. 5. Linear analysis (EDS) of the $Al_2O_33TiO_2$ coating*

### 3b. Structure and composition of coatings after heat treatment

The analysis of the coating microstructure showed that the reduction process had influence on the particular components. The morphology of the $Al_2O_33TiO_2$ coating (Fig. 6a) did not change.

The point and linear analyses showed no difference in the composition of the phases, either. Yet, we observe some modification of the structure and the chemical composition of the NiO coating. The boundaries between the badly adherent lamellae, the pores, the micropores, and the microcracks increased considerably due to the occurrence of vapour (Fig. 6b). The hardly visible boundaries between the well adherent lamellae vanished. The analysis of the chemical composition of the NiO coating showed that it was completely reduced to pure nickel. Similar behaviour was observed after the process of reduction. (Fig. 6c). The amount of nickel oxide in the $Al_2O_33TiO_2$ matrix, not modified either structurally or chemically, was reduced. The test results concerning the chemical composition of the nickel oxide phases based on the point analysis before and after heat treatment are presented in Table 3 and in Fig. 7.

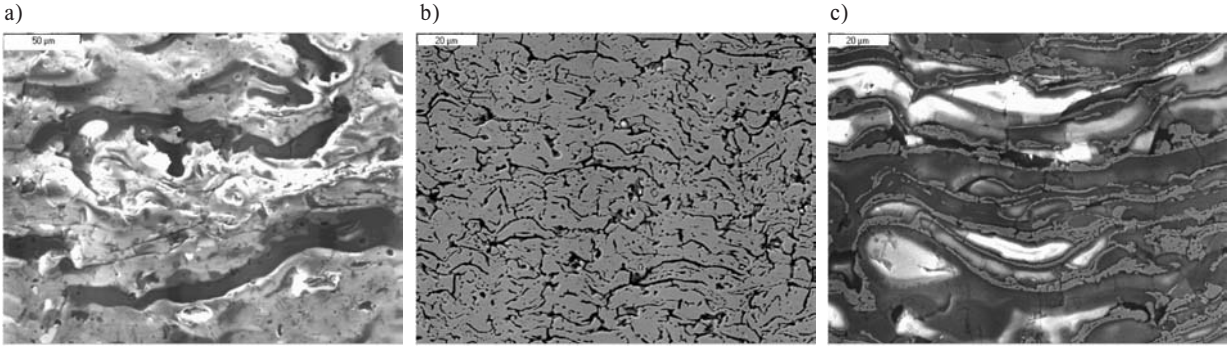


*Fig. 6. Microstructure of the coating after heat treatment a) $Al_2O_33TiO_2$ b)NiO c) $Al_2O_33TiO_2$/NiO*

Chemical composition of the NiO phase before and after heat treatment (EDS). Table 3.

| NiO phase | |
|---|---|
| Before heat treatment [%wt.] | After heat treatment [%wt.] |
| NiO – 98.09 | Ni – 98.97 |
| CoO – 1.24 | Co – 1.23 |
| MgO – 0.67 | – |

The vapour observed in the composite structure, i.e. in the nickel lamella, caused the formation and partial defragmentation of micropores.

## 4. Conclusions

1. The plasma spraying process makes it possible to obtain composite coatings by mixing two or more powders, each with a different granulometeric composition.

2. Nickel oxide was reduced at an atmosphere of dissociated ammonia. The chemical composition of alumina did not change due to its greater affinity with oxygen.

3. The reduction of a plasma sprayed Al2O33TiO2/ NiO coating resulted in the formation of an Al2O3/Ni composite coating.

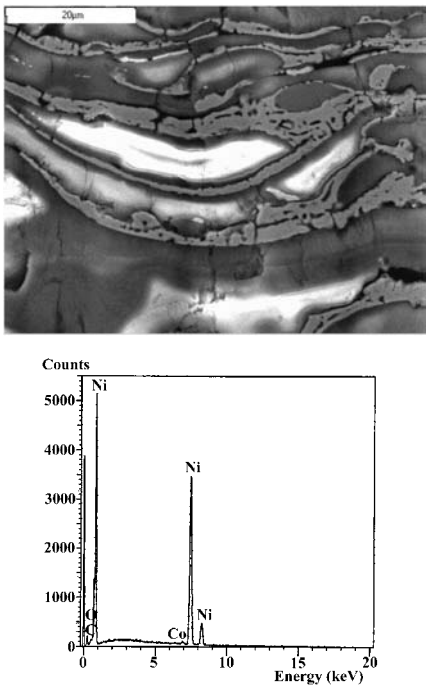


*Fig. 7. Point analysis (EDS) of the $Al_2O_33TiO_2$/NiO coating after heat treatment*

## References

[1] PAWLOWSKI, L.: *The science and engineering of thermal spray coatings.* John Wiley & Sons Ltd, Chichester 1995.

[2] Art. LLORCA-ISERN, N., LUCCHESE, P., JEANDIN, M.: *Advances in plasma spraying technologies and applications,* Finishing 2/1997.

[3] NESTLER, M. C., SPIES, H. J., HERMAN, K.: *Improvement of coating characteristics and end-use performance of thermal spray coatings through post-treatments like hardening, nitriding or carburizing.* Proc. of United Thermal Spray Conference, Düsseldorf 1999.

[4] WIELAGE, B., STEINHÄUSER, S., PAWLOWSKI, L., SMUROV, I., COVELLI, L.: *Laser treatment of vacuum plasma sprayed CoCrAlY alloy.* Surface Engineering, Vol. 14, No 5, 1998.

[5] BINSHI, X., SHICAN, L., XIANGYANG, X., MEILING, Z.: *Structure and fretting wear resistance of electron beam remelting CoCrW coating.* Proc. of International Thermal Spray Conference, Essen 2002.

[6] MATEOS, J., CUETOS, J. M., VIJANDE, R., FERNÁNDEZ, E.: *Tribological properties of plasma sprayed and laser remelted 75/25 Cr3C2/NiCr coatings.* Tribology International 34 (2002) 345-351.

[7] ŻÓRAWSKI, W., RADEK, N.: *Influnce of laser treatment on the tribological properties of thermally sprayed nickel based alloys.* Przegląd Spawalnictwa Nr 8-10/ 2002.

https://doi.org/10.26552/com.C.2004.1.19-25



Mirosław Wendeker *

# ADAPTIVE FUELLING OF THE SI ENGINE

*The paper presents some investigations concerning implementation of the adaptive control methods for the control of the fuel injection in an automotive gasoline engine. As quality index the difference between a current emission level and the level obtained during the stoichiometric combustion was chosen. Stoichiometric mixture provides maximal conversion ratio of the catalytic converter. The paper presents mathematical procedures of the direct adaptive control, based on the adaptive algorithms, which use competitive estimators. Theoretical analysis was supplied with the results of computer simulation of the single point gasoline injection engine model.*

## 1. Introduction

Despite various demands on fuelling of the engine during operation, there is one global quality index of the control algorithm, which affects the whole vehicle. This quality index is represented by the amount of consumed fuel – optimal control algorithm provides the highest fuel energy to engine output conversion efficiency, what meets the driver's expectations. Some limitations have to be taken into account during optimisation of the control algorithm and their influence on the optimisation procedures cannot be neglected. These limitations have character of the inequalitive (acceptable level of toxic emissions) or equalitive (driving comfort and engine durability) restrictions.

Experiments confirmed that the highest increase in hydrocarbons and CO emissions occurs during the engine warm-up test phase. Lambda probe is unable to estimate mixture content and the cold catalytic converter is ineffective, therefore vehicle cannot meet any exhaust emission standards. Counteraction is usually based on the use of the heated lambda probe and heated catalyst or application of a so-called start-up catalyst. Optimisation of the algorithm-controlling amount of fuel injected during the test warm-up phase requires labour-consuming experiments.

After completing the warm-up phase (i.e. when the catalyst reaches its proper operation temperature) fuelling control procedures become more important. Only 1 % deviation from the stoichiometric mixture causes 50 % reduction of the catalyst efficiency with only about 1 % difference in the fuel consumption level. It means that in mathematical task of optimising the fuel consumption, a certain level of the exhaust emissions serves as a penalty function. When the oxygen sensor becomes active, deviations of the mixture composition $\lambda(t)$ from the stoichiometric value can be treated as a quality measure $J_\lambda$ of the fuelling control algorithm, what can be described by the following equation:

$$J_\lambda = \int_{t\in\{T_\lambda\}} (\lambda(t) - 1)^2 \cdot dt = MIN \qquad (1)$$

where: $T$ indicates time intervals, in which the rule of stoichiometric mixture is obligatory (so without periods like engine start-up, engine breaking, full throttle opening). Minimising the quality index $J$ is a basic problem during the synthesis process of the control algorithm designed for the spark-ignited engine.

Mixture stabilisation around stoichiometric composition is a common problem met in many scientific researches, patents and applications [1, 2, 5]. This problem (e.g. oxygen content in the exhaust gases) is solved by means of a feedback control, where oxygen sensor serves as a feedback signal source and the amount of fuel in the inlet pipe is a controlled quantity. Fig. 1 presents a simplified control scheme. The quality of control depends on the proper controller structure and its calibration. Automatic control mostly requires controllers with parameters adjustable in a wide range. Proper selection of the parameters (tuning of the mixture controller) should lead to:

- stabilisation of the mixture at the stoichiometric ratio,
- stable operation of the controller,
- suppression of noise which influences exhaust composition and can be transmitted to the controller,
- insensitiveness to changes of the dynamic properties of the engine.

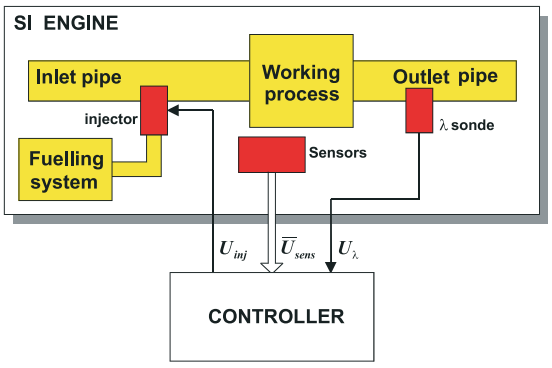


*Fig. 1 A control scheme of the fuel injection in a SI engine*

* **dr hab. inż. Mirosław Wendeker, prof PL**
Department of Internal Combustion Engines, Technical University of Lublin, ul. Nadbystrzycka 36, 20-618 Lublin, Poland
Tel.: +48-81-5381272, E-mail: wendeker@archimedes.pol.lublin.pl

Designing an efficient fuelling control algorithm is not a simple task. Such an algorithm should provide stoichiometric mixture, despite such factors as:
- fast changes of the engine operating conditions,
- signal noise, errors in the memorised map of the engine,
- engine cyclic variations,
- changes of the engine characteristics and exploitation interference.

Quality of the control is influenced by:
- type of the fuel injection system (SPI, MPI, GDI),
- method of the airflow measurement,
- structure and parameters of the engine model written into controller's memory
- type of the control algorithm.

Because of a great variety of available solutions, which can be implemented into electronic control systems of the SI engines, any comparison requires detailed experiments. Moreover, the most promising adaptive control systems are seldom described in literature [3, 4, 7].

An attempt to analyse adaptive control systems of the automotive engines requires computer-aided methods. In consequence, a mathematical model of the engine is necessary as a test object for the investigated control algorithms. Modelling of the engine needs to be compact and one of the main factors influencing this task is the availability of the data describing the object. Usage of the very complex model can be as well dangerous as to much simplification. Model of the engine should be easily identified, having enough complexity for the control purposes. Structural and parametric identification of the model requires experiments on the test bed, which are also the final verification of the simulated control algorithms.

This paper describes an implementation of the adaptive mixture control for the fuel injection controlling in a 1500 ccm four-cylinder SPI gasoline engine [6].

## 2. Adaptive mixture control

The fuel control system is the SISO (Single Input Single Output) system, where the input signal is dose of fuel and the output signal is the lambda signal. The mathematical description of the model is now

$$y(t) = -\sum_{i=1}^{n} g_i(t) \cdot y(t-i) + \sum_{i=1}^{m} h_i(t) \cdot u(t-i) + \eta(t) \qquad (2)$$

where $y(t)$ means lambda signal as a function of time, $u(t)$ means quantity of the fuel and $g_i$ and $h_i$ are the coefficients of the model. We can write

$$y(t) = \vartheta^T(t) \cdot \varphi(t) + \eta(t) \qquad (3)$$

where

$$\vartheta^T(t) = [g_1(t), ..., g_n(t), h_1(t), ..., h_m(t)]i \qquad (4)$$

$$\varphi^T(t) = [-y(t-1), ..., -y(t-n), u(t-1), ..., u(t-m)] \qquad (5)$$

and $\eta(t)$ is the output noise with $\rho = \sigma_n^2$.

The method of estimation can be expressed as:

$$\hat{\vartheta}(t) = \hat{\vartheta}(t-1) + \boldsymbol{P}(t) \cdot \varphi(t) \cdot \epsilon(t) \qquad (6)$$

$$\epsilon(t) = y(t) - \hat{\vartheta}^T(t-1) \cdot \varphi(t) \qquad (7)$$

$$\hat{\boldsymbol{P}}(t) = \frac{1}{\beta}\left[\hat{\boldsymbol{P}}(t-1) - \frac{\hat{\boldsymbol{P}}(t-1) \cdot \varphi(t) + \varphi^T(t) \cdot \hat{\boldsymbol{P}}(t-1)}{\beta + \varphi^T(t) \cdot \hat{\boldsymbol{P}}(t-1) \cdot \varphi(t)}\right] \qquad (8)$$

where $\beta$ is the learning factor.

The problem of discrete models of controlled analog plants and the issue of identification of nonstationary object is the choice: velocity of identification versus quality of identification. Here is proposed a new approach to identification: parallel operating of competitive adaptive filters. The efficiency of the parallel estimation technique in self-tuning control systems is much better than using only one estimator. In this proposition, a few results of estimations (with few learning factors $\beta$) are compared

$$\hat{\vartheta}_j(t) = \hat{\vartheta}_j(N_j, y, \varphi \,|\, t) \qquad (9)$$

and the best one is used for prediction of the next input

$$\overline{\vartheta}(t) = \hat{\vartheta}(t) = \sum_{j=1}^{j} \mu_j(t) \cdot \hat{\vartheta}_j(t) \qquad (10)$$

where $\mu_j$ is equal to 1 or 0.

In the next parts of the paper, some numerical experiments are shown for checking a new method of adaptive control.

## 3. Computerised research system

Computer simulation is often the only way leading to comparative analysis of the control rules of the nonlinear objects, with stochastic parameters and operating conditions. Such simulations reduce costs of the experiment and allow precise analysis, which is free from disturbances unavoidable during test stand experiments. Moreover, in case of the automotive engine, fast exhaust gas analysis requiring precise and very costly equipment can be avoided.

In order to investigate adaptive control algorithms used for controlling mixture composition, a computer system was designed. The core of this system was a mathematical model of the single point fuel injection engine. Having an engine model capable of detailed representation of internal processes [5], the model of the controller was designed. It described reactions of the control algorithm (time of injection, spark advance, bypass air valve position) triggered by the data coming from on-board sensors. The most

common structure of the control system was accepted, typical for SPI automotive engines. It configured also the object of research: 1500 ccm engine of the Polonez GLI vehicle. Several simplifications were made. Such factors like: voltage of the wiring system, spark energy, ignition angle, hydraulic effects in the fuel system (caused by the fuel pump and fuel pressure governor), damping of the exhaust flow caused by the catalytic converter, impulse conversion of the rotational speed sensor, position of the ignition switch and vehicle speed were taken into account as factors influencing the controller, but with no search for detailed relations. The influence was described as a part of general deviation of the measurement-control qualities from the preset values. Other elements were described in the model as logical values or numbers. After reduction the modelled control system simulates indications from several sensors (crankshaft position, rotational speed, coolant temperature, throttle position, intake air pressure, oxygen content in exhaust gases) and simulates operation of actuators. Figs. 2 and 3 describe accepted model of the measurement-control system.

The model assumes that control system reacts when the crankshaft reaches TDC of the current piston in a compression stroke - for the 4-cylinder engine it happens every 180 deg. At this moment control algorithm has data from the sensors gathered between consecutive TDCs as a voltage course. The algorithm (e.g. to calculate mean values) can process regarding to actual needs these signals, but the readouts can be simulated by the algorithm for a given period as well. According to the quality index and limitations, control qualities are calculated for the cylinder being in the compression stroke. Injection starts immediately after determining injection time, stepper motor of the bypass air valve begins the movement towards its new position and ignition advance is triggered with advance to next estimated TDC position.

The model assumes that sensors have their specific metrological properties: precision, linearity, dynamic. Simulated measurement noise was added to their indications so as to reflect the engine cyclic variability. Successive sensors were described using the first-degree inertia model:

$$\frac{dy_P(t)}{dt} = \frac{1}{T} \cdot y_P(t) + \frac{k_P}{T_P} \cdot y_M(t) \qquad (11)$$

where $y_M$ denotes value of the physical quantity in the engine model, $y_P$ is an indication of the physical to electrical converter, $k_P$ – converter gain, $T_P$ – conversion time constant.

The sensor indication has an error with normal distribution and variance dyp. Using the method of determining the deviation of normal distribution the following equation describes indication $y_C$ of the sensor:

$$y_C = y_P(t) + \sqrt{-2 \cdot \Delta y_P \cdot \log(RND)} \cdot \cos(2 \cdot \pi \cdot RND) \qquad (12)$$

where *RND* denotes random function within the range (0, 1). It is assumed that the calculated value $y_C$ cannot exceed limits for the signal level:

$$y_{C,\,min} \leq y_C(t) \leq y_{C,\,max} \qquad (13)$$

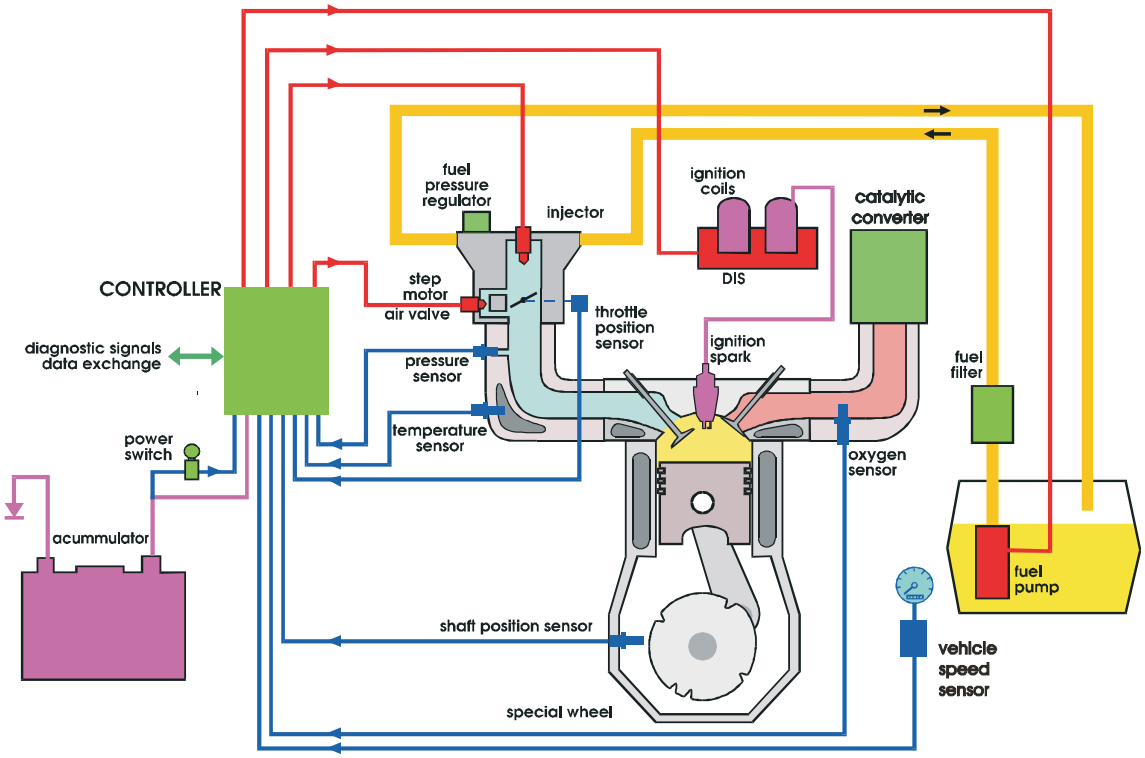


*Fig. 2 General view on the control system accepted in the model*

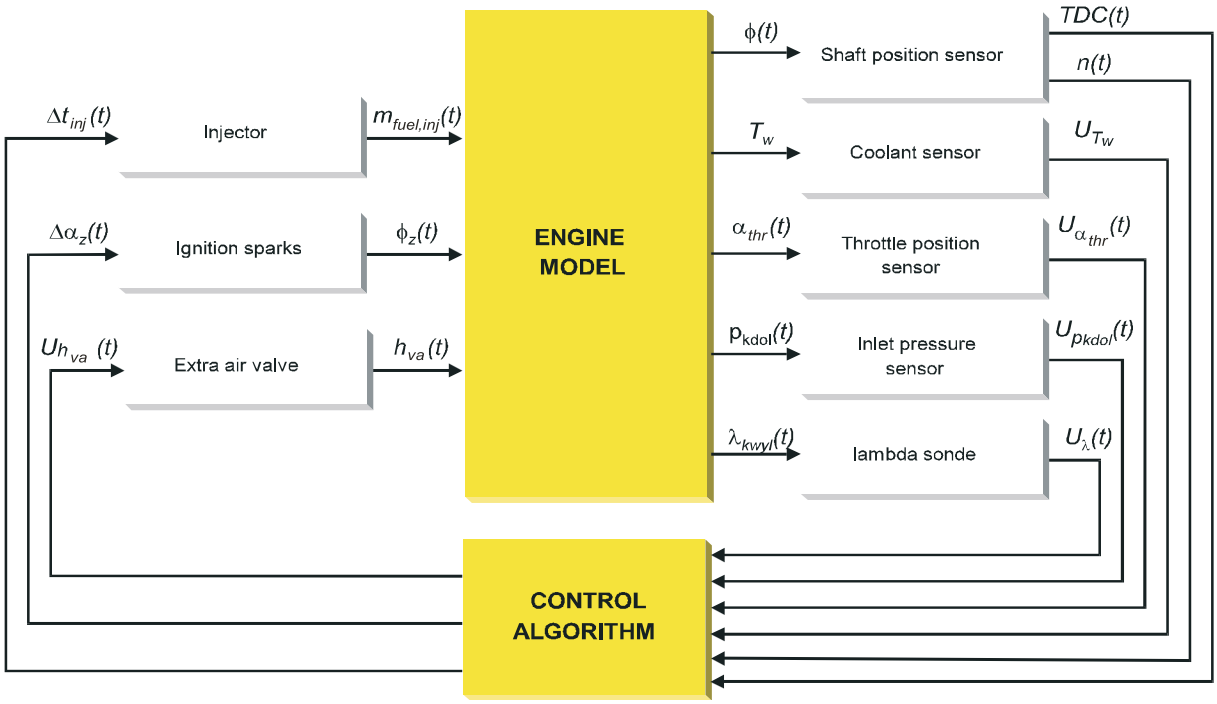


*Fig. 3 Scheme of the control system accepted in the model*

Corresponding quantities $k_P$, $T_P$, $y_{C,min}$, $y_{C,max}$ and $d_{yp}$ for successive sensors are calculated on the basis of a manufacturer's data and experimental results. Rotational speed is calculated from the time difference between consecutive $(k-1, k)$ TDCs of the engine (with the assumed measurement error), according to the formula:

$$n(t) = \frac{30 \cdot N}{t_{TDC}(k) + t_{TDC}(k-1)} \tag{14}$$

It is also assumed that time of the injection $\Delta t_{inj}$ calculated by the control algorithm is subject to various interferences influencing the fuel injection process, which leads to the difference between the assumed mass of injected fuel and the actual mass of injected fuel. Calculations are made on the basis of the following equation:

$$m_{fuel,\,inj}(t) = \hat{m}_{fuel,\,inj}(\Delta t_{inj}(t)) + \\ + \sqrt{-2 \cdot \Delta m_{inj} \cdot \log(RND)} \cdot \cos(2 \cdot \pi \cdot RND) \tag{15}$$

where stands for theoretical dependence between injected fuel and injection duration, $\Delta m_{inj}$ is a variance of the injected mass of the fuel, both these quantities were identified on the engine test bed.

The computer system enabled modifications of the control algorithm. Having in mind necessity of stoichiometric mixture composition, it was possible to determine the influence of the algorithm controlling injection time on the exhaust gases composition for the consecutive engine cycles. The verified and identified mathematical model of the engine was used for the calculations. The engine model was able to simulate thermodynamic processes in the inlet pipes and in successive cylinders.

## 4. Simulations

Simulations were made according to the previously established plan of the experiment, which included three steps. The first step was to select the most valuable methods of estimation of the fuel and air mass reaching cylinders both at steady state and transient conditions. The second step was supposed to establish optimal structure and parameters of the controller according to the rules: PID, model adaptation and estimators cooperation. After the optimal structure was found, the third step of the experiment was initiated. 4 types of controllers were compared in conditions of significant deviations of the model parameters from their original values, written in the controller's memory. This comparison enabled to evaluate reactions of the controllers on the deviations, especially in the context of confirming the advantage of the controller based on the estimator battery cooperation.

Calculations of the engine work for the single investigation point were done both for the steady state and transient throttle positions. During the experiment the rotational speed and the coolant temperature of the engine remained constant as well as parame-

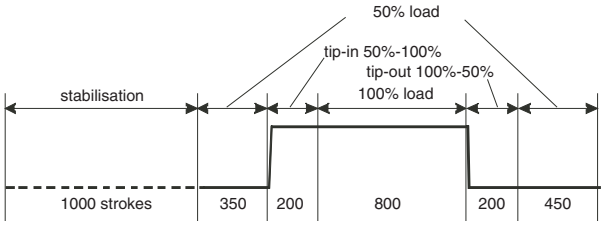


*Fig. 4 Throttle position during one-point calculations*

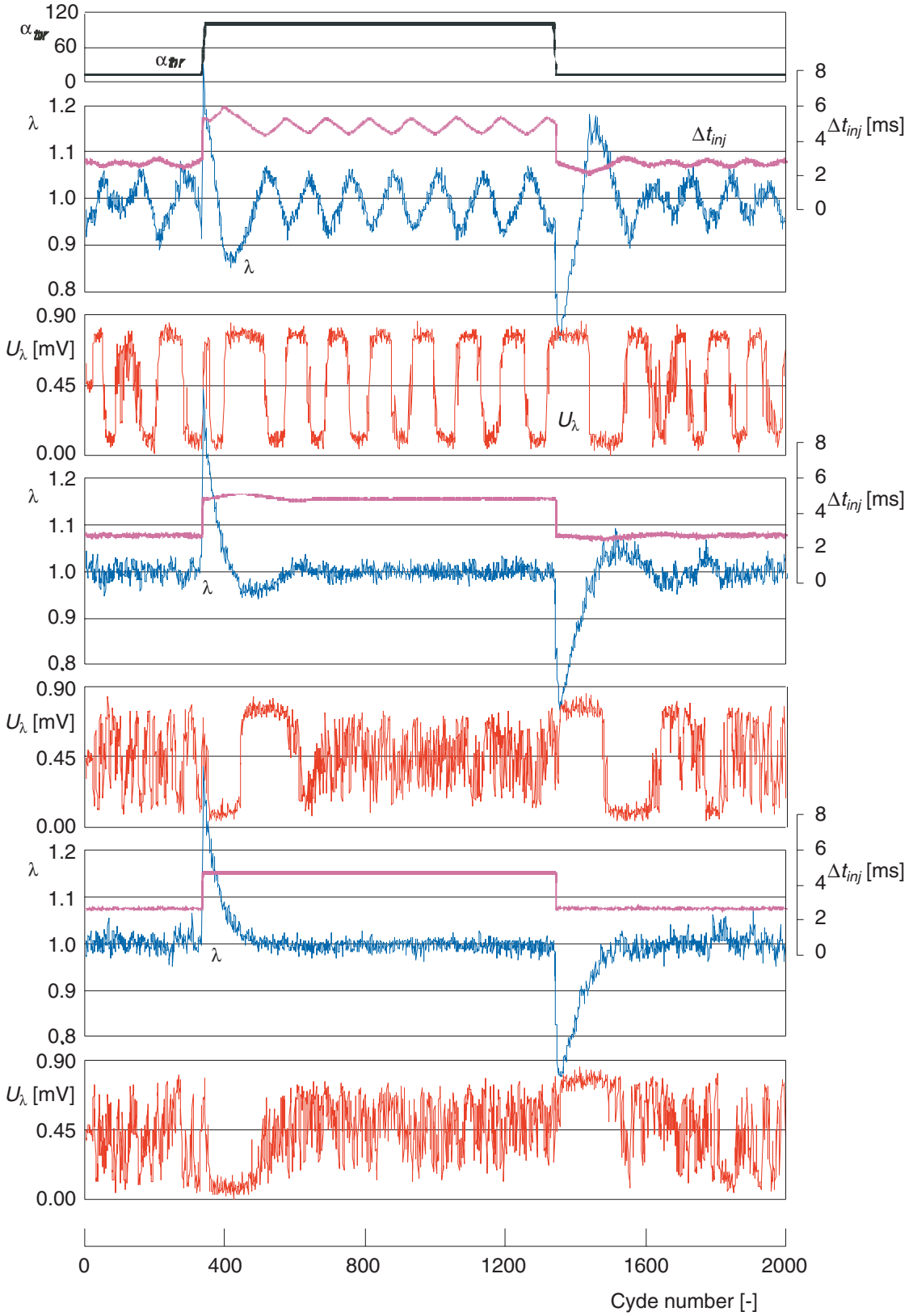


*Fig. 5 Examples of the throttle movement, injection time, exhaust gases composition and lambda probe signal for the one point calculations for the three adaptive control algorithms characterised by different values of the learning ratio - from the top: 0,7, 0,8, 0,9.*

ters of the surrounding air. Before the proper calculations, engine was running for 1000 consecutive cycles at the speed of 1500 rpm and throttle position giving mean inlet pressure level of 50 kPa (14 % throttle opening). The second steady state was set for the fully opened throttle and constant speed. Transient states were realised by the fast throttle repositioning (tips) between these two steady conditions. Fig. 5 shows throttle movement and steps of the calculations.

For the investigated control algorithm calculations were repeated five times. It was caused by the simulated signal noise, giving stochastic deviation values of the mixture composition, inlet pressure or on-board sensors readouts. The results of the calculations consisted of many quantities characterising physical processes in the engine and calculation process of the control algorithm. The most important were mixture composition signal and lambda signal (voltage) from the exhaust pipe. There were five indexes describing quality of the control:

- global control error – deviation of the mixture from the stoichiometric composition

$$\Delta\lambda_g = \frac{1}{T} \cdot \sum_{i=1}^{i=T} (\lambda_i - 1)^2 \qquad (16)$$

- static control errors – deviations of the mixture from the stoichiometric composition in steady state conditions (for the 50 % and 100 % engine load)

$$\Delta\lambda_{S1} = \frac{1}{T_{S1}} \cdot \sum_{i=1}^{i=T_{S1}} (\lambda_i - 1)^2 \qquad (17)$$

$$\Delta\lambda_{S2} = \frac{1}{T_{S2}} \cdot \sum_{i=1}^{i=T_{S2}} (\lambda_i - 1)^2 \qquad (18)$$

- dynamic control errors – of the mixture from the stoichiometric composition in transient conditions (for the load changes)

$$\Delta\lambda_{D1} = \frac{1}{T_{D1}} \cdot \sum_{i=1}^{i=T_{D1}} (\lambda_i - 1)^2 \qquad (19)$$

$$\Delta\lambda_{D2} = \frac{1}{T_{D2}} \cdot \sum_{i=1}^{i=T_{D2}} (\lambda_i - 1)^2 \qquad (20)$$

Additionally an index for the lambda probe voltage was calculated, characterising deviation around 450-mV value

$$pU_\lambda = p(U_\lambda = 450 \pm \Delta U_\lambda) \qquad (21)$$

Fig. 6 shows results of the calculations in the time domain. The following figures show influence of the inlet air and fuel mass assessment on the quality of the control both for the steady and non-steady conditions.

Fig. 7 depicts results of the calculations for the various parameters of the adaptive controller.

Fig. 8 shows comparison of the control quality with four types of control for deviations of the model parameters from their values preset in the algorithm. These parameters [percent values] are:

- k1 – difference in the fuel remaining on the inlet pipe walls,
- k2 difference in the time constant of the fuel evaporating from the walls
- k3 difference in the air reaching the cylinder.

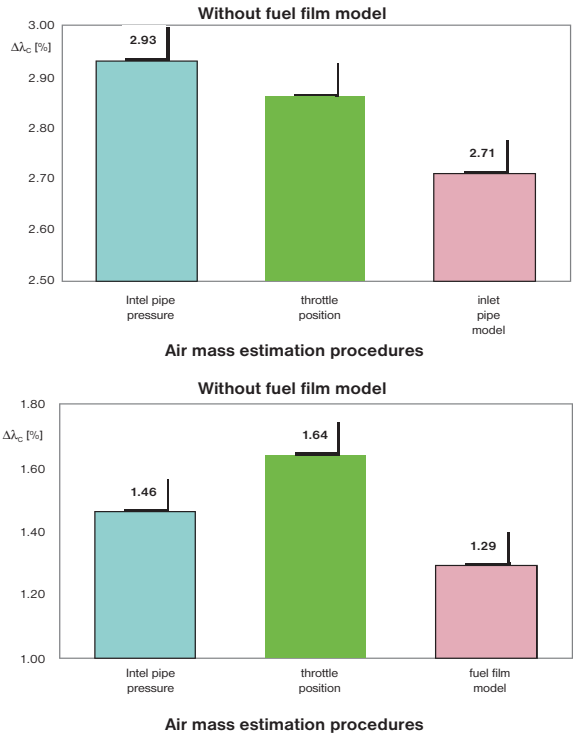


*Fig. 6 Comparison of the total control error for the three methods of the cylinder air assessment and two methods including influence of the fuel film phenomena.*

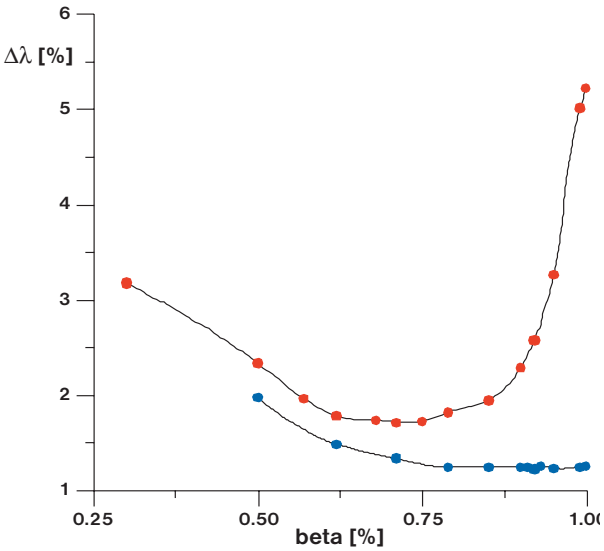


*Fig. 7 Influence of the learning ratio on the total control error for the two different methods of including fuel film phenomena: no film (above), film present (below)*

Types of controllers are:
PID1 – optimal (for the whole test procedure) PID controller,
PID2 – dynamic PID controller (useful at occurrence of rapid changes of model parameters)

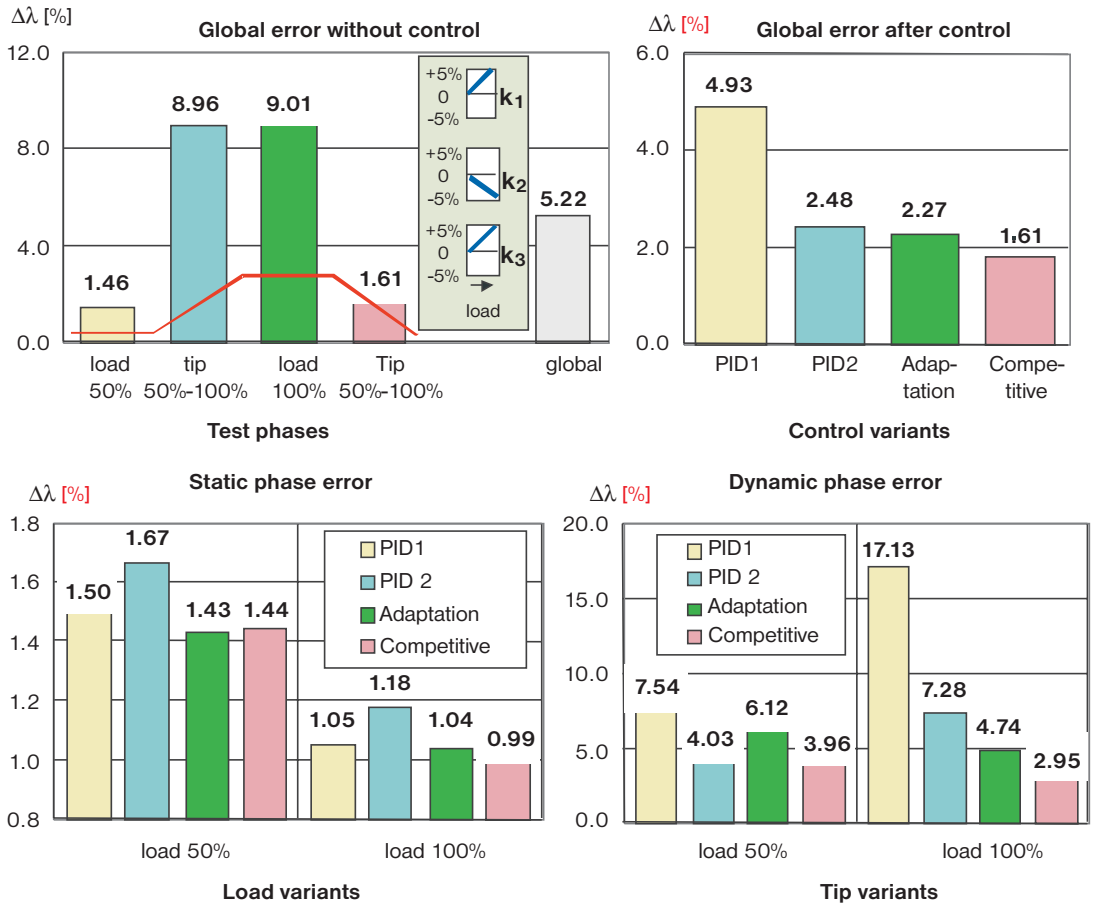


*Fig. 8 Calculation results for the four types of the controller with presence of deviations in engine model parameters from their preset values.*

Adaptation – optimal adaptive controller ($\beta = 0{,}90$)
Competitive – cooperating three adaptive estimators with different learning rations.

## 5. Conclusions

The results of the simulations have confirmed that:

- the best method of the in-cylinder air assessment is based on the inlet pipe modelling, considering fuel deposition and evaporation from the walls significantly increases control efficiency,
- optimal adaptation speed can be established,
- controller based on the set of competitive estimators is more efficient than other investigated types, operation in conditions of erratic model results in smaller control error.

## References

[1] BENNINGER N., PLAPP G.: *Requirements and Performance of Engine Management Systems under Transient Conditions.* SAE Technical Paper No 910083, 1991.
[2] HENDRICKS E. e, a.: *Transient A/F Ratio Errors in Conventional SI Engine Controllers.* SAE Technical Paper No 930856, 1993.
[3] LENZ U., SCHROEDER D.: *Transient Air-To-Fuel Ratio Control Using Artificial Intelligence.* SAE Technical Paper No. 970618, 1997.
[4] SHAFAI E., RODUNER CH., GEERING H.: *Indirect adaptive control of a three-way catalyst.* SAE Technical Paper No. 961038, 1996, pp. 185-193.
[5] WENDEKER M.: *Experimental Results of the Investigation of the Mixture Preparation in Spark Ignition Engine.* SAE Technical Paper No 98456.
[6] WENDEKER M.: *Adaptive Control of the Fuel Injection in the Spark Ignition Engine.* Technical University of Lublin 1998, 176 pp. (in Polish).
[7] YAOZHANG B., YIQUN H.: *Decrease emissions by adaptive air-fuel ratio control.* SAE Technical Paper No 910391, 1991.

https://doi.org/10.26552/com.C.2004.1.26-28

kamUNikácie
COMMUNICATIONS

Rastislav Isteník – Dalibor Barta – Wladyslaw Mucha *

# INFLUENCE OF THE WHEELS ON THE AUTOMOBILE DYNAMICS

*The analysis of the vehicle dynamics with various types of wheels (R13, R14, R15) in two shifting modes and at the driving on a horizontal plane, at downhill- and uphill- driving as well as with different vehicle total mass is described in this paper.*

## 1. Introduction

Contemporary automotive producers allow to equip each of their cars with disks and pneumatics of various sizes. In general, there are several combinations available among them. The influence analysis of some disks and pneumatics combinations on chosen dynamical characteristics of the automobile starting up is made in the paper. The vehicle Škoda Felicia 1.3MPI 40 kW was chosen for the solution of the problem. There were compared combinations of these disks and pneumatics: 165/70 R13, 155/80 R14, 195/65 R15. Especially, rotational speed of the engine was monitored in detail from a large number of parameters.

## 2. Analysis of the car wheels type influence

A numerical simulation with utilization of the program DYNAST [1] solved the problem of the vehicle starting up. The mathematical model [2] consists of a motion equation and supplementary equations defining resistances against movement and functional dependences of important quantities [3]. The speed characteristic of the considered engine 1.3 MPI 40 kW is in Fig. 1.

Analyses of the running up dynamics were made for two values of RPM at gear change - 5500 $min^{-1}$ (maximum, given by the engine characteristic) and 4000 $min^{-1}$ (a lower value for usual drive). Other analyses were made for various values of the road inclination - horizontal road, uprising +10% (+5.71°), decreasing −10% (−5.71°) and for various values of the total vehicle mass (standard value 1025 kg, maximum 1420 kg).

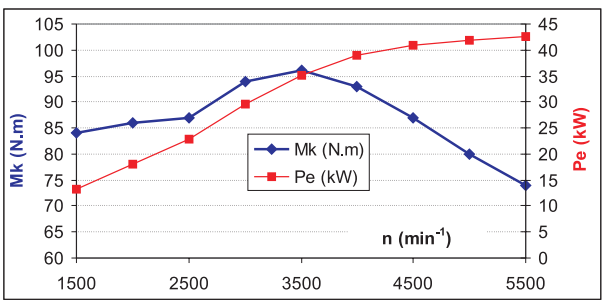


*Fig. 1 Speed characteristics of the engine ŠKODA 1.3 MPI / 40 kW*

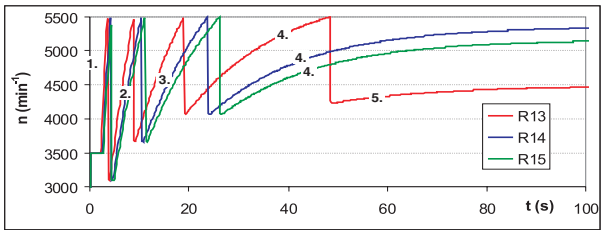


*Fig. 2 Dynamic characteristics of the engine rotational speed, gear change at 5500 $min^{-1}$*

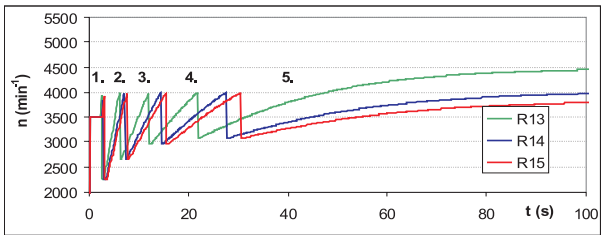


*Fig. 3 Dynamic characteristics of the engine rotational speed, gear change at 4000 $min^{-1}$*

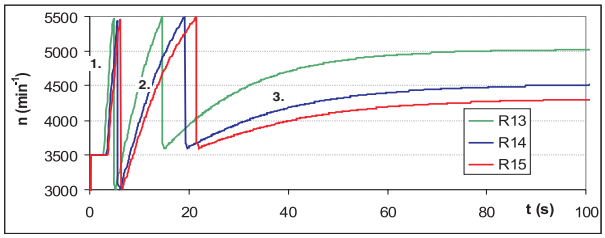


*Fig. 4 Dynamic characteristics of the engine rotational speed, up rise +5.71°.*

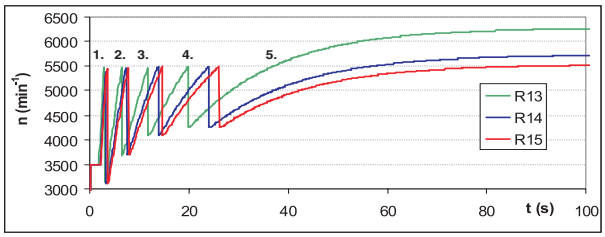


*Fig. 5 Dynamic characteristics of the engine rotational speed (unlimited), decrease −5.71°.*

* **doc. Ing. Rastislav Isteník, PhD., Ing. Dalibor Barta, Ing. Wladyslaw Mucha,**
Department of Railway Vehicles, Engines and Lifting Equipment , Faculty of Mechanical Engineering, University of Žilina, Moyzesova 20, 010 26 Žilina, Slovak Republic, Tel.: ++421-41- 6462660, fax: ++421-41-53016,
E-mail: rasto_istenik@kkvmz.utc.sk, dalibor@kkvmz.utc.sk, wladyslaw_mucha@kkvmz.utc.sk

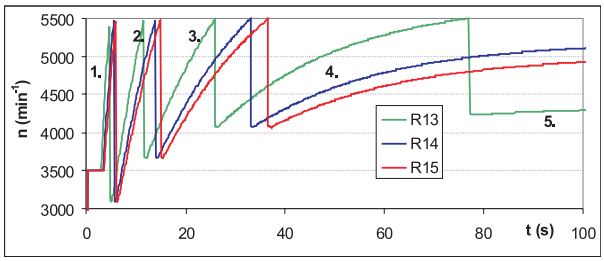


*Fig. 6 Dynamic characteristics of the engine rotational speed, vehicle mass 1420 kg, 0°*

Influence of rotational speed at the gear change (road inclination 0°, total vehicle mass 1025 kg) Tab. 1

| Wheel type | Gear change at 5500 $min^{-1}$ | | Gear change at 4000 $min^{-1}$ | |
|---|---|---|---|---|
| | Time to 100 km/h | Maximal velocity | Time to 100 km/h | Maximal velocity |
| R13 | 16.215 s | 153.09 $km.h^{-1}$ | 19.664 s | 153.08 $km.h^{-1}$ |
| R14 | 16.568 s | 155.11 $km.h^{-1}$ | 20.410 s | 150.50 $km.h^{-1}$ |
| R15 | 16.773 s | 154.75 $km.h^{-1}$ | 20.701 s | 148.72 $km.h^{-1}$ |

Influence of the road inclination - decreasing, (gear change at 5500 $min^{-1}$, road inclination −5.71°, total vehicle mass 1025 kg) Tab. 2

| Wheel type | Without rotational speed limitation | | Limitation to n = 5500 $min^{-1}$ | |
|---|---|---|---|---|
| | Time to 100 km/h | Maximal velocity | Time to 100 km/h | Maximal velocity |
| R13 | 10.512 s | 213.95 $km.h^{-1}$ at n = 6273.77 $min^{-1}$ | 10.517 s | 187.58 $km.h^{-1}$ |
| R14 | 10.639 s | 214.1559 $km.h^{-1}$ at n = 5732.71 $min^{-1}$ | 10.637 s | 205.47 $km.h^{-1}$ |
| R15 | 10.726 s | 214.0691 $km.h^{-1}$ at n = 5537.44 $min^{-1}$ | 10.727 s | 212.62 $km.h^{-1}$ |

Influence of the road inclination – uprising, (gear change at 5500 $min^{-1}$, road inclination +5.71°, total vehicle mass 1025 kg) Tab. 3

| Wheel type | Time to 100 km/h | Maximal velocity |
|---|---|---|
| R13 | (inaccessible 100 km/h) | 98.85 $km.h^{-1}$ |
| R14 | (inaccessible 100 km/h) | 97.41 $km.h^{-1}$ |
| R15 | (inaccessible 100 km/h) | 96.20 $km.h^{-1}$ |

Influence of the total vehicle mass (gear change at 5500 $min^{-1}$, road inclination 0°) Tab.4

| Wheel type | Total mass of the vehicle 1025 kg | | Total mass of the vehicle 1420 kg | |
|---|---|---|---|---|
| | Time to 100 km/h | Maximal velocity | Time to 100 km/h | Maximal velocity |
| R13 | 16.215 s | 153.09 $km.h^{-1}$ | 22.012 s | 147.88 $km.h^{-1}$ |
| R14 | 16.568 s | 155.11 $km.h^{-1}$ | 22.537 s | 150.32 $km.h^{-1}$ |
| R15 | 16.773 s | 154.75 $km.h^{-1}$ | 22.804 s | 149.86 $km.h^{-1}$ |

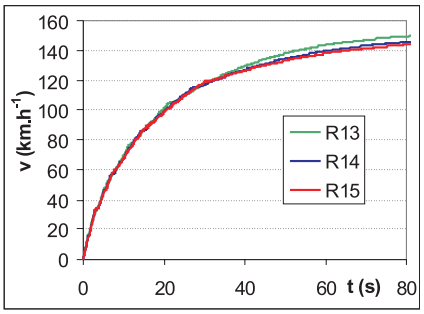


*Fig. 7 Gear change at 4000 $min^{-1}$*

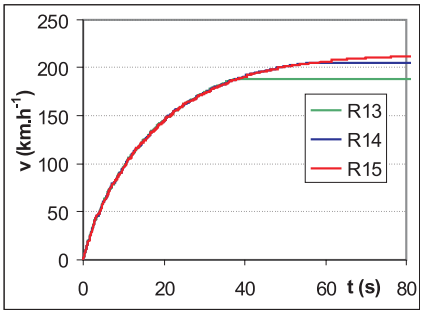


## 3. Conclusion

The results of analysis show that the parameters as the maximal vehicle velocity and the time of achieving 100 $km.h^{-1}$ velocity are not clearly equivalent to the wheel size (with respect to the chosen value of rotational speed during the gear changing and the time variances of the gear changing).

For example, as shown in the table 1, from the compared wheels R13, R14 and R15 in the case of the gear changing at 5500 rpm ($min^{-1}$), the maximal velocity is achieved by the wheels R14 and the maximal acceleration is achieved by the wheels R13. With the wheels R15 the value of the maximal vehicle speed is the lowest, which is due to a smaller traction force on the bigger driving wheel,

in addition, the engine also operates at a little smaller rotational speed with an equivalent lower power. In the case of a gear changing at 4000 rpm ($min^{-1}$) the maximal speed of vehicle is achieved by the wheels R13 due to the highest traction force on the small driving wheels.

In spite of worse vehicles dynamic properties, the big wheels can be advantageous on the score of the lower fuel consumption - the engine operates at a lower rotational speed (in the case of equal vehicle speed) and (also) the rolling resistance is smaller too.

**Reference:**

[1] ISTENÍK R., FITZ P.: *The program DYNAST – solved examples from area of transport and handling machinery (in Slovak)*, EDIS, University of Žilina, ISBN 80-7100-829-X, Žilina, 2001.
[2] ISTENÍK, R., BARTA, D.: *Simulation analysis of a type of engine on dynamical characteristics of an automobile (in Slovak)*, In: PERNER'S CONTACT 2003, Section 3, University Pardubice, DFJP, Pardubice, 2003, ISBN 80-7194-522-6.
[3] LABUDA, R.: *Experimental results from the combustion engine electronic regulator research (in Slovak)*, Mechanical engineering in economy and industry 3/1999, Žilina, 1999, ISSN 1335-2938.

https://doi.org/10.26552/com.C.2004.1.29-33



Peter Choroba *

# DYNAMIC AIR TRAFFIC CONTROL WAKE VORTEX SAFETY AND CAPACITY SYSTEM

*International regulations require aircraft to be separated in approach phase of flight by up to six nautical miles (11.12 km) due to the potential hazard caused by the swirling air left in their wakes. This 'wake vortex' is now the subject of intense worldwide research to understand the nature of the phenomenon and find ways of making air travel safer while reducing congestion around airports. "With the world airline fleet expected to double in size over the next 15 years and the giant A380 entering service in 2005, solutions to the wake-vortex problem cannot come too soon for the aerospace industry and therefore there is a strong need for developing a dynamic air traffic control wake vortex safety and capacity system." [1] This paper describes the concept of integrated transportation system regarding the current state-of-the-art technologies.*

## 1. Introduction

Just as a ship leaves a wave behind it in the sea, an aircraft leaves a wake in the air. An aircraft's wake is in the form of two counter-rotating swirling rolls of air – the wake vortices – that trail from the wings of the aircraft. The wake vortex pair may last for several minutes and may stretch for many kilometres behind the aircraft. The strength of the vortices basically depends on the aircraft weight, divided by the product of air density, flying speed and wingspan. This property generally increases with aircraft weight. The lifetime of a vortex depends upon local meteorological conditions. Vortices last longer in calm air and atmospheric turbulence hastens their decay.

Why do wake vortices matter? It is a question of safety. The rapidly swirling air in a vortex can catch the wings of a following aircraft with potentially disastrous results. Tests with experienced test pilots have shown that even heavy size commercial airliners can be thrown out of control if they follow too close behind a large aircraft such as a Boeing 747. Wake vortices are normally invisible and pilots have no warning that they are flying into one. For this reason, the International Civil Aviation Organization (ICAO) lays down strict rules about the permitted spacing between aircraft, based on their size. In instrument flying conditions aircraft may follow no closer than three nautical miles (5.56 km), and a small aircraft must follow at least six nautical miles (11.12 km) behind a heavy jet such as a Boeing 747.

Many airline pilots have had encounters with vortices, usually on the final approach to airports. They are experienced as a buffeting of the aircraft. While of little concern to passengers and crew who are wearing seat belts at this stage, pilots regularly report minor injuries to crewmembers standing up or moving around the cabin. However, thanks to ICAO regulations on separations (Fig. 1), there have been no serious accidents reported with passenger airliners until November 12 2001, when an Airbus 300 crashed in New York and one of the mentioned reasons was the wake encounter.

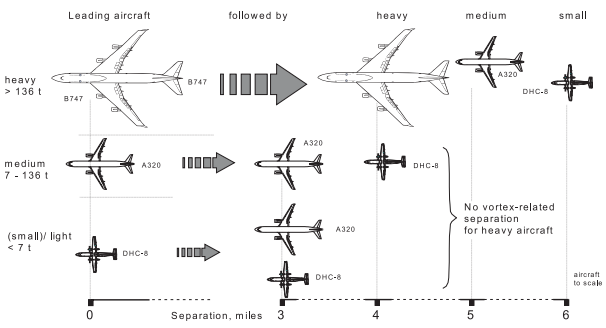


*Fig. 1. ICAO separation scheme for single runway approaches*

"ICAO separations are conservative: they do not completely avoid the effects of wake vortices, but they are sufficient to be safe in most meteorological conditions." [2] Particularly noteworthy is that appropriate regulation for closely spaced parallel runways (separated by less than 2500 ft) is lacking, resulting in inefficient use of some of the runway configurations. The present regulation prescribes that such runways must be used as single runways when the spacing is less than 2500 ft (or 760 m) and in case of instrument meteorological conditions (IMC). Since building an additional closely spaced parallel runway at existing European airports is often the only possible feasible extension possibility, this matter is of crucial importance to increase airport capacity.

Since new high capacity aircraft (such as the Airbus A380) will be heavier and larger, and air traffic has grown continuously with an average rate of 4 % per year, today's aircraft separation rules are considered increasingly inefficient, and may result in unnecessary delays. An integrated Air Traffic Control (ATC) wake vortex safety and capacity system (including a controller Human Machine

* **Peter Choroba**
This work was supported by Eurocontrol Experimental Centre. The author is with the Eurocontrol Experimental Centre, Centre des Bois des Bordes, B.P. 15, F-91222 Bretigny sur Orge Cedex, France (Tel: +33-1-6988-7858; E-mail: peter.choroba@eurocontrol.int).

Interface (HMI)) used in combination with new modified wake vortex safety regulation is expected to provide the means to significantly enhance airport capacity, basically on runway throughput.

## 2. The components of the system

The impact of weather on wake vortex safety is a crucial aspect, and the uncertainty in predicting the behavior of wake vortices in different weather conditions implies that continuous monitoring of both wake vortices and weather will be necessary. This will enable continuous verification – and possibly update – of safe predictions of required aircraft spacing (separation minima). The integrated wake vortex safety and capacity system should therefore integrate the following subsystems:

- Wake detection sensors
- Weather forecast and now cast systems
- Wake vortex prediction tool
- Air Traffic Controller Human Machine Interface (HMI)

### A. Wake detection sensors

The basic requirements for a wake vortex sensor are to detect, locate and quantify the strength of aircraft wake vortices. There are several tools (systems), which enable detection of wake vortices with different limitations in range, accuracy, and weather sensibility. The simplest one is WINDLINE, based on mechanical approach of vortex detection by set of anemometers. This system is highly accurate, but cannot be used for higher altitudes, since anemometers are placed on the ground. On the other hand, advantage of this sensor is usability in all weather conditions.

Vortices can be detected by ground-based or in the future by onboard-pulsed lidars. LIDAR (LIght Detection And Ranging) is similar to the more familiar radar and can be thought of as laser radar. In radar radio waves are transmitted into the atmosphere, which scatters some of the power back to radar's receiver. LIDAR transmits and receives electromagnetic radiation but at a higher frequency (ultraviolet, visible and violent region). Different types of physical processes in the atmosphere are related to different types of light ring. Choosing different types of scattering processes allows atmospheric composition, temperature and wind to be measured. LIDAR in general consists of 3 main parts: transmitter, receiver and detector system (Fig.2).

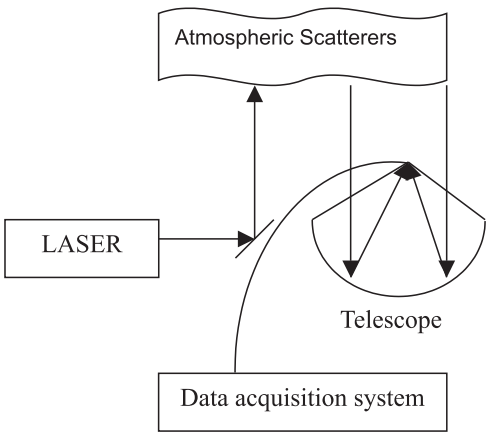


*Fig. 2. Schematic view of LIDAR's architecture*

LIDARs use extremely sensitive detectors so called photo multiplier tubes. An individual quantum of light is converted first into electric currents and then into digital photo counts, which can be stored and processed on a computer. The received photo counts are recorded for fixed time intervals during the return pulse. The times are converted to heights called range bins since the speed of light is well known. The range-gated photo counts are then stored and analysed by a computer.

"CW (continuous wave) lidar has the best range resolution but is limited to about 300 meters in range, so it used close to the runway threshold. The pulsed lidar can measure wakes out to several kilometers, but has poorer resolution (∼30 meters)." [3] However, LIDAR capability in rain and fog has not been demonstrated.

The SODAR (Sound detection and ranging) may also be capable to detect wake vortex. The newest SODAR systems use steered beam, phased array technology. Three independent beams are generated: one directed vertically and two tilted in perpendicular directions. Their compact design is ideal for measuring and providing high-resolution wind and wind turbulence profiles from a wide variety of platforms such as ships, buildings, trailers and trucks. The SODAR acoustic signal processor is engineered for reliable, unattended field operation. Data analysis software is also available to process SODAR data, including automatic generation of data reports and summary plots. SODAR's height range is depending on the model in interval 15 – 750 meters, with resolution 5- 20 m.

A building block necessary to build sufficient confidence in the model predictions for wake vortices evolution in relation to weather will be to use data from a C-Band Doppler weather radar for weather monitoring but also wake vortex detection. Several US references in scientific literature put forward the idea that a Doppler radar can detect wake vortices, and it must be stated that currently some research centers are starting to use C-band Doppler radar data as experimental trials relevant data. The interest of radar for weather analysis is that of a system complementary to the lidar system:

- It can provide additional meteorological parameters besides performing turbulences detection (especially for mapping of precipitations areas where lidar is not efficient)
- The potential detection range on wake vortex is at least the same as for lidar in clear air, but is larger in humid air and in rain.

Principles and algorithms (for e.g. atmospheric turbulence detection and weather forecasting) previously developed within three European studies of the 4th Research Technology and Devel-

opment Framework Program. These algorithms improve significantly the Doppler radar analysis performances and are well adapted for wake vortex monitoring. Some principles have already been validated on low altitude wind-shears detection.

Nevertheless, the limitations as well as uncertainties in measurements of wake turbulence detections are yet to be evaluated as most technologies are still under development.

### B. Weather forecast and now cast systems

Since the weather impact on wake vortex behavior is significant, the weather forecast and now cast must be provided as one the required data sets for further calculations, especially for vortex prediction computing. Weather subsystem is crucial and must provide detailed wind, vertical wind shear, atmospheric turbulence and temperature gradient information to the prediction subsystem for the current time and up to an hour in the future. Besides the common used airport weather radars (mostly C-Band Doppler radars) it is necessary to use wind profilers to get accurate wind and temperature profiles.

"Wind profilers are pulse-Doppler radars that look into the atmosphere and make high-resolution measurements of wind, turbulence, and echo strength in a vertical column above the radar site." [4] Typically, wind measurements are made by pointing the radar's antenna beam in three (or sometimes five) different directions. The Doppler shifts of the echoes from each direction are compared to determine the wind speed and direction. Profilers can operate continuously, providing wind measurements approximately every 5 minutes. The scattering targets from which echoes are received depend on the wavelength used. In the case of UHF-band profilers, the targets include rain, snow, and turbulent fluctuations (causing changes in refractive index) of clear air. Some profilers can also measure temperature using a Radio Acoustic Sounding System (RASS) in which sound waves are also emitted and tracked by the radar head. The measured speed of the sound is related to air temperature.

The effective altitude range of a profiler depends on the wavelength used and other factors such as the antenna size, transmitter power, and the availability of scattering targets. "For a typical profiler, the range in fair weather is from about one half to five kilometers during the summer, although on cold, clear, winter days sometimes no measurements can be made at all." [4] In rain or snow, measurements can be made from as low as 100 meters and often up to ten-km altitude or higher. These profilers are often called boundary layer profilers because of the region in which they are most effective. Other profilers, operating in the VHF band, are designed to make measurements higher in the atmosphere; some, for example, probe the mesosphere, stratosphere, and troposphere.

### C. Wake vortex prediction tools

The core of the integrated system is the prediction subsystem. The predictor utilizes weather data and an aircraft characteristic database to predict the wake and threshold of wake vortex strength for an acceptable encounter, airport layout data and wake sensor feedback.

Two most capable prediction tools in Europe nowadays are: P2P developed by DLR (Deutsches Zentrum fur Luft- und Raumfahrt) and Vortex Forecast System (VFS) developed by Transport Canada but with European cooperation.

"A new parametric wake vortex transport and decay model is proposed that predicts probabilistic wake vortex behavior as a function of aircraft and environmental parameters in real-time." [5] The Probabilistic Two-Phase wake vortex decay model (P2P) accounts for the effects of wind, turbulence, stable stratification, and ground proximity. The model equations are derived from the analytical solution of the spatial-temporal circulation evolution of the decaying potential vortex and are adapted to wake vortex behavior as observed in large eddy simulations. Vortex decay progresses in two phases, a diffusion phase followed by rapid decay. Vortex descent is a non-linear function of vortex strength. Probabilistic components account for deviations from deterministic vortex behavior inherently caused by the stochastic nature of turbulence, vortex instabilities and deformations, as well as uncertainties and fluctuations that arise from environmental and aircraft parameters. The output of P2P consists of confidence intervals for vortex position and strength.

To reliably assign a defined degree of probability to the predictions, the model design allows you for the continuous adjustment of decay parameters and uncertainty allowances, based on a growing amount of data. "The application of a deterministic version of P2P to the Memphis wake vortex database yields favorable agreement with measurements." [6]

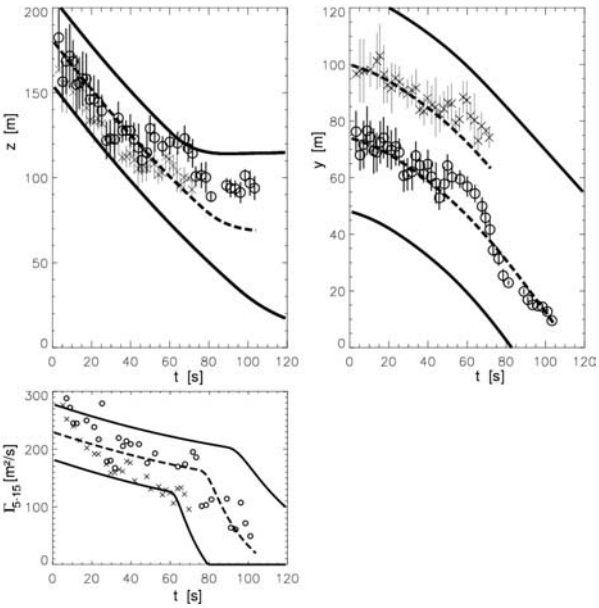


*Fig. 3. Comparison of prediction and detection (DLR project Wirbelschleppe)*

Comparison between wake vortex prediction made by P2P and measurements conducted by LIDAR is shown in Fig. 3. The bold lines present the predicted confidence interval in vertical ($z$) and lateral ($y$) plane, as well as circulation ($\Gamma$) data. Measurements were made by two lidar systems.

"Vortex Forecast System (VFS) is a prediction tool based on a combination of theory (method of discrete vortices) and experimental data. Its accuracy and speed in predicting potentially dangerous wake vortices may allow the safe distances between aircraft to be reduced, thus increasing capacity of congested airport." [7]

VFS uses real-time information about the environment and the aircraft, predicted meteorological conditions, and accurate real-time modeling of vortex transport and decay to predict conditions under which the separation may be safely reduced below the current wake vortex standards. The principal components of VFS are the Near Wake, Far Wake, and Danger Area Models. The Near Wake Database (NWDB) is calculated offline for each aircraft type based on the information available on the aircraft geometry. The far wake evolution is calculated in real time. The far wake calculation may start from the NWDB, or alternately from a universal near wake profile. The far wake calculations are based on the 2-D cross-plane method of discrete vortices equations describing the vortex motion in incompressible flows.

### D. Air Traffic Controller Human Machine Interface (ATC HMI)

The role of the ATC HMI is to provide the traffic situation picture and automated support for various ATC tactical roles e.g. approach, tower. It is foreseen to integrate wake vortex related information together with flight information (position, altitude, ground speed, aircraft type) in order to improve the safety and capacity. Current ATC systems do not take into account wake turbulence information, hence controllers rely on the ICAO separation standards or very often just on their own experience. The AVOSS (Advance vortex spacing system) study shows [8], that in specific weather conditions even the ICAO separations are not enough and there is a potential of wake vortex encounter. On the other hand, separations are quite often too conservative, thus limiting capacity. Wake vortex information visualization can be integrated in any of the current air traffic control human machine interfaces and can be used for optimization of separations.

HMI has to be developed and optimized for tower and Terminal Area / en-route controllers, under the commitment to the principles of human centered automation. That means, with priority to providing optimal decision support to the controllers, who will keep the ultimate responsibility for their decisions, HMIs will have to reflect a synthesis between

- Specific controller needs for information and decision support
- Usability and acceptability of the HMIs
- Airport operational requirements and constraints
- Traffic demands (e.g. amount of inbound/outbound traffic)
- Technical functionality provided by the integrated system, particularly for wake vortex prediction and monitoring, and aircraft spacing prediction.

A further issue is merging those functionalities with other functions at the controller working positions (e.g. approach planning, departure planning). This issue has to be addressed through an analysis of the interoperability with existing ATC systems and the usability and acceptability of the system.

### 3. Sensor and data fusion

To develop an integrated wake vortex safety and capacity system it is necessary to combine all the components mentioned above and to deal with the data fusion. Fig. 4 illustrates the data flow.

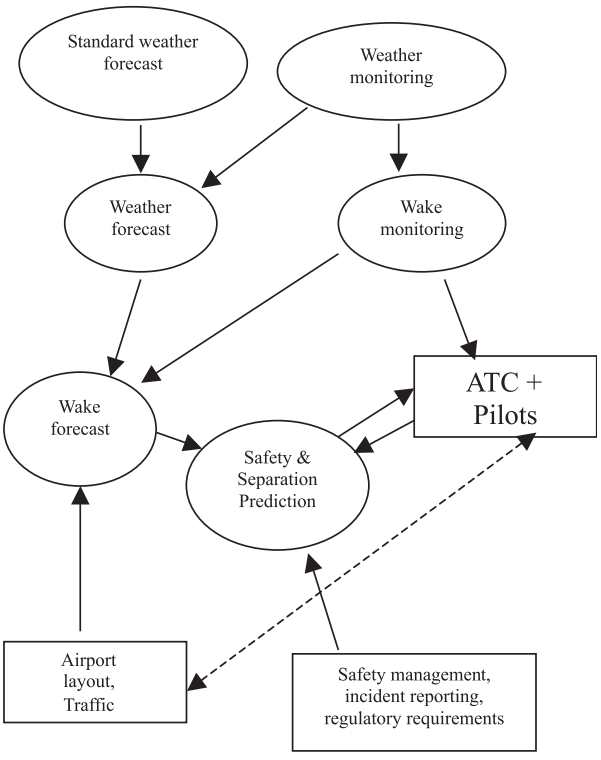


*Fig. 4. Diagram of data flow in the integrated system*

Standard weather forecast data are used as input for local weather forecast at the particular airport using also data from weather monitoring at the same airport. Wake monitoring (detection) requires also input from local weather monitoring subsystem and also provides wake information to pilots and air traffic controllers, especially in the case of detected very strong wake turbulence to avoid an encounter.

Wake vortex prediction is computed with an input of airport layout and traffic data including weather forecast and wake moni-

toring data. After the wake prediction, safety and separation prediction can be computed regarding to safety management, incident reporting and regulatory requirements. Output of this step provides "new" spacing criteria to controllers and pilots.

Integration of the heterogeneous subsystems requires state-of-the-art facilities, including a variety of methods for integration (e.g. static/dynamic interaction, tool chaining, workflow chains). Design of the integrated platform comprises the design of system architecture, interfaces, common database, scenario manager, and human-machine interfaces (including controller HMI).

## 4. Conclusion

The local installation of the integrated system at the airports will require new safety regulation, since the present wake vortex safety recommendations and best practices do not take new modified ATC systems into account. Specific attention must be given to the issue of development and harmonization of new wake vortex safety regulation. To enhance acceptability of the integrated system (and other new technologies, including high capacity aircraft such as the Airbus A380 and on-board wake detection and warning instrumentation), possible end-users and regulatory authorities should be involved in the development of such system to achieve the goal as soon as possible. The concept of the integrated system will be validated firstly through the fast-time simulation followed by real-time simulation, including assessment of safety and capacity benefit.

## References

[1] EUROPEAN COMMISSION RESEARCH PROJECTS OVERVIEW: *Wake vortex*, 2002
[2] GERZ, T., HOLZAPFEL, F, DARRACQ, D.: *Aircraft wake vortices* (A position paper), 2001
[3] HINTON, D. A.: *An aircraft vortex spacing system* (AVOSS), NASA Langley, 2001
[4] CARTER, L. A.: *Developments in UHF lower troposphere wind profiling at NOAA*, 1995
[5] HOLZAPFEL, F.: *A probabilistic two-phase wake vortex decay and transport model*, DLR 2001
[6] HOLZAPFEL, F., ROBINS, E. R.: *Probabilistic wake vortex decay model predictions compared with observations*, DLR 2002
[7] JACKSON, W.: *Wake vortex prediction - an overview*, Transport Canada 2001
[8] Wake vortex measurements data – DFW Deployment of September 15 to October 3, 1997

Peter Choroba is a Ph.D. student in the Innovative R&D of Eurocontrol Experimental Centre in Bretigny sur Orge/Paris. He holds a Master in Air Transportation engineering from the University of Zilina in the Slovak Republic.

https://doi.org/10.26552/com.C.2004.1.34-37

komunikácie
COMMUNICATIONS

Gergely Biczók – Kristóf Fodor – Balázs Kovács *

# HANDOVER LATENCIES IN BCMP NETWORKS

*In this article, we give a short overview on wireless access networks and the BRAIN Candidate Mobility Protocol (BCMP). The two different handover mechanisms of BCMP are introduced. With the help of standard network tools and an own measurement program, latencies caused by both kinds of handovers were examined. We show that latency values are largely hardware-dependent and that by an adequate hardware configuration, BCMP provides smooth and fast handovers. This makes BCMP suitable for using with real-time applications, such as packet-switched voice or video.*

## 1. Introduction

Nowadays, wireless local area networks are of increasing importance. They provide comfortable network connectivity in such places, where cables are not affordable or disturbing. In the past few years, the evolution of radio technology made high bandwidth links available so that they are also suitable for audio and video applications.

Driven by the increasing demand for mobile and cordless broadband services, the BRAIN (Broadband Radio Access for IP based Networks) project [1] was to provide a true broadband multimedia IP-based radio technology. In addition, BRAIN offers the integration of end-to-end services over IP and evolves IP towards mobility. The project MIND [2, 3] (Mobile IP-based Network Developments) has been formed to research the extension of IP-based radio access networks (ANs) to include ad-hoc and wireless elements both within and attached to the fixed infrastructure. MIND is a follow up to the successful BRAIN project. The project will take an IP core as a starting point, accessed by a variety of technologies. They put the focus on the access network, where different IP QoS protocols could run and where IP micro-mobility management would be introduced.

One of the most important requirements in wireless access networks is to provide fast and smooth handovers because of real-time applications. There are several ongoing research projects to lessen handover latency, for example, BETH [4] is an extension to the Fast Mobile IPv6 handover protocol, which reduces layer 3 latency to zero. There is also a need to lower the handover latency caused by the link layer of IEEE 802.11 [5], to make it VoIP-enabled.

As a large umbrella project, BRAIN/MIND includes the development of a number of IP-based technologies. One of them is BCMP (BRAIN Candidate Mobility Protocol) an IP micro-mobility solution. As it was mentioned earlier, on the way to voice and other real-time applications, latency is a key point. That is why we conducted an experiment-based analysis of latency caused by different kinds of handovers (HO) in a BCMP-enabled access network.

## 2 A Short Overview on Access Networks and BCMP

For a better understanding of the measurement results, a brief description of the participating entities in an AN is needed [6]. These are the following:

- *Mobile Hosts (MHs)* are computers which can move from a location to another one and from a network to another one. They have to be supported by IP-mobility enabled routers.
- *BCMP Access Routers (ARs)* are situated at the border of the AN and offer IP-connectivity to the MHs. They act as the default router to the served MHs.
- *Anchor Points (ANPs)* are located inside the AN at selected positions. They own and allocate IP addresses, authenticate users, maintain user records and tunnel packets towards MHs.
- *Access Network Gateways (ANGs)* form an explicit boundary of the AN. They work as standard border routers, so they do not need to implement mobility functions.
- *Internal Routers (IRs)* are supporting routers between an ANP and ARs.

Mobility management in the access network is considered as a single problem in most cases, but the BRAIN concept treats it as several separate issues. According to this idea there are three main responsibilities of an IP-mobility solution.

*Packet forwarding and Path Updates:* this refers to the mechanism for installing information in the interior of the AN so that packets can be successfully delivered to the MH at its new AR. It has to be well scalable (to support large networks), robust (to have a quick recovery process from failures) and it should allow multiple gateways (for improved scalability and reliability).

*Handover Management:* this refers to the impact of handovers on the MH. It deals with the local signalling involving the MH and

* **Gergely Biczók, Kristóf Fodor, Balázs Kovács**
High Speed Networks Laboratory, Department of Telecommunications and Mediainformatics, Budapest University of Technology and Economics,
E-mail: biczok@tmit.bme.hu

the ARs to facilitate re-attachment to a new AR. The primary goal here is to minimize packet loss and delay during a handover.

*Support for Idle Mobile Hosts:* an idle mobile host (i.e. one not actively involved in data transmission) can lessen its signalling messages over the air and save on its terminal power. Its location is tracked through a combination of paging and location updates, which reduces router states in the AN.

From the article's point, the most interesting one among these functions is handover management. BCMP supports two basic kinds of handoffs [2].

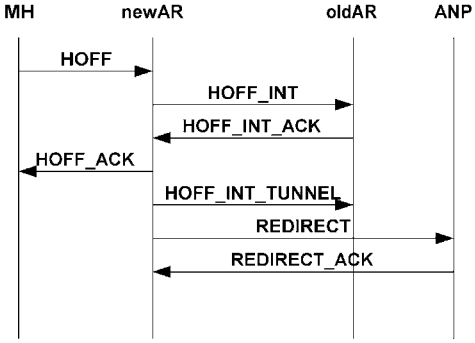


*Fig. 1 Non-planned handover*

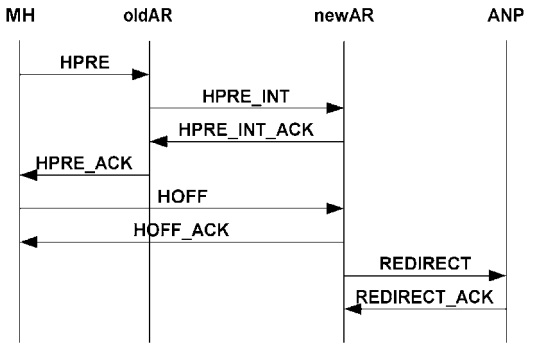


*Fig. 2 Planned handover*

*Regular handoff (non-planned):* if the MH wants to hand off to a new AR, but it has no contact to its current AR, then the procedure that can be seen in Fig. 1 takes place.

*Prepared handoff (planned):* this handoff occurs if the MH knows in advance which AR it is moving to, and it is still in contact with its current AR. In this case, first, the new AR processes the context data sent by the old AR, and if the new AR has sufficient resources, then a temporary tunnel is constructed by the old AR towards the new AR, which stores the incoming packets in its buffer. After that, the process is quite similar to the one in the previous case (Fig. 2).

As it can be expected, the prepared handoff has better performance in the field of packet loss, but latency – which is a key factor in real-time applications – is lower at non-planned handovers.

## 3. Design of the Experiment

The experiment was done in two phases at the BCMP testbed of the High Speed Networks Laboratory (HSNLab) at the Department of Telecommunication and Telematics, Budapest University of Technology and Economics. At the first stage, the network consisted of an ANG, an ANP, an IR and two ARs. The ARs' configuration was: Pentium 133Mhz processor, 32 MB of RAM, but AR2 had 64 MB. The ANG was also built upon P133 with 32 MB RAM. The IR and the ANP had an AMD Duron 700Mhz processor with 128MB RAM. The AN was linked with 100Mbit/s Ethernet connections. The wireless interface of the ARs and the MH was type 802.11b, up to 11Mbit/s maximum throughput. For the MH we used a notebook with Pentium III 800 MHz processor and 128MB RAM. All of the computers were equipped with the same Linux distribution and kernel.

The ARs were quite close to each other so a program initiated the different types of handovers. The test bed used MAC filtering which disables packets arriving from the old AR of a MH. The experiment was logged on the MH.

During our experiment we measured packet inter-arrival times to analyze handover outage effects. We used two methods: `tcpdump` and an own test program. These programs let us show both the low and the user level handover outage impacts.

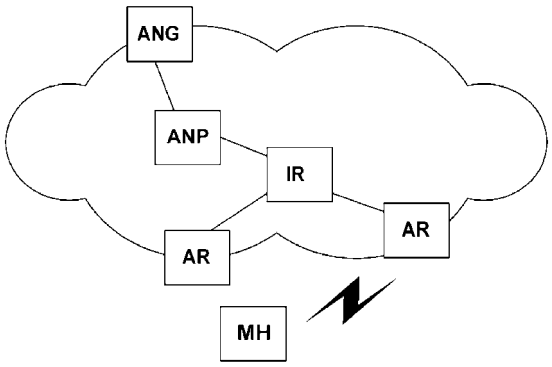


*Fig. 3 Topology of the test bed*

Our program consists of a packet sender and a packet receiver. The packet sender emits 65-byte-long UDP packets at a defined rate. We used the UDP transport protocol to avoid TCP's traffic control mechanisms. The receiver logs the sequence number of the packet arrived, the inter-arrival times, packet loss and if there was exchange in the packet sequence.

At the second stage, we had an opportunity to use a test bed having more powerful machines. All the fixed computers (ANG, ANP, ARs) had AMD Athlon 1800+ and 512MB of system memory,

the MH was a notebook equipped with a 1800 MHz Pentium 4-M processor and 256 MB RAM.

## 4. Stage 1: Results and Analysis

As it was mentioned earlier, our measurements were based on two kinds of handovers. Fig. 4 shows the planned handover latencies. We can see two mean values changing (60ms and 100ms). This is due to the different AR hardware configuration. If we do not take this into consideration we can say that the outage time caused by handovers is quite deterministic. In Fig. 5, it can be seen that the packet-sending interval is 10 ms (as we set it), the handover outage time – which includes the creation of the tunnel as well – hits nearly 60ms, but after the preparation phase the queued packets are re-sent towards the MH through the tunnel at maximum performance. After the "equalization" of the impact of the delayed packet, arriving intervals are set back to normal. The results of the measurement show that packet loss is close to zero in the case of planned handovers, except for very high sending rates. Exchanges in the packet sequence are also more common at smaller inter-departure times.

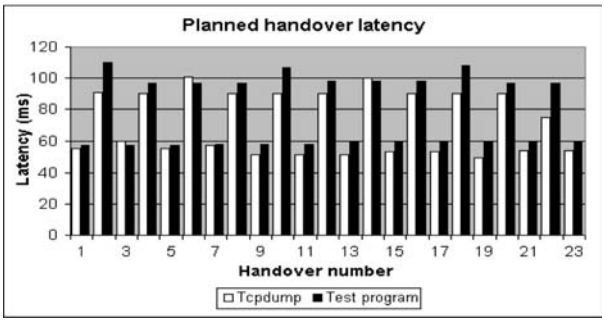


*Fig. 4 Planned HO latency*

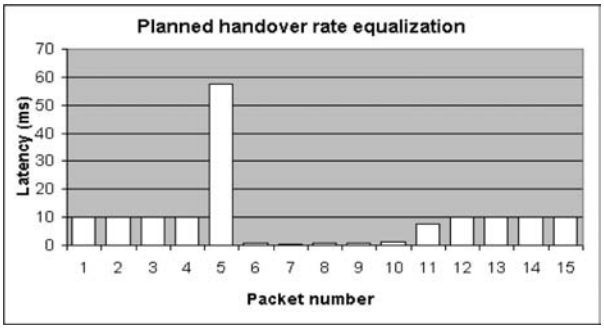


*Fig. 5 Planned HO rate equalization*

In the case of non-planned handovers, outage times are a little bit lower due to a lack of the preparation phase and the construction of a temporary tunnel, but accordingly, it has disadvantages in the quality of transmission. We can see handover latency values, oscillating between 60 and 75 ms (Fig. 6), instead of the 80 ms average of a planned handover. However, upon inter-arrival times caused by non-planned HOs, we cannot draw the interfere that for how long exactly the HOs last. In order to do that, checking packet types in `tcpdump` output are necessary. Fig. 7 shows the time values elapsed from the HOFF message to the HOFF_ACK. (In the planned case, latency and real HO duration are fairly equal.) In the non-planned case the presence of packet loss is quite stationary and changes in the packet sequence are more frequent than in the planned case.

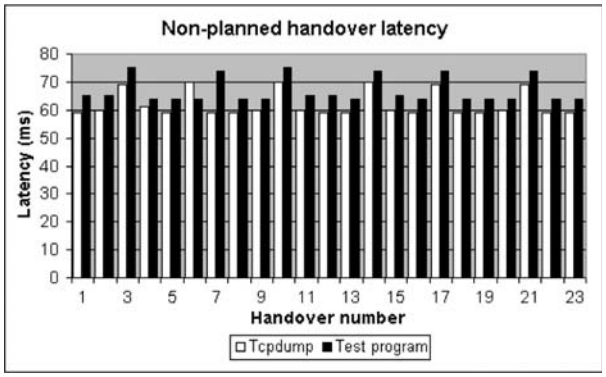


*Fig. 6 Non-planned HO latency*

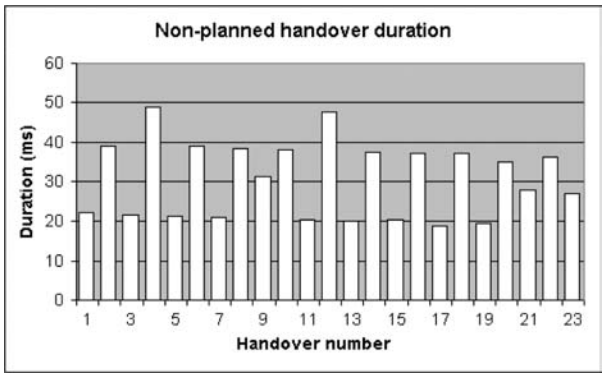


*Fig. 7 Exact duration of non-planned HO*

## 5. Stage 2: Results and Analysis

The second batch of measurements was conducted in order to observe if serious hardware upgrades could result in a significant drop of handover latency values. Meanwhile, a new measurement technique was designed to achieve better efficiency. As we knew the frequency of handovers and the packet-sending interval in advance, we could well localize the first arriving data packet in the data flow after a handover. In this way, we do not take "pseudo-handovers" into consideration (when packets are delayed due to some other reason). This method enhances the quality of the experiment. Since the aim of the second stage was to show the difference in latencies caused by new hardware, only handover outage times were logged with `tcpdump`. A packet is sent every 10 ms, and handovers are performed with a period of 2 seconds (as in the first stage).

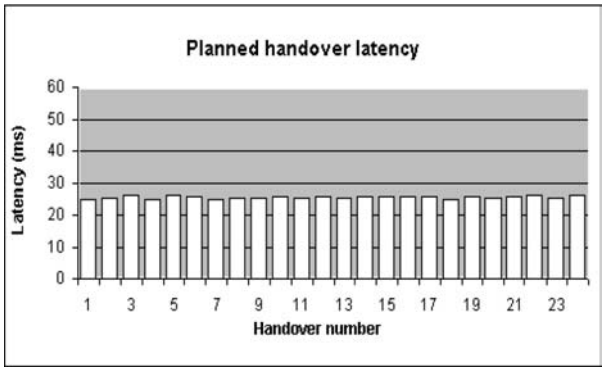


*Fig. 8 Planned HO latency (Stage 2)*

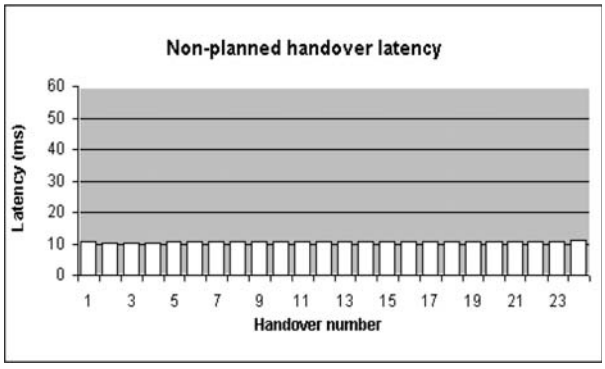


*Fig. 9 Non-planned HO latency (Stage 2)*

Fig. 8 shows planned handover latency values. As it follows from the upgraded hardware resources, values are around 25 ms: a significant reduction occurred (see Fig. 4 for comparison). As we expected, BCMP performed even better at the second stage.

There is some improvement in the case of non-planned handovers, as well (Fig. 9). The average latency is around 10.7 ms, which is only 0.7 ms more than the normal packet inter-arrival time (i.e. without switching Access Routers). Although non-planned handover latencies are smaller than that of planned handover, packet loss may occur. For this very reason, planned handover is preferred, since its performance is more than enough for real-life applications, such as packet-switched voice data or streaming video.

## 6. Conclusion and Future Work

It can be recognized that more powerful hardware has an advantageous effect on BCMP handover duration and data outage times. This explains the variation of values in the diagrams. Fast and smooth handovers are crucial for ensuring micro-mobility, while transceiving e.g. packet-switched voice data (a maximum delay of 50 ms is acceptable). According to the results, it seems that with the support of adequate hardware infrastructure BCMP is able to make the mobile hosts capable of sending and receiving real-time data. In the future, we plan to examine more complex access networks, which are equipped with more access routers, furthermore, to investigate the effects of simultaneous handovers caused by the presence of multiple mobile hosts.

## References

[1] BRAIN HOME PAGE: *www.ist-brain.org*
[2] IST MIND: *Core Report*, November 2002
[3] MIND HOME PAGE: *www.ist-mind.org*
[4] KEMPF, J. et al.: *Bidirectional Edge Tunnel Handover for IPv6,* Internet Draft, September 2001.
[5] MISHRA, A., SHIN, M., ARBAUGH, W.: *An Empirical Analysis of the IEEE 802.11 MAC Layer Handoff Process,* ACM CCR, 2002.
[6] KESZEI, CS., GEORGANOPOULOS, N., TURÁNYI, Z., VALKÓ, A.: *Evaluation of the BRAIN Candidate Mobility Management Protocol,* IST Global Summit, Barcelona, 2001.

https://doi.org/10.26552/com.C.2004.1.38-41

komunikácie
COMMUNICATIONS

Martin Kuchař – Pavel Brandštetter *

# DEVELOPMENT AND DSP IMPLEMENTATION OF ANN-BASED VPWM IN A VOLTAGE SOURCE INVERTER

*This paper deals with development, simulation and DSP implementation of space vector modulator based on artificial neural network. The modulator is designed for a voltage source inverter utilization. In the contribution an explanation of presented ANN-based VSI-VPWM is described. Main features and advantages of the used algorithm are summarized too. The entire AC electrical drive consists of a frequency converter, induction motor and microprocessor control system. In the paper a description of the control system with TMS 320C40 DSP is also given. A very important part of the development is simulation, because it is necessary to verify rightness of the algorithm. The entire drive was simulated in the program Matlab with Simulink toolbox.*

***Keywords:*** *DSP, Artificial Neural Network (ANN), Vector Pulse-Width Modulation (VPWM), Voltage Source Inverter (VSI), Induction motor, Simulation*

## 1. Introduction

Induction motors are often a preferred choice in variable-speed drive applications. The PWM inverters are most commonly applied in such induction motor drives. The PWM voltage source inverter, based on IGBTs, has gained a dominant position in AC drives market due to its ease of application, good power factor and potential to provide good dynamic performance.

Pulse-width modulation (PWM) has been one of the most intensively studied areas of power electronics in the past three decades. The fast development of the switching capabilities of power semiconductor switches requires faster, more accurate and simpler modulation techniques. Although the digital implementation of a space-vector modulator is simple, the required computations for the pulse times and the corresponding execution times limit the minimum sampling time. However, to reduce hardware and software complexity, to increase the accuracy, and to reduce the required computation times, it is also possible to use an ANN-based space-vector modulator, which utilizes vector classification concepts associated with competitive ANNs [1].

The on-line implementation of the conventional space-vector modulator requires that at every sampling time the sector where the space-vector reference lie must be established, and pulse times must be evaluated too. It follows that the trigonometric function sin must also be computed on-line. In one possible form of the conventional implementation, the sine function is stored in a look-up table.

However, this approach has two main disadvantages:

- Use of any look-up table requires additional memory.
- Interpolation of non-linear functions leads to poor accuracy and thus to increased harmonics in the PWM waveforms.

It is possible to use such technique where the direct computation of trigonometric functions is completely avoided. The technique is presented in the paper and it does not require a complicated computation.

## 2. Description of presented ANN-based VPWM

The space-vector modulation is basically a classification problem. Therefore, it is possible to use competitive type artificial neural network. The entire structure is shown in Fig. 1. For this purpose it is necessary to modify conventional competitive type ANN. Similarly that is a feedforward two-layer ANN and the inputs are stator reference voltages $u_{S\alpha}^*$, $u_{S\beta}^*$. This is followed by a layer of six neurons (the outputs – $n_1$, $n_2$, ... , $n_6$). These outputs correspond to the real part of the product of the reference voltage space vector $\underline{u}_1^*$ and one of the normalized nonzero switching vectors $\underline{u}_k$ ($k = 1, 2, ..., 6$; modulus is equal to 1).

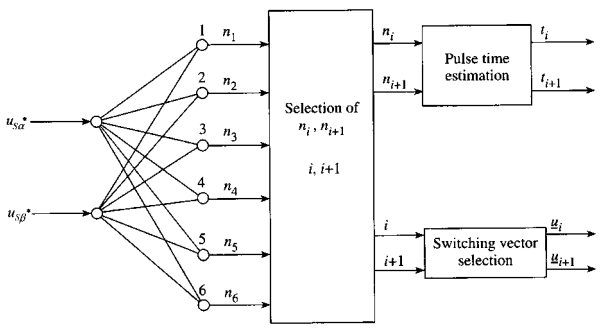


*Fig. 1 ANN-based VPWM method*

* **Ing. Martin Kuchař, Prof. Ing. Pavel Brandštetter, CSc.**
Department of Power Electronics and Electrical Drives, Faculty of Electrical Engineering and Computer Science, VŠB - Technical University of Ostrava, 17. Listopadu, 708 33 Ostrava - Poruba, Czech Republic, Tel. +420-59-6994283, E-mail: martin.kuchar@vsb.cz

Main equations leading to the final relation of the algorithm will be described here.

The non-zero switching vectors can be expressed as follows:

$$\underline{u}_{\underline{k}} = \exp[j(k-1)\pi/3] \tag{1}$$

Real parts of the products of the reference voltage space vector and one of the normalized nonzero switching vectors are as follows:

$$n_k = \mathrm{Re}(u_k\, u_S^*) = \mathrm{Re}[\exp[j(k-1)\pi/3](u_{S\alpha}^* + j\, u_{S\beta}^*)] =$$

$$= \cos[(k-1)\pi/3]u_{S\alpha}^* - \cos[(2k+1)\pi/6]u_{S\beta}^*;$$

$$\mathrm{k} = 1, 2, ..., 6 \tag{2}$$

From the relation (2) it is easy to express the weight matrix for competitive type ANN. Each neurons of ANN realises the inner product of the reference voltage vector and corresponding non-zero-switching vector.

$$\mathrm{w} = \begin{bmatrix} 1 & 0 \\ 0.5 & \sqrt{3}/2 \\ -0.5 & \sqrt{3}/2 \\ -1 & 0 \\ -0.5 & -\sqrt{3}/2 \\ 0.5 & -\sqrt{3}/2 \end{bmatrix}$$

It is clear that the presented weight matrix allows simple implementation of the ANN onto the microprocessor control system.

The pulse times can be evaluated from the largest network values in the following way.

Conventional VPWM utilizes the trigonometric function for determining right pulse times:

$$t_i = mT_s \sin(60 - \vartheta) \tag{3}$$

$$t_i + 1 = mT_s \sin\vartheta \tag{4}$$

$$t_0 = T_s - t_i - t_i + 1 \tag{5}$$

where $\vartheta$ is the angle between the reference stator voltage vector and the closest clockwise switching vector, $m$ is the modulation index and $T_s$ is the sampling period.

For the final equations of the pulse times it is necessary to use the following relations:

$$n_i = I\underline{u}_{\underline{s}}^*\, I\cos\vartheta \tag{6}$$

$$n_{i+1} = I\underline{u}_{\underline{s}}^*\, I\cos(60 - \vartheta) \tag{7}$$

then, by considering the trigonometric relationships

$$\cos\vartheta = \left[\frac{2}{\sqrt{3}}\right]\left[\sin\frac{(60-\vartheta)}{2} + \sin\vartheta\right] \tag{8}$$

$$\cos(60-\vartheta) = \left[\frac{2}{\sqrt{3}}\right]\left[\sin(60-\vartheta) + \sin\frac{\vartheta}{2}\right] \tag{9}$$

and also equations (6), (7), (8), (9), it possible to obtain the following pulse times equations from the relations (3), (4):

$$t_i = (2T_s/3)(2n_i - n_{i+1}) \tag{10}$$

$$t_{i+1} = (2T_s/3)(2n_{i+1} - n_i) \tag{11}$$

The pulse time for zero switching vector can be obtained in the same way as in the conventional method:

$$t_0 = T_s - t_i - t_{i+1} \tag{12}$$

It can be seen that the pulse times are estimated simply from the largest net values.

To summarise the important steps of the mentioned ANN-based VPWM:

1. Competitive type ANN evaluates the inner product of vectors $\underline{u}_{\underline{s}}^*$ and $\underline{u}_{\underline{k}}$, ($k = 1, 2, ..., 6$).
2. Determination of the two largest values $n_i$, $n_{i+1}$ and corresponding indexes $i$, $i+1$.
3. The pulse times for adjacent switching space vectors are obtained by simple equations using $n_i$, $n_{i+1}$.
4. The switching combinations $\underline{u}_i$, $\underline{u}_{i+1}$ are selected according to the values $i$ and $i+1$.

## 3. Simulation

The induction motor drive was simulated in the program MATLAB-Simulink. The simulation stage was important to verify rightness of the presented algorithm and to find out behaviour of the drive. The simulation results have confirmed our assumptions, then the algorithm has been implemented into DSP. Stator voltage and current of the induction motor working in steady state are shown in Fig. 2.

## 4. Induction motor drive implementation

The mentioned algorithm was implemented into a digital signal processor TMS320C40. The processor works with 32-bit data in floating-point arithmetic. To test the method a wound-rotor induction machine 2,7 kW supplied by a frequency converter was used. The entire control system is shown in Fig. 3., and it was realized at the Technical University of Ostrava (Czech Republic).

The core of the system is the mentioned DSP, which utilizes additional information from other peripherals – Analog to Digital and Digital to analog converter (A/D, D/A), Block of Switching Pulses (BSP), Block of Evaluation of Rotor Position (BEPR) pro-

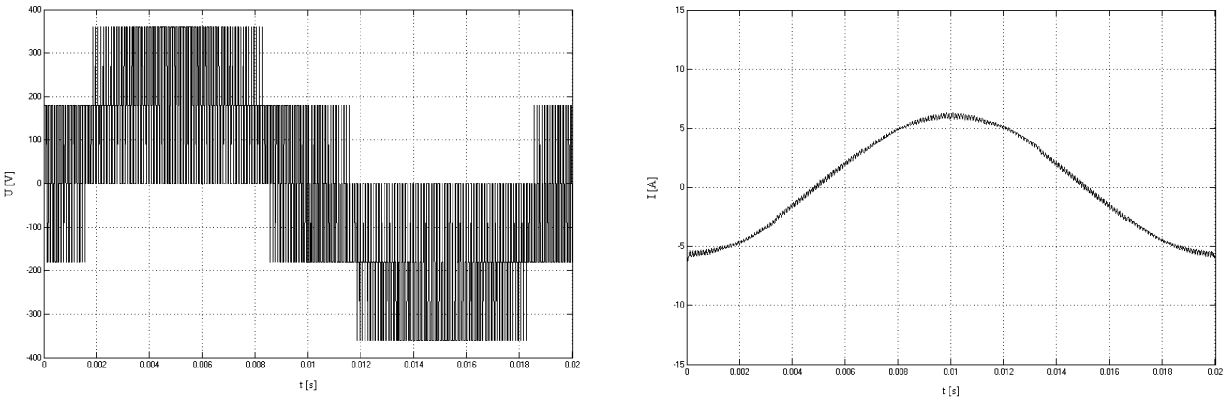


*Fig. 2. Stator voltage and corresponding stator current while the motor is working in steady state ($f_s$ = 10 kHz, $f_{Uout}$ = 50 Hz (MATLAB simulation))*

cessing the signals from the incremental encoder. BSP is needful for right communication with a modern IGBT frequency converter (TFC). A Block of Isolated Amplifiers (BIA) is important to get signals of stator currents, which are monitored by means of LEM current sensors.

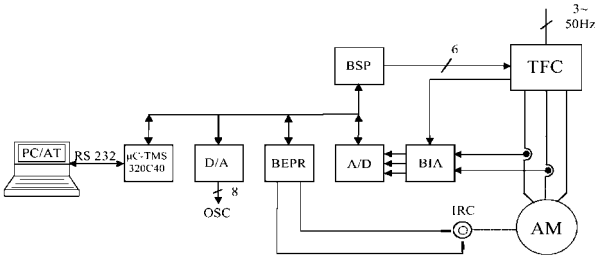


*Fig. 3. DSP control system*

## 5. Experimental results

In the chapter measured stator voltage and ANN-based vector pulse width modulator controls current of the motor will be presented. You can then set the desired magnitude of output voltage and the desired output voltage frequency. The presented results were obtained by U/f = const control. The switching strategy optimisation was implemented in the algorithm. The method is based on choosing the right switching vectors in the corresponding instants. After the zero switching vector the algorithm chooses one of two selected non-zero switching vectors by the following condition: the mentioned right vector has to cause minimum changes of IGBT switches in the frequency converter. This algorithm allows reduction of switches changes per one vector from 1.33 to 1. It is clear that it reduces the switching losses of the converter. This application was used as the function block in vector control of an induction motor.

## 6. Conclusions

Conventional vector pulse-width modulation requires on-line computations with trigonometric functions. It causes the disadvantages mentioned at the beginning of the paper. It is possible to avoid the problems by means of the presented algorithm. The method utilizes a competitive artificial neural network and it works with

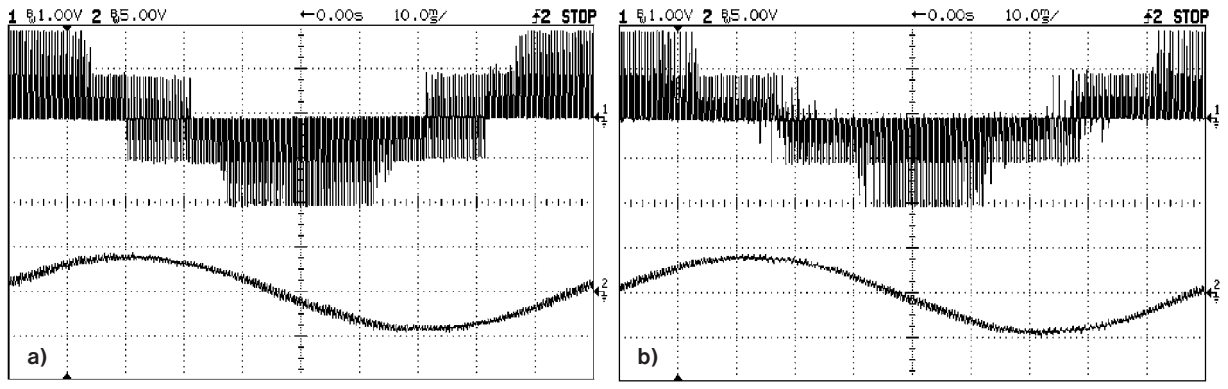


*Figure 4. Stator voltage and corresponding stator current while the motor is working in steady state, ch1: $u_s = f(t)$, ch2: $i_s = f(t)$, $V_{DClink}$ = 300V, $f_s$ = 2 kHz, $f_{Uout}$ = 10Hz, $m_u$ = 100 V/V, $m_i$ = 1,5 A/V a) not optimised switching strategy, b) optimised switching strategy*

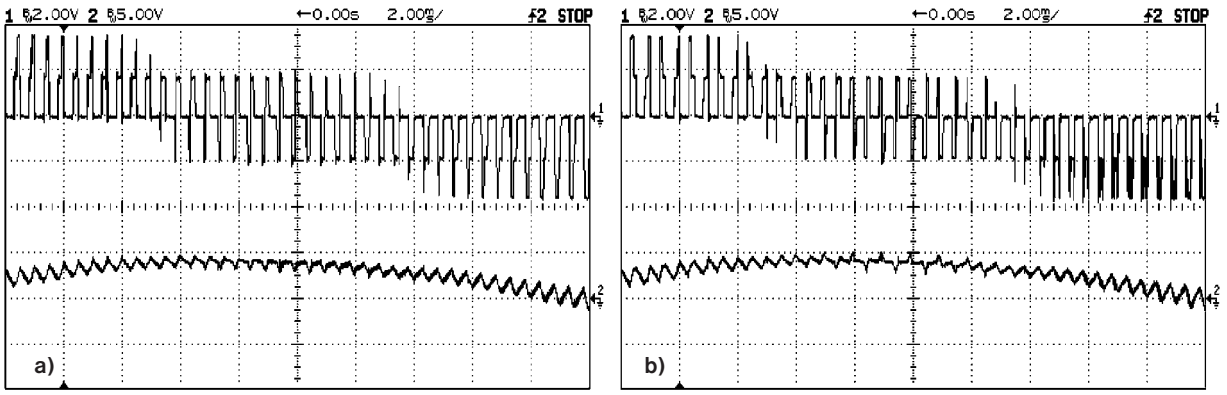


*Figure 5. Stator voltage and corresponding stator current while the motor is working in steady state, ch1: $u_s = f(t)$, ch2: $i_s = f(t)$, $V_{DClink} = 540$ V, $f_s = 2$ kHz, $f_{Uout} = 20$ Hz, $m_u = 100$ V/V, $m_i = 1{,}5$ A/V a) not optimised switching strategy, b) optimised switching strategy*

simple mathematical operations. It is clear that this type of VPWM is very simple to be implemented into microprocessor systems. Rightness of the algorithm has been verified by the simulations, then the method including the switching strategy optimisation was implemented into DSP powered by Texas Instruments. The mentioned strategy reduces switching losses of the converter. In the end, VPWM was integrated into vector control of an induction motor and all experimental results were presented at the EPE 2003 conference.

**Acknowledgement**

In the paper there are results of the project LN00B029, which was supported by The Ministry of Education of the Czech Republic.

## References

[1] VAS, P.: *Artificial-Intelligence-Based Electrical Machines and Drives,* Oxford Science Publication, 1999, ISBN 0 19 859397 X
[2] BRANDSTETTER, P.: *AC regulation drives - Modern control methods,* VSB-TU Ostrava 1999, ISBN 80-7078-668-X
[3] NEBORAK, I.: *Modelling and simulation of electrical regulation drives,* VSB-TU Ostrava 2002, ISBN 80-248-0083-7
[4] TEXAS INSTRUMENTS: *TMS 320C40 Users Guide,* Digital Signal Processing Product, 1995
[5] BRANDSTETTER, P., KUCHAR, M., PALACKY, P., VINKLAREK, D.: *Sensorless Induction Motor Drive with Vector Control,* EPE-PEMC 2002, Dubrovnik 2002
[6] DEMUTH, H., BEALE, M.: *Neural Network Toolbox,* for use with Matlab, ver. 4.
[7] FEDOR, P., PERDUKOVA, D., TIMKO, J.: *Study of Controlled Structure Properties with Reference Model,* Acta Technica, ISSN 0001-7043, CSAV 46, 2001.

https://doi.org/10.26552/com.C.2004.1.42-45

komunikácie
COMMUNICATIONS

Libor Štěpanec – Pavel Brandštetter *

# DSP IMPLEMENTATION AND SIMULATION OF IM DRIVE USING FUZZY LOGIC

*This paper deals with vector-controlled induction motor drive, which uses fuzzy logic as a part of artificial intelligence. There are three phases: development, simulation and DSP implementation, which are discussed in this paper. In the first part of the paper fuzzy logic and development of the given problem are described. Next, there is a description of the used control structure. Important simulations were realised, which confirm the rightness of proposed structure and good behaviour of developed fuzzy controller. The simulation results are also given. In the end part of the paper, there are presented a control system with DSP TMS 320C40 and experimental results. There are also presented advantages of fuzzy logic and main features of used method are summarised too.*

***Keywords:*** *Fuzzy logic, Vector Control, Induction Motor, DSP, Simulation*

## 1. Introduction

Variable-speed drives are being continually innovated. Their development is characterised by process made in various areas including power and microelectronics, control systems etc. The introduction of various vector-controlled drives has allowed the dynamic performance of AC drives to match or sometimes even to surpass that of the DC drive. Vector-controlled drives provide high-dynamic performance and they are used in many industrial applications. Induction motors are often a preferred choice in variable-speed drive applications. Nowadays low cost microprocessors enable the development of cost effective digital drives and the widespread availability of DSPs enable the development of a large variety of drives with advanced features and, of course, use of new control methods. The applications of artificial intelligence (AI) in electrical drives can lead to improved performance, enhanced tuning and adaptive capabilities. There are further possibilities for much wider range of AI-based applications in variable-speed AC and DC drives [1].

Considerable research has been performed in the field of AI. Recent trends and advancements in this field have stimulated the development of various systems for electrical machine and drive application. Fuzzy logic control is receiving great interest worldwide. The essential part of fuzzy logic controller is a set of linguistic control rules related by the dual concepts of fuzzy implication and compositional rule of inference. Thus fuzzy logic control provides an algorithm into an automatic control strategy. Experience shows that fuzzy logic control may yield results superior to those using conventional control algorithms. A main advantage of the use of fuzzy logic is that fuzzy logic controllers can work well without having to construct any mathematical model of the process (or plant). Their application can also lead to reduced development times. In general, the application of artificial intelligence, including fuzzy logic, in drives can lead to increased performance and robustness to parameter and load variations.

## 2. Structure of vector controlled induction motor

For vectors control it is used indirect orientation on magnetic rotor flux (indirect FOC). In the paper a speed regulation of the drive is discussed. Controller uses Mamdani type of fuzzy logic (fuzzy logic controller FLC). The overall structure of the system is shown in Fig. 1. The system contains a voltage-source inverter (TFC) with PWM, induction motor, fuzzy logic controller for speed, classical PI controllers and blocks for processing signals. As shown in Fig. 1, in the induction motor (IM) drive there are four controllers: controller 1 is the speed controller, controller 2 is the torque producing stator current controller, controller 3 is the rotor magnetizing current (rotor flux) controller and controller 4 is the flux producing stator current controller.

Voltage signals of measured stator currents are transformed from the stationary reference frame [$\alpha$, $\beta$] into the reference frame oriented on the rotor flux linkage space vector [x,y], which is done in the Block of Vector Shift 2 (BVS2). Outputs of this block are real stator currents $i_{1x}$, $i_{1y}$, which are feedback signals to the current controllers $R_{i1x}$, $R_{i1y}$. The decoupling rotation voltage components $u_{xe}$, $u_{ye}$, which are evaluated in the Block of Decoupling Circuit (BDC), are added to the outputs of the mentioned controllers. The inverse shift (from the reference frame oriented on the rotor flux linkage space vector to the stationary reference frame) is done in the Block of Vector Shift 1 (BVS1). It is necessary to determine the oriented angle $\gamma$, which is used in BVS1, BVS2. The angle is evaluated in the Block of Evaluation of Oriented Quantities (BEOQ). Rotor position (angle $\varepsilon$) is obtained by means of a speed sensor. BEOQ is based on the so-called current

* **Ing. Libor Štěpanec, Prof. Ing. Pavel Brandštetter, CSc.,**
Department of Power Electronics and Electric Drives, Faculty of Electrical Engineering and Computer Science, VŠB - Technical University of Ostrava, 17. Listopadu 15, 708 33 Ostrava - Poruba, Czech Republic, Tel. +420-59-6994283, E-mail libor.stepanec@vsb.cz

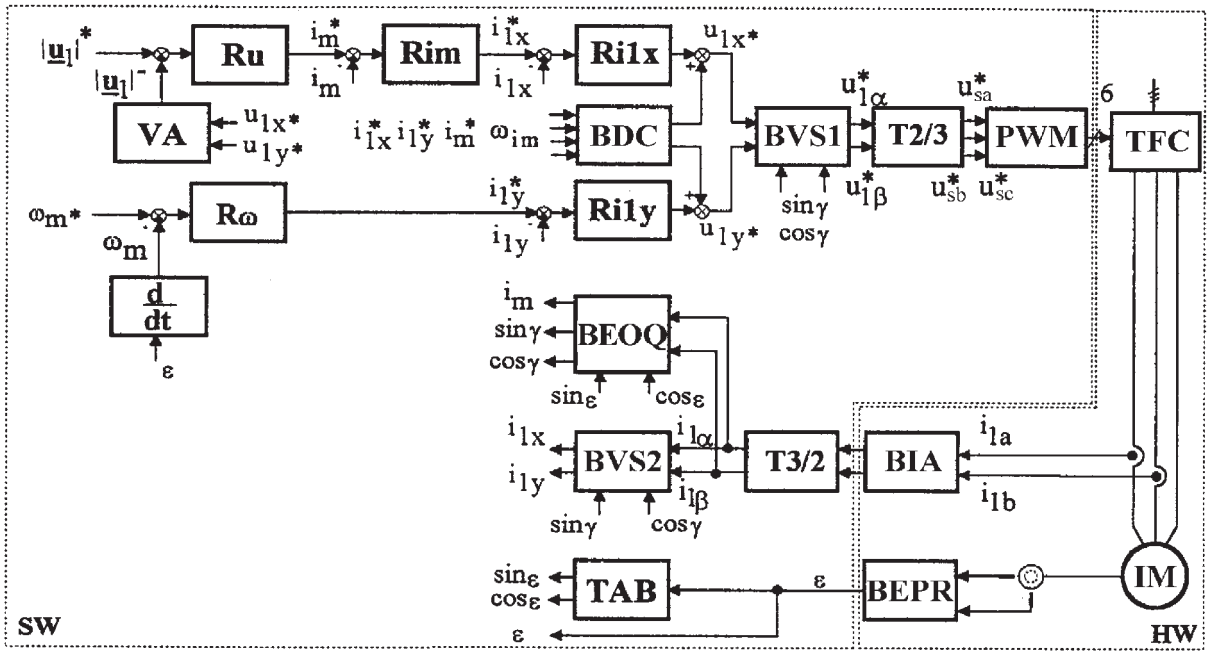


*Fig. 1 Structure of vector controlled induction motor drive*

model. The controller $R_\omega$ processes a control error between the measured $\omega_m$ and reference value $\omega_m$* of mechanical speed.

## 3. Brief description of presented fuzzy controller

There are many types of fuzzy logic controllers (FLC), but now the classical structure of Mamdani type of fuzzy logic controller is used. It should be noted that, in general, this type of fuzzy logic controller contains four main parts: fuzzifier, knowledge base (rule base + data base), inference engine and defuzzifier (Fig. 2). The real FLC consists of pre-processing (matching of input values) and post-processing, which is very important for tuning FLC.

Mentioned facts are used for the fuzzy logic controller in program Matlab – Simulink and the implementation to DSP.

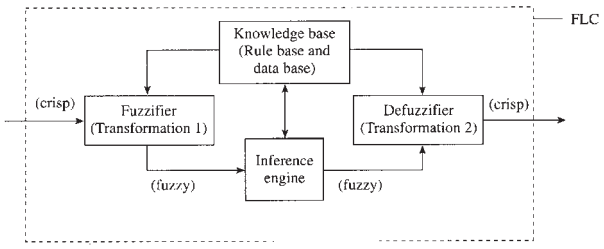


*Fig. 2 Block scheme of fuzzy controller*

In this case the fuzzy logic controller is used as an analogy to PI-type controller, but it is possible to set its non-linear behaviour by means of base rules in the other side of a classical PI controller. A fuzzy controller is an expert system where a set of base rules is based on knowledge and experience of a system expert.

The result of the proposed fuzzy controller is control surface shown in Fig. 3, which is a more easily implemented, for example, as a table to the microcontroller. Figure 3 shows the highly non-linear three-dimensional control profile. The control profile of the PI controller is simpler due to its linear nature.

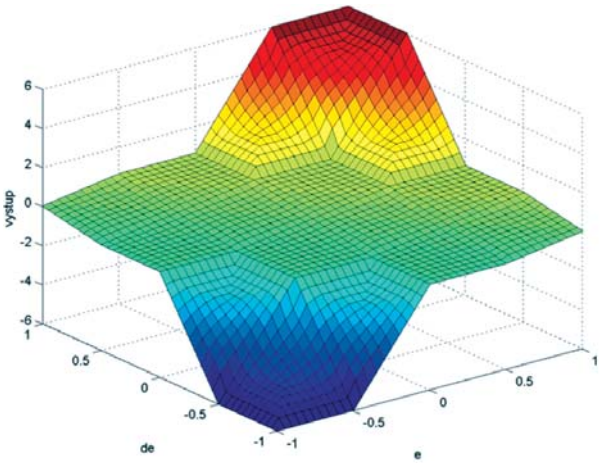


*Fig. 3 Non-linear three-dimensional control profile*

## 4. DSP implementation

The DSP controlled vector drive contains single fuzzy logic controller, which is the speed controller. The DSP (digital signal processor) used is the Texas Instruments TMS320C40. The

processor works with 32-bit data in floating-point arithmetic and provides high computing power for presented control. Instruction cycle interval is 50 ns, while most instructions are performed in one machine cycle. The overall structure of the system is shown in Fig. 4 and was realised at the Technical University of Ostrava (Czech Republic). The system contains a voltage-source inverter, a 2,7 kW wound-rotor induction motor, analogue circuits for the voltage and current transformations, a TMS320C40 DSP system board and interface boards. There are A/D converter (12-bit includes four-channel), D/A converter with 8 channels, Block of Switching Pulses (BSP), Block of Evaluation of Rotor Position (BEPR), which process signals from the incremental encoder (1024 pulses per rotation with two shifted outputs => overall 4096 pulses/rotation). BSP is needful for right communication with modern IGBT frequency converter (TFC). The Block of Isolated Amplifiers (BIA) is important to get signals of stator currents, which are sensed by means of LEM current sensors. Communication between DSP and PC is ensured by serial interface.

The DSP software contains the algorithms for the fuzzy controllers, vector control and control of inverter. During operation up to 8 inner drive quantities can be simultaneously shown by a D/A converter.

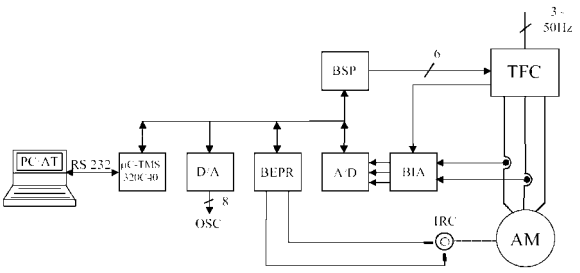


*Fig. 4 Entire control system*

## 5. Simulation and experimental results

Based on the description of the presented FLC and structure of vector controlled induction motor, the fuzzy logic controller and the whole structure of the vector controlled IM in the program Matlab-Simulink were created. The conventional PI controller is replaced by a fuzzy controller, where it is possible to set its non-linear behaviour by means of rule base in the other side of a classical PI controller. A fuzzy controller is an expert system, where the set of rule base is based on knowledge and experience of the system expert.

An extensive range of digital simulations has been performed to obtain the appropriate values of scaling factors, membership functions and rule base. Two types of simulation have been performed, the former uses direct calculation and the latter uses look-up tables. The execution time of the table lookup form was found to be approximately half of the direct form. In this way it was also possible to verify the suitability of the look-up table based on the FLC approach in the vector drive. The simulation stage was made to verify fuzzy controller features and to get information about behaviour of the drive. The used scheme of FLC is shown in Fig. 5. This stage was followed by the real-time implementation of the fuzzy logic controller considered. Entire control of the drive was implemented onto DSP.

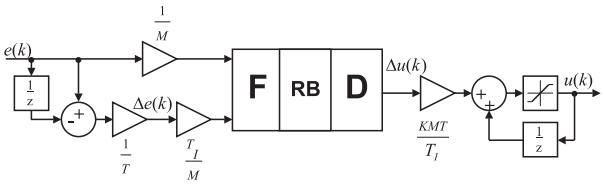


*Fig. 5 Structure of FLC in program Matlab - Simulink*

In real implementation of the fuzzy controlled drive a fuzzy logic controller (speed controller) was implemented, the other controllers are classical PI controllers. Thus, in this case, the two inputs to the fuzzy speed controller are the speed error and the change of the speed error respectively.

Figures 6 to 8 show the responses of the DSP controlled drive. It can be seen from figures in the left column that the drive runs up to 300 rpm with load. In the right column the reference rotor speed is first set to zero then to 300 rpm and then to −300 rpm. In Fig. 6 the rectangular curve is the reference rotor speed, the "trapezoidal" curve is the real angular rotor speed. Torque producing stator current is shown in Fig. 7.

## 6. Conclusion

The absence of widespread industrial application of fuzzy controllers in variable-speed drives is also related to the fact that there are no straightforward procedures for the tuning of fuzzy controllers. Only a few papers discuss implementations and mainly concentrate on simulations. However, techniques for determination of classical controller can be time-consuming and fixed controllers cannot necessarily provide acceptable dynamic performance over the complete operating range of the drive. Performance will degrade mainly because of machine non-linearity, parameter variation, etc. Considerable advantage of fuzzy controller is possibility to create a suitable controller by means of base rules. As fuzzy controllers are generally non-linear system we can achieve better regulation results. Not always the use of a fuzzy controller is a better solution. It depends on the system complexity and its linearity. For a simple linear system it is not suitable to implement a fuzzy controller. As folow from the experimental results fuzzy control brings a better utilisation of the proposed vector control. Rightness of the controller has been verified by simulations, so then the fuzzy controller has been implemented into DSP powered by Texas Instruments. The dynamics of the drive is better for the proposed controller.

**Acknowledgement**

The paper is based on the results of the project LN00B029, which was supported by The Ministry of Education of the Czech Republic.

*Run-up to 300 rpm with load* *Run-up to 300 and reversation to −300 rpm without load*

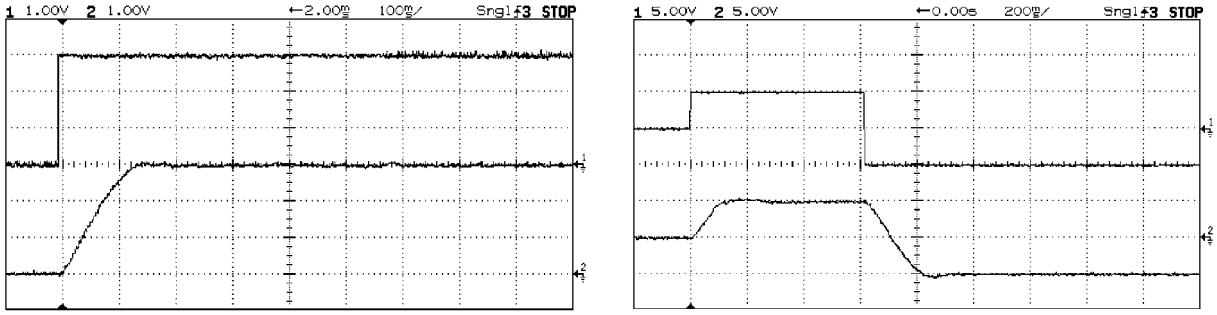


*Fig. 6 Reference and real speed (ch1: n* = f(t), ch2: n = f(t), mn = a) 100 b) 60 rpm/V)*

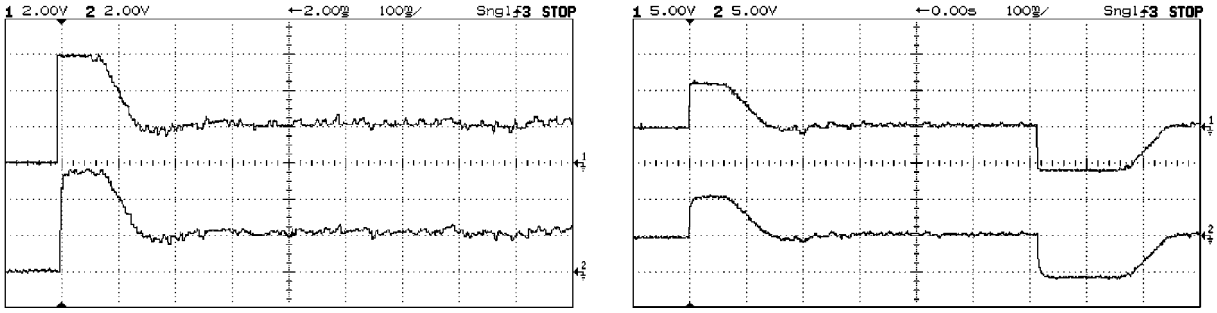


*Fig. 7 Reference and real torque producing stator current (ch1: $i_{Sy}$* = f(t), ch2: $i_{Sy}$ = f(t), $m_i$ = 1 A/V)*

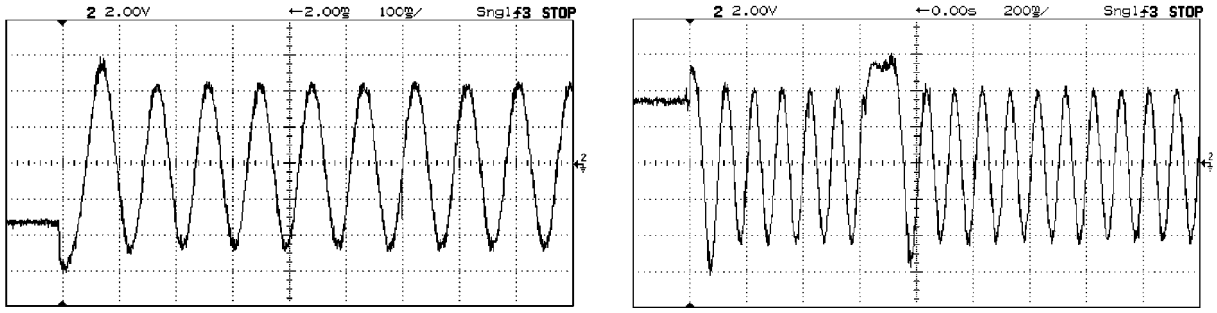


*Fig. 8 Phase stator current ($i_{Sa}$ = f(t), $m_i$ = 1,5 A/V)*

## References

[1] VAS, P.: *Artificial-Intelligence-Based Electrical Machines and Drives.* Oxford Science Publication, 1999. ISBN 0 19 859397 X.
[2] BRANDSTETTER, P.: *A.C. Control Drives - Modern Control Methods.* VŠB-Technical University of Ostrava, 1999. ISBN 80-7078-668-X.
[3] NEBORAK, I.: *Modelling and Simulation of Electrical Control Drives.* VŠB-Technical University of Ostrava, 2002. ISBN 80-248-0083-7.
[4] TEXAS INSTRUMENTS: *TMS 320C40 Users Guide.* Digital Signal Processing Product, 1995
[5] LEONHARD, W.: *Control of Electrical Drives.* Springer - Verlag Berlin, 1997. ISBN 3-540-59380-2.
[6] THE MATH WORKS: *Fuzzy Logic Toolbox for Use with Matlab,* ver. 2.
[7] FEDOR, P., PERDUKOVA, D., FEDAK V.: Reference Model Robust Control of MIMO Systems with an Incomplete Access to State Variables. *Proceedings of International Conference Motion Control for Intelligent Automation.* Vol. II, Perugia, 1992, p.183

https://doi.org/10.26552/com.C.2004.1.46-49

komunikácie
COMMUNICATIONS

Martina Blašková *

# INDIVIDUAL AND SECTIONAL COMMUNICATION SYSTEMS IN MANAGEMENT AND DEVELOPMENT OF HUMAN POTENTIAL

*The article deals with identification of communication systems existing inside the organization: individual, group and organizational. The article deals with possibility to perceive human potential management and development processes as communicational processes, it means, the processes, which we can understand through prism of communication. The quality of basic communicational skills using (active listening, assertivity, empathy and persuasion) is an important condition of permanent growth of human potential management and development system.*

***Keywords:*** *communication systems, communication, human potential, efficiency, feedback*

## 1. Introduction

Each single company and all its integral parts (individuals, groups, teams, departments, sectors) have their own communication system. This system provides immediate or mediate information and communication exchange among the participants of work and extra-work relations in a company. Whereupon it is possible to regard the company, sectional and individual communication systems, which all together form the communication platform of the internal as well as relevant external business environment.

## 2. Specification of Communication Systems

*Communication system of a company* presents a complex system inside a company, used communication channels, forms, sources, "dictionaries", communication situations and resources, reciprocal sharing, understanding and feedback and implanted visions and expectations of all communicating participants, now members of a company. It can be pointed out that it is the widest form of the sectional communication system, while the setting of the communication in this case, is the whole company. It involves and reflects all the individual and sectional communication systems that exist in the business environment. Despite the fact that company communication system retroacts with the sectional and individual communication systems, which are its immanent parts, it also aims at correct alignment of progress and requisite influence and adaptation to the context of a real and current company situation.

*Sectional communication systems* in a narrow sense present communication systems of offices, departments, sectors, sections etc. In a larger view, the communication system of the whole hierarchic level of the company management can be taken into the consideration, e.g. communicational system of the lowest, middle or the highest level of management. All the sectional communication systems imply and reflect the individual communication systems. However, compared to simple "sum" of individual communication systems, this system is complicated as well as enriched by necessary integration of group values, norms, habits, visions, preferred communication channels and dictionaries and also by obstacles and barriers occurring in effective communication in a particular environment. From this point of view, sectional communication systems are able to influence in negative and positive sense, both individual communication systems as well as the company one.

*Individual communication systems* present subjectively built and alleged patterns and forms of communication of an individual (manager or employee) with other individuals or groups inside or outside of the company. Each of these individual systems is in a great part formed by a personality of a particular communicant. It is formed by lifelong working and extra-working experiences, feedback from the others, subjective appraisal of reaction accuracy of a particular individual in communication situations (pleasant, usual or confrontational). It is marked by achieved qualification, pursuit of permanent improvements, aspirations and ambitions of an individual, as well as by influence of the other individual and sectional communication systems.

Moreover, it is usually heavily marked and it is characterised by the occurrence of many communicative errors. Out of these inadequacies the most common are inappropriate formulation of particular information, selective perception, drawing of early and incorrect conclusions, filtration of information, incapability to choose a reliable source of information, inability to ask for, accept and provide a feedback, information overload etc. As these communication faults occur quite often and can have large-scale consequences in a field of possible destruction of individual, sectional and business communication systems, it is necessary to pay an appropriate attention and seriousness to their identification and elimination.

* **Ing. Martina Blašková, PhD.**
University of Žilina, Faculty of Management Science and Informatics, Tel. +421-41-5134455, E-mail: blaskova@fria.fri.utc.sk

## 3. Management and Development of Human Potential by Prism of Communication

Management and development of a human potential is represented by systematically and meaningfully realised processes of judgment and strategically directed level raising of motivation, skills and knowledge of all employees and management personnel in a company. All the processes connected with the human potential can be viewed through the prism of continuous and open communication led in internal and external business environment. It means *that the processes of work with people (including processes of strategic preparation of suitable conditions) can be considered as communication processes* (scheme 1).

For example, the vision and mission of a company motivate and communicate the future conceptions and present the purpose of a company existence. To have a clear vision and strategy is insufficient. It is necessary to overcommunicate it and clearly understand it in an entire company [3]. Culture and philosophy represents the verbalisation and reflection of values, norms, persuasion, priorities and principles of company manners in a relation to employees, customers, own development, public and nature. Strategic objectives of development of the human potential constitute desired conditions and wanted results in this field. Personal strategy and politics imply trajectories, constraints, sources, principles, practices and effective realisation of particular personal processes.

Work analysis is communication about difficulty, responsibility, merits and character of a particular working place – e.g. by the use of questionnaires, interviews, observations (acquisition of verbal manners and monitoring of non-verbal manners of employees as well as management personnel in their job performance). Acquisition, i.e. process of gaining and selection, means representation of requirements and attraction of both communication sides – company representatives as well as applicants. Orientation is a communication-adaptation-socialisation process, which in full lean on preliminary, running and consecutive informative interviews. Allocation implies, on the basis of communication of visions and real output as well as company potentials, movement of employees in a company. Yet, always with an essential and early notice of future impacts on employees and managers.

In an evaluation process of a complex working output, employees expect an opportunity to confront their own visions about themselves and their potentials with the visions of their superior and according to that they orientate their own working and qualifying endeavour. They also expect to gain the feedback, i.e. information about their job performance. All the same they need to have a space to submit their own conception of remuneration [1]. Concurrently, managers in a position of evaluators need a feedback about the efficiency of their motivation-communicational endeavour exerted on their subordinate colleagues.

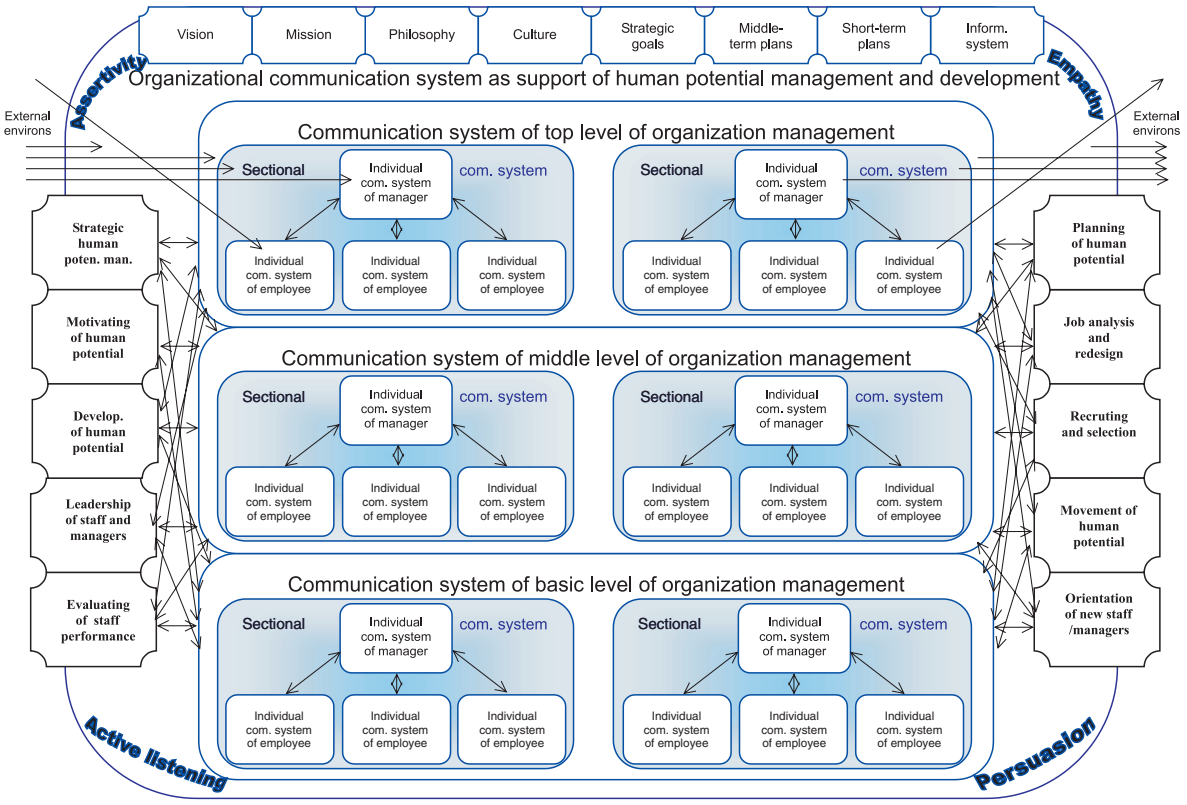


*Scheme 1 Communication systems and human potential management and development system*

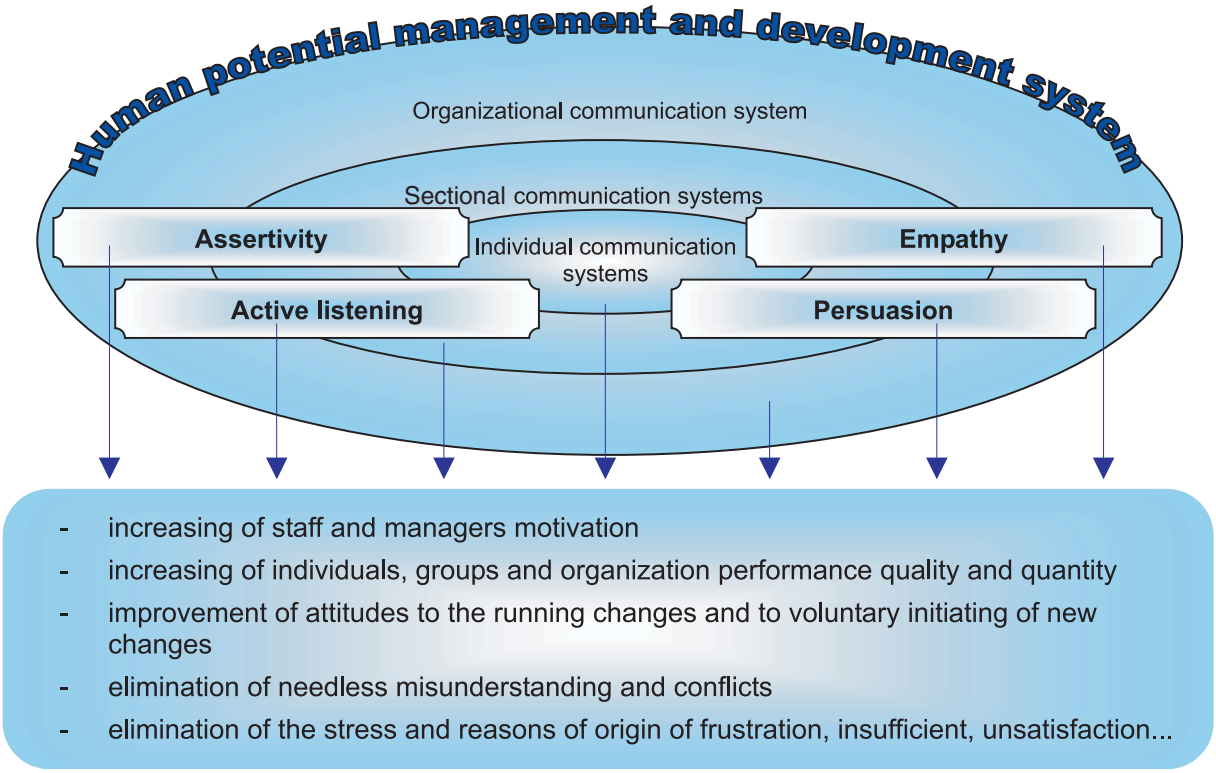


*Scheme 2 Positive consequences of communicational skills implying in organization*

Leadership is based on communication and direction of employees and managers to adjust their individual aims and individual communication systems with the sectional and company ones. Education and development of knowledge and skills represent communication of all the other possibilities of the professional and personal development, while quite often it concentrates on the communication skills training and elimination of basic communication mistakes and barriers.

Motivation presents recognition and accosting of value scales, needs and aims of employees by open verbal and also non-verbal communication (application of persuasion, active listening and emphaty). Relevance of effective communication in motivation stress out the fact, that "the highest value is achieved when employees identify themselves with their working tasks and are convinced about their importance." [2].

## 4. Development of Communication Skills

Common way of enhancement and harmonisation of individual and sectional communication systems with the company one, and also dynamisation of all processes of management and development of human potential, is the way of development and application of basic communicative skills of all employees and managers. These skills, in contemporary understanding, are *assertivity* (skill to actively and "ethically" communicate), *emphaty* (skill to understand the view and experiences of a communication partner), *active listening* (skill to show the interest in communication topic and communication partner) and *persuasion* (skill to positively persuade). Suitable integration or creation of these communication skills into communication systems of individuals and sections will be definitely reflected in enhancement of complex results of employees, managemers as well as a company in future (scheme 2).

Call for meaningful and balanced application of these communication skills can be directed from the *complex company communication system.* However, individuals or groups in a company can also invoke it so it can be directed even from the *individual and sectional communication systems*. This call can be also invoked by *individual processes of management and development of human potential* in a company as a natural reaction to a need to eliminate the faults and demonstrative inefficiency.

## 5. Conclusion

*Enhancement of individual, sectional and company communication system can positively influence and generate certain pressure on dynamisation of particular processes of management and development of human potential and vice-versa.* This positive reciprocal influence of quality of communication systems and working processes with the human potential is realised mostly by application and acceptation of direct and indirect feedback and by use of ideas and suggestions made by employees and management in a company. It is also realised by common sharing of communicated expectations and duties and by endeavour to gain, maintain and communicate "the wisdom" of all members of the company on the basis

of learning from the previous positive and negative experiences, reciprocal knowledge and skill beneficiation and effective use and development of unique human potential.

*Enhancement of communication systems* can be achieved by, e.g. meaningfully directed arrangements, which are identified as knowledge of outputs of evaluation processes of complex employees and management job performance. It could be achieved by higher motivation effort of managers, staff managers and ordinal employees and by application of creative (participative) management centred on this field. Desired planing of human potential and its development in short-term, medium-term and long-term time and logical perspective can form it. In this layer an analysis of working places and especially the way and philosophy of creation of new and redesign of already existing places can be very helpful. Equally, the process of new employees orientation and their consecutive placement can obtain the view of balanced and desired reinforcement of communication skills and communication systems of individuals, sections and company.

*Enhancement and dynamisation of system of management and development of human potential* can be achieved by creation of reciprocal, open and unblocked communication environment, and by high quality and balanced function of individual as well as sectional communication systems of a company.

**Acknowledgement**
This paper is supported by the grant of VEGA 1/1243/04.

## References

[1] HITKA M.: *Hodnotenie práce riadiacich pracovníkov vo výrobnom podniku.* Zvolen. Vydavateľstvo TU Zvolen. 2002
[2] KACHAŇÁKOVÁ A.: *Podniková kultúra.* Bratislava. Ekonóm. 2003
[3] KUCHARČÍKOVÁ A. – VODÁK J.: *Dnešný pohľad na zajtrajšiu budúcnosť – tvorba a implementácia stratégie.* In: Produktivita 5/2002.

https://doi.org/10.26552/com.C.2004.1.50-53

kamUNikácie
COMMUNICATIONS

Michal Žarnay *

# HUMAN FACTOR IN DECISION-MAKING IN SIMULATION MODEL OF TRANSPORTATION SYSTEM AND APPROACHES TO ITS MODELLING

*The article deals with human factor in decision-making in simulation model of transportation system. It points to the difference between the management in reality and in a model, where it is more difficult to represent the human thinking. The consequence of this is a higher probability of deadlock appearances that can be developed after operation has deflected from the plan. The effort to minimize the operation deviations leads to processing larger amount of information and to more complicated decision-making algorithms, which makes the simulation model more complicated and slower. The task of the developer is to set the level of details in the decision-making subsystem.*

*In the end of the article, few different approaches to the modelling of human decision-making are mentioned.*

## 1. Introduction

Computer simulation model of transportation system represents one of tools that help us in solving problems and making improvements in transportation systems. This tool may have a various level of capture of details from real transportation system – its master, depending mainly on what is it designed for.

When we focus on detailed analysis and improvement of technological processes, we may happen to work with complex simulation models containing hundreds of objects and thousands of parameters. In such models, management of interaction of objects gains high importance and more sophisticated decision-making is required.

In this paper, I'll discuss more in detail what problems in decision-making may be encountered when modelling a transportation system.

## 2. Decision-Making in Simulation Model

Simulation models intend to model real systems as closely as possible. Objects with their attributes in reality serve as masters for creation of objects in a simulation model. Relations among objects in a model also reproduce relations among objects in the master system. In this way also decision-making processes in the models are made based on decision-making processes in real systems.

There is one significant difference in decision-making in a real transportation system and in its simulation model: human factor. While it is people who make decisions in a real system, in its simulation model built on the computer, they are supposed to be made by the computer.

As we know, modelling of human thinking is not as an easy task as modelling of non-human objects and their behaviour. With growing complexity of the transportation system grows importance of human decision-making, and also difficulties in modelling it in a simulation model rise.

## 3. Deadlock

A major problem is appearance of deadlocks. Deadlock is a name for a situation when a process in the system is waiting for another process to be finished and at the same time, the latter process is waiting for the former process to be finished. Neither of them can finish, because they wait for each other. This happens commonly when more processes can use the same resources.

For instance (fig. 1), the locomotive A is moving from a locomotive depot to a train in the station, where it is assigned. At the same time, the locomotive B is moving from the station to the locomotive depot. Both locomotives are supposed to use the same route between the depot and the station, the former in one direction, the latter in the opposite direction. They get their routes assigned gradually, section by section, as they move. They are moving simultaneously until they come to a point, when next section in the route of the locomotive A is occupied by the locomotive B and

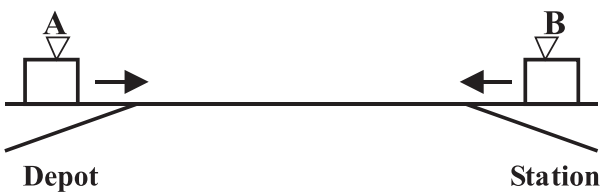


*Fig. 1 Deadlock*

* **Ing. Michal Žarnay**
Department of Transportation Networks, Faculty of Management Science and Informatics, University of Žilina, Moyzesova 20, 010 26 Žilina, Slovak Republic, Tel: +421–41–5134224, E-mail: Michal.Zarnay@fri.utc.sk

next section in the route of the locomotive B is taken by the locomotive A. They stop to wait for their resources to be assigned. And if they have no alternatives for movement, they can wait forever – they are in deadlock.

## 4. Plan and Management

In most transportation systems (e.g. railway station, airport, local bus network), an operation is planned in advance. A plan assumes time points when events will happen and contains actions that should follow the events in context of current situation. Because of stochastic influence, events do not happen always according to the plan. Thus deviations from the plan appear – e.g. deviations in time or in selection of used resources.

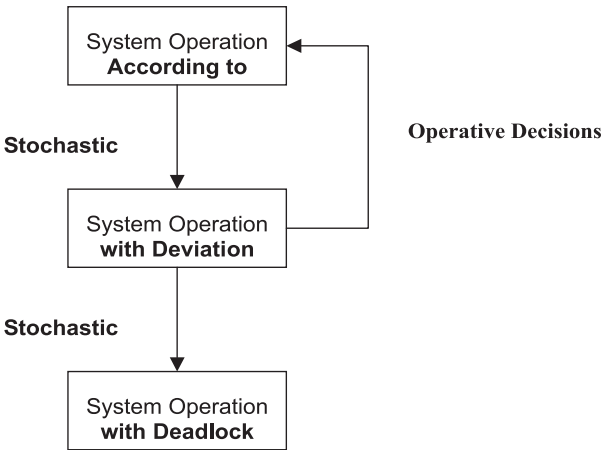


*Fig. 2 Stochastic influence and operative management in transportation*

In this situation, it is a task of an operative management subsystem to adapt the plan to the reality. It must take such actions that the system comes back to the plan. If there are enough resources to cope with the deviation (time reserves, available personnel or equipment), the management subsystem can remove the deviations and bring the system back to the plan. If any of required resources fails, the deviation may grow, and come to a deadlock eventually (fig. 2).

For instance, in a railway station, the plan is represented by a timetable that predicts events of departures and arrivals of trains. Based on this, plans of corresponding technological processes and services to passengers are developed. In this way, employees at the station know when the train should be shunted, cleaned, or inspected. Each employee has an individual working plan with a list of time points and train numbers to work on.

Stochastic influence causes that trains may run late, cargo trains may contain more loaded cars, or any cars for special manipulation, or unexpected failures may cause delay of technological operations.

The deviations in this example could be: using a track that was not planned for the given train, delay in processing of the train or using another personnel group for certain operation than originally planned.

## 5. Problem in Modelling of Human Decision-Making

In a real transportation system, the management subsystem contains human factor, which is able to spot deviations that may lead later to a deadlock. This person monitors the system and does necessary operations to keep it running closely to the plan.

In a simulation model, in most cases, the human being in the management subsystem is replaced by computer logic. The subsystem contains also tools for monitoring the system and for performing necessary operations. These are prescribed in a form of algorithms by a human being in advance. Each algorithm is supposed to make a decision in a given situation. The situation is recognised from available information about the current situation in the system. Based on it, a decision is made.

Quality of the decision depends on two factors: quality of processed information and quality of decision-making algorithm. The processed information must contain basic data that is absolutely necessary for the decision-making. It can also contain additional information that can influence quality of the solution. Similarly, the decision-making algorithm must contain some absolutely necessary minimum to make the requested decision. To ensure higher quality of solution, the algorithm may be also more sophisticated and contain mechanisms for processing additional information and evaluating additional criteria when choosing a decision.

Let's see an example (fig.3). Passenger train No. 340 comes to a train station delayed. According to the plan, it is supposed to use the platform track No. 3 in the station. However, at its delayed arrival another train No. 2801 should occupy the track. To solve this conflict, an additional track must be used.

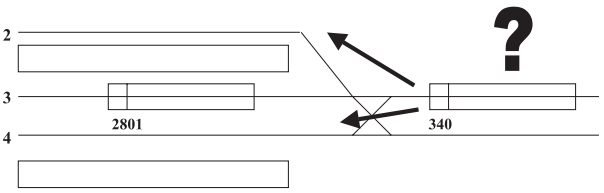


*Fig. 3 Example of conflict situation*

We have two options: platform tracks No. 2 or No. 4. This information (list of additional tracks for use) is the necessary minimum to solve the situation. A simple algorithm may use the First-In-First-Out method. According to this the train No. 340, as coming later, will use the track No. 2, which is selected as the first in the list.

However, as consequence of this decision, the evident deviation from the plan may be spread further to other trains and tracks,

because use of the track No. 2 will influence the processing of another train planned for that track. Another decision, use of the track No. 4 in this case, could have other consequences. It could spread the deviations from the plan to other parts of the model as well, more or less than the former decision. Our simple algorithm does not compare them.

If additional information about consequences was available or the decision-making algorithm processed available information in more sophisticated way, another solution could be chosen bringing the deviation closer to its end in near future. In this example, it could use information from the occupation plan of the platform tracks No. 2 and No. 4 in the next 10 minutes, or check how modified routes of trains through the station will influence other movements. This information could be compared with additional criteria for use of the platform tracks and for movements in the station planned in the near future. Results of this evaluation could contribute to the selection of one of the two alternatives.

It is obvious that making decisions of better quality would require more information in the phase of monitoring or more detailed processing of available information in the phase of decision-making (fig. 4). However, the more parameters a simulation model has, the larger is variety of different situations to solve, the more sensitive is model to stochastic events and probability of deadlocks is higher.

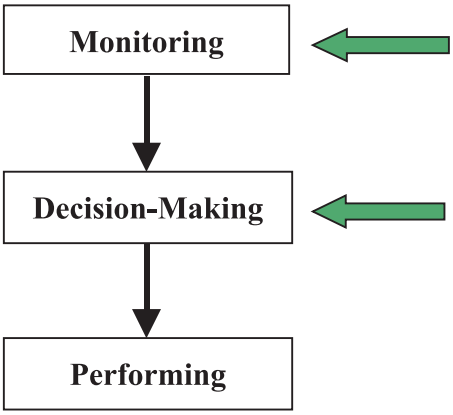


*Fig. 4 Phases of focus when improving decision-making*

In order to prevent a complex simulation model from deadlocks and to keep it in line with the plan, requirements on the computer management subsystem are higher which means a larger scale of information needed for decision-making and more complicated algorithms. Both aspects require deeper knowledge of management subsystem in the transportation system by a simulation model designer. Information from more sources in the model and more ways of combining it must be taken into account.

Apart from that decision-making processes last longer and require more computing power. This makes simulation models slower.

## 6. Possible Approaches in Modelling of Human Decision-Making

There is a wide range of possible approaches for solving this issue: from application of exact algorithms (e.g. from mathematical programming), through heuristic algorithms to application of artificial intelligence with fuzzy logic. It can be also a combination of all.

Exact algorithms can be used in only a small extent of situations, since their application usually requires unacceptable simplification of the problem or they need too long time to come to a solution, or both. That is why heuristic algorithms and artificial intelligence are applied in most of the cases.

In the described area, in our department, so far we have used the exact algorithms for solving simple problems. For complicated decision-making situations, heuristic algorithms are used. The development goes on and we are improving heuristic algorithms and investigating the area of artificial intelligence.

Another way that can help in solving, is modelling with help of Petri Nets. This formal tool allows not only modelling, but also simulation and analysis of the modelled system. There are different classes of Petri Nets used in different cases, e.g. coloured Petri Nets, timed Petri Nets or fuzzy Petri Nets.

An idea that we would like to investigate is to use coloured Petri Nets and their analysis space for solving individual decision-making situations that will be extracted from the modelled system. It is also possible that for representation of facts and rules for decision-making, fuzzy logic will be used.

## 7. Conclusion

A result of the development of management subsystem to a more complex version is its complexity and slower speed of the simulation model. This can harm some of the advantages of simulation models: speed and clarity.

In this way, a simulation model designer is between two extreme approaches leading to:

- On one side a faster and clearer model with simpler management subsystem, but with more difficult task of managing stochastic events in the model (deviations from plan),
- On the other side a more robust model able to deal with more various situations as results of stochastic events, but slower with more complex management subsystem.

It is a task for a designer to find a compromise between the two approaches and to define how close the compromise will be to any of them. This compromise depends most often on goal(s) carried out by simulation.

Possible approaches in modelling of human decision-making are various. One of them, connected with application of Petri Nets, is to be investigated.

**References:**

[1] ŽARNAY, M.: *Decision-making support in simulation models of nodes of railway network.* Perner's Contact 2001, Pardubice, 2001
[2] ŽARNAY, M.: *Analysis of decision-making in simulation model of node of railway network.* Perner's Contact 2001, Pardubice, 2001
[3] KAVIČKA, A., KLIMA, V.: *Interactive problem solving in simulation model of marshalling yard operation.* In: Proceedings of the 3rd international symposium "ŽEL 96", Žilina, 1996, pp. 229-233
[4] KLIMA, V., KAVIČKA, A.: *Agent-based simulation model design.* In: Proceedings of European simulation multiconference, SCS Budapest, 1996, pp. 254-258.

https://doi.org/10.26552/com.C.2004.1.54-57

komunikácie
COMMUNICATIONS

Mariana Strenitzerová *

# CHANGE MANAGEMENT: THE PEOPLE DIMENSION OF CHANGE

*Change management is the process, tools and techniques to effectively manage people and the associated human resource issues that surface when implementing business changes. Change management as a field of study finds its roots in two areas: business process improvement and psychology. The ADKAR model for change management as the diagnostic tool helps employees understand where they are in the change process. A manager can use this tool to identify gaps in his change management process and to provide effective coaching for his employees.*

## 1. Introduction

Change management is the process, tools and techniques to effectively manage people and the associated human resource issues that surface when implementing business changes. Some authors integrate change management techniques with business improvement methodologies. This integrated approach is neither right or wrong. What is important is that you can recognize the difference between the two and understand the relationships between business improvement techniques and change management.

Change management as a field of study finds its roots in two areas: business process improvement and psychology. From the business process improvement disciplines such as total quality management (TQM) and business process reengineering (BPR), change management came about after many project failures. The root cause of many failures was a lack of change leadership and poor management of employee resistance to change.

In fact many process improvement disciplines that were "engineering" centric and problem solving in nature ignored change management.

From the psychology field, change management was recognized early on as a necessary component to manage the "human side" of change in the workplace. However, the soft and personal approach to managing change, sometimes referred to as the "touchy feely" approach, did not fit well with the problem-solving staff members so often picked to tackle critical business issues.

As a result, the marriage of business process improvement (meant in this case to comprehensively cover any business change including new business models, business processes, technology or restructuring) and change management took many years to develop. Early change management books were authored beginning in the early 80's. However, integrated models for designing business solutions and managing the change process did not appear until the late 90's and many of these models are still not widely recognized.

Research has shown clearly that projects that effectively integrate change management as a part of their business change are more successful and received better by those impacted by the change.

Change management occurs on two levels: the organizational level and the individual level. This framework of viewing change management from the management view and the employee view is critical for understanding.

The field of change management can be confusing and sometimes complicated to research and study, especially for new practitioners. Change management is the application of many different ideas from the engineering, business and psychology fields. As changes in organizations have become more frequent and a necessity for survival, the body of knowledge known as "change management" has also grown to encompass more skills and knowledge from each of these fields of study.

While this may be a good trend overall, the result for many change leaders is growing confusion about what change management really means.

Change Management: The convergence of two fields of thought

To understand change management as we know it today, you need to consider two converging and predominant fields of thought: an engineer's approach to improving business performance and a psychologist's approach to managing the human-side of change.

The table below summarises the key differences and contrasts the two approaches in terms of focus, business practice, measures of success and perspective on change.

* **Ing. Mariana Strenitzerová, PhD.**
Department of Communications, Faculty of Operation and Economics of Transport and Communications, University of Žilina, Moyzesova 20, 010 26 Žilina, Slovak Republic, Tel.: +421-41-5133131, Fax: +421-41-5655 615, E-mail: Mariana.Strenitzerova@fpedas.utc.sk

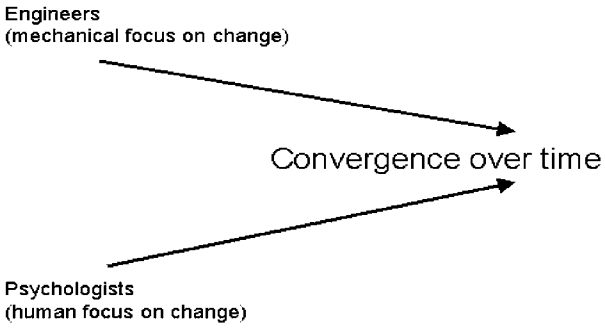


| | Engineer | Psychologist |
|---|---|---|
| Focus | Processes, systems, structure | People |
| Business practices | BPR, TQM, ISO 9000, Quality | Human resources, OD |
| Starting point | Business issues or opportunities | Personal change, employee resistance (or potential for resistance) |
| Measure of success | Business performance, financial and statistical metrics | Job satisfaction, turnover, productivity loss |
| Perspective on change | "Shoot the stragglers, carry the wounded." | "Help individuals make sense of what the change means to them." |

Today, the term "change management" takes on a variety of meanings. The most practical and useful definition is:

*Change management is the process, tools and techniques to manage the people-side of business change to achieve the required business outcome, and to realize that business change effectively within the social infrastructure of the workplace.*

This definition allows practitioners to separate change management as a practice area from business improvement techniques. So whether you are doing Six Sigma, BPR, TQM or some other technique to improve business performance, change management can be viewed as an essential competency to overlay and integrate with these methods.

## 2. Change Management: Definitions and Strategies

In thinking about what is meant by "change management," at least three basic definitions come to mind:

1. The task of managing change
2. An area of professional practice
3. A body of knowledge

*The Task of Managing Change*

The first and most obvious definition of "change management" is that the term refers to the task of managing change. The obvious is not necessarily unambiguous. Managing change is itself a term that has at least two meanings.

One meaning of managing change refers to the making of changes in a planned and managed or systematic fashion. The aim is to more effectively implement new methods and systems in an ongoing organization. The changes to be managed lie within and are controlled by the organization. However, these internal changes might have been triggered by events originating outside the organization, in what is usually termed "the environment." Hence, the second meaning of managing change, namely, the response to changes over which the organization exercises little or no control (e.g., legislation, social and political upheaval, the actions of competitors, shifting economic tides and currents, and so on). Researchers and practitioners alike typically distinguish between a knee-jerk or reactive response and an anticipative or proactive response.

*An Area of Professional Practice*

The second definition of change management is "an area of professional practice."

There are dozens, if not hundreds, of independent consultants who will quickly and proudly acknowledge that they are engaged in planned change, that they are change agents, that they manage change for their clients, and that their practices are change management practices. There are numerous small consulting firms whose principals would acknowledge these same statements about their firms. And most of the major management consulting firms claim to have a change management practice area.

Some of these change management experts claim to help clients manage the changes they face, the changes happening to them. Others claim to help clients make changes. Still others offer to help by taking on the task of managing changes that must be made. In almost all cases, the process of change is treated separately from the specifics of the situation. It is the task of managing this general process of change that is laid claim to by professional change agents.

*A Body of Knowledge*

Stemming from the view of change management as an area of professional practice there arises yet a third definition of change management: the content or subject matter of change management. This consists chiefly of the models, methods and techniques, tools, skills, and other forms of knowledge that go into making up any practice.

The content or subject matter of change management is drawn from psychology, sociology, business administration, economics, industrial engineering, systems engineering, and the study of human and organizational behaviour. For many practitioners, these component bodies of knowledge are linked and integrated by a set of concepts and principles known as General Systems Theory (GST). It is not clear whether this area of professional practice should be termed a profession, a discipline, an art, a set of techniques, or a technology. For now, suffice it to say that there is a large, reasonably cohesive albeit somewhat eclectic body of knowledge underlying the practice and on which most practitioners would agree – even if their application of it does exhibit a high degree of variance.

To recapitulate, there are at least three basic definitions of change management:

1. The *task of managing change* (from a reactive or a proactive posture)
2. An *area of professional practice* (with considerable variation among practitioners)
3. A *body of knowledge* (consisting of models, methods, techniques, and other tools)

To use the ADKAR model effectively, you will need to understand the underlying framework for change initiatives. In the diagram below, change happens on two dimensions: the business dimension (vertical axis) and the people dimension (horizontal axis). Successful change happens when both dimensions of change occur simultaneously.

The table below summarises four basic strategies of change management.

| Strategy | Description |
|---|---|
| Rational-Empirical | People are rational and will follow their self-interest - once it is revealed to them. Change is based on the communication of information and the proffering of incentives. |
| Normative-Reeducative | People are social beings and will adhere to cultural norms and values. Change is based on redefining and reinterpreting existing norms and values, and developing commitments to new ones. |
| Power-Coercive | People are basically compliant and will generally do what they are told or can be made to do. Change is based on the exercise of authority and the imposition of sanctions. |
| Environmental-Adaptive | People oppose loss and disruption but they adapt readily to new circumstances. Change is based on building a new organization and gradually transferring people from the old one to the new one. |

## 3. "ADKAR" – A Model for Change Management

Prosci developed the ADKAR model in 2001 after research with more than 700 companies undergoing major change projects. This model is intended to be a coaching tool to help employees through the change process. The ADKAR model is not an organizational change management model or strategy.

The ADKAR model for change management as the diagnostic tool helps employees understand where they are in the change process. As a manager, you can use this tool to identify gaps in your change management process and to provide effective coaching for your employees. The ADKAR model can be used to:

- Diagnose employee resistance
- Help employees transition through the change process
- Create a successful action plan for personal and professional advancement during change
- Develop a change management plan for your employees

The ADKAR model has the ability to identify why changes are not working and help you take the necessary steps to make the change successful. You will be able to break down the change into parts, understand where the change is failing and address that impact point.

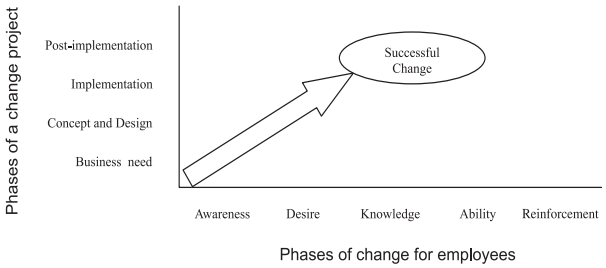


*Business dimension of change*

The business dimension of change includes the typical project elements.

- Business need or opportunity is identified.
- Project is defined (scope and objectives).
- Business solution is designed (new processes, systems and organizational structure).
- New processes and systems are developed.
- Solution is implemented into the organization.

These are the standard elements of a business change that managers feel most comfortable managing.

*People dimension of change*

The people dimension of change is how employees experience the change process. Research shows that problems with this dimension of change are the most commonly cited reason for project failures. In a study with 248 companies, effective change management with employees was listed as one of the top-three overall success factors for the project. Helping managers be effective sponsors of change was considered the most critical success factor overall.

Effective management of the people dimension of change requires managing five key phases that form the basis of the ADKAR model:

- **A**wareness of the need to change
- **D**esire to participate and support the change
- **K**nowledge of how to change (and what the change looks like)
- **A**bility to implement the change on a day-to-day basis
- **R**einforcement to keep the change in place

## 4. Conclusion

This contribution presents an overview of the ADKAR model for change management. This diagnostic tool helps employees understand where they are in the change process. As a manager, you can use this tool to identify gaps in your change management process and to provide effective coaching for your employees.

The power of the ADKAR model is that it creates focus on the first element that is the root cause of failure. When you approach a change using this model, you can immediately identify where the process is breaking down and which elements are being overlooked. This avoids generic conversations about the change that rarely produce actionable steps.

## References

[1] JURAJ CAJCHAN, OĽGA PONIŠČIAKOVÁ: Principles of process managing, V. International conferences in Transport, Vysoke Tatry, October 2002
[2] www.change-management.com
[3] www.prosci.com

https://doi.org/10.26552/com.C.2004.1.58-63

kamUNikácie
COMMUNICATIONS

Eva Remišová *

# THEORY AND MEASUREMENTS OF BITUMEN BINDERS ADHESION TO AGGREGATE

*The pavement as unit is able to perform services, provided that we ensure good synergy of layers and especially good adhesion between used materials. Adhesion knowledge allows to design suitable technology by preventing defects and to ensure service ability and life of pavement.*

*In the paper there is a theoretical analysis of problem of bitumen binders adhesion to aggregate, basic methodologies to evaluate this property and specific results achieved at measuring by the method STN 65 7089 and EN 12272-3. At the same time the results are compared from the type of aggregate point of view as one of the most important factors that influenced adhesion.*

## 1. Introduction

The wearing surface of the road is exposed to both vertical and tangential forces caused by the moving vehicle. The bitumen elements and aggregate stripping from the tyre are torn out by the suction effect of the wearing course, thus causing the continual destruction of the wearing course. The loss of bitumen cohesion and adhesion between the bitumen and aggregate is a major cause of defects in bitumen road surfacing. By the traffic effects, ravelling occurs. It is caused by material fatigue and stress pressure in tyre/surface contact area, weather effects, especially water which results in stripping the aggregate grains in the wearing surface (water is forced by the tyre engravement into the tyre/pavement contact area, and arises forces with similar effect as suction) and the ageing of the bitumen binder in the wearing surface which becomes harder and more fragile to the breaking.

The basis for the construction of the high quality wearing course with a long service life is the adhesion between the binder and the aggregate. It is important to achieve a strong bond among all materials during the service life at the varied climatic conditions. Adhesion knowledge allows to design a suitable technology, thus preventing defects and ensuring longer service life of the wearing course.

## 2 Methodological Approach

### 2.1 Adhesion

Generally, *adhesion* is defined as the affinity force between surface molecules of two materials that cause a close contact without chemical change. It depends on the interfacial surface tension and the binder wetting.

The ability of binder to cover aggregate (wetting ability) is called *active adhesion. Passive adhesion* expresses the binder coat resistance to the stripping from aggregate surface by the water effect. If the conditions of coating are properly designed and performed, there is no active adhesion [1].

Besides the mechanical interaction at the contact surface (liquid bitumen penetration into the pores of solid material), which depends on the physical properties of aggregate and bitumen – also *mechanical adhesion* exists. It is also necessary to ensure sufficient bond strength of physical and chemical bonds between contacted binder and aggregate – *specific adhesion*. Incipient *chemical cohesion* caused by the effect of chemical (interatomic) bonds is more energetically stable than *physical cohesion* initiated by a physical (intermolecular, van der Waals) bond effect [2].

### 2.2 Theories of adhesion mechanism

From the general point of view, adhesion is the force that bonds the binder to solid surfaces and prevents its tearing away. Several mechanisms have been used to explain adhesion between

Theories of adhesion mechanism Tab. 1

| Theory | Mechanism | Strength of interaction |
|---|---|---|
| adsorption (Bruyne) | van der Waals, H-bonding | moderate to strong |
| diffusion (Voyutskii) | inter-diffusion binder molecules to solid material | variable |
| bonding (Bickerman, mechanical interlock) | mechanical diffusion of binder to aggregate pores, close contact wetting | variable |
| surface energy theory | binder and aggregate surface with more critical surface tension, wetting | variable |
| reactive theory, chemical bonding | covalent bond | very strong |

* **Eva Remišová**
Faculty of Civil Engineering, University of Žilina, Slovakia, E-mail: remisova@fstav.utc.sk

materials [3]. We can say about none of them to be perfect and general. Some of them are presented in Table 1.

The adhesion is closely related to the surface properties of materials – binders and aggregates. Generally, material surfaces are characterized by the surface energy, esp. surface tension that influences their ability to adhere to each other and to a create strong bond.

Excess of acting forces in the surface level per length unit of a line on the surface is surface tension. Surface tension is positive when affects following the direction of surface contracting. If the bitumen surface tension is low and if the bitumen has affinity to aggregate surface, the bitumen is able to cover aggregate and adhere to its surface [4].

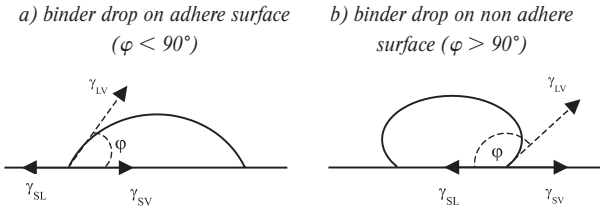


*Fig. 1 Surface tensions between liquid and solid phases*

Performance of bitumen – aggregate bond (liquid – solid phases) is with the presence of the gas phase, if this bond does not occur in vacuum. The calculation of the surface tension of the triple contact is difficult because surface interface tension is effected by all contact phases – solid phase, liquid phase and gas phase where the surface tension of solid phase is $\gamma_{SV}$, surface tension of liquid phase is $\gamma_{LV}$ and $\gamma_{SL}$ is interface tension between solid and liquid phases (fig.1).

The equilibrium (or stability) of surface tensions of interface of solid – liquid – gas phase is expressed generally in Young – Dupré equation:

$$\gamma_{SV} - \gamma_{SL} = \gamma_{LV} . \cos \varphi \qquad (1)$$

where $\varphi$ [°] is contact angle between liquid drop and surface of solid material with the presence of air.

Direct relation exists between perfection of wetting and intensity of adhesion strength stability. Bond strength is changed analogously as cos $\varphi$. Interface tension increases directly proportional with cos $\varphi$, and the ability to coat solid material with the binder. If $\varphi = 0$, total and spontaneous coating and adherence occur. If $\varphi = 180°$ coating cannot come into force.

Initial surface energy decreases during bitumen aggregate coating due to the absence of air membranes covering the liquid (bitumen) and solid materials (aggregate),while performing the work $W$:

$$W = \sigma_{SV} + \sigma_{LV} - \sigma_{SL} \qquad (2)$$

where: $\sigma_{SV}$ is surface energy of solid phase,
$\sigma_{LV}$ is surface energy of liquid phase,
$\sigma_{SL}$ is energy of solid – liquid phase interface.

Measurement of surface energies, interface energies and contact angles are difficult under the conditions of conventional laboratories. Thus, the comparison of properties of different surfaces with the binder is difficult because the measurement of the contact angle requires even surface of solid material and then the surface must be modified [5].

Specific value of the surface tension of the binder and aggregate contact above which spontaneous coating does not occur is *the critical surface tension*. Only binders with surface tension less than critical value will cover solid surfaces spontaneously.

It is necessary that bitumen have good wetting ability to create the stable coat on the aggregate. Wetting and adhesion perform on the phases interface and relate to the intermolecular forces. The bitumen covers aggregate surface well if its surface tension is low. Surface tension of bitumen decreases when temperature increases. The viscosity of bitumen decreases at higher temperature; bitumen covers aggregate well and adheres to the aggregate surface.

## 3 Experimental measuring

As mentioned above, it is difficult to measure adhesion as the force that bonds bitumen to aggregate therefore methodological techniques have been developed for evaluating adhesion by measuring the properties of the bitumen mixtures. Methods used to adhesion measurement are based on one of following principles:

- visual evaluation by estimation of uncovered surface of the aggregate by the water effect,
- adhesion measurement by the mechanical test (adhesion evaluating as the resistance to mechanical stresses),
- adhesion evaluation as the resistance to water by measuring mechanical property of mixture before and after tempering in water,
- evaluating the chemical adhesion.

The basic test method of adhesion evaluating in the Slovak Republic is the procedure which follows the technical standard *STN 65 7089 - Determination of Adhesion of Asphalt Products to Aggregates* from year 1982 [6]. According to this standard the adhesion of asphalt products to aggregates is the resistance of the asphalt film on the aggregate surface to the water displacement (passive adhesion). The adhesion influences asphalt mixtures quality and service life. This method also indicates the efficiency of adhesion additives.

The methods able to evaluate adhesion of the binders penetration 35 – 210, cut-back bitumen with the flow time C/5/60 to 170 s and C/5/25 to 70 s and asphalt anionactive emulsions to the aggregates. Dry aggregates and wet aggregates are covered by the

tested bitumen. After 24 hours of tempering it is exposed to the effects of tempered water (at the temperature of +60 °C res. +40 °C) for one hour. Adhesion is expressed as a mean value of stripping of the asphalt film on the grains of the aggregate surface. Thus, adhesion is accepted if some uncovered points appear on the surfaces of covered aggregate grains or stripped borders and corners on more than two grains of the aggregate. If there are larger stripped areas on the grains of aggregate surface (two and more aggregate chippings), adhesion is not acceptable.

The degree of stripped asphalt on aggregate surface is evaluated visually. In this way, the evaluation becomes subjective depending on the technician performing the test. Methodology, test specimen, and test procedure predetermine this test to the asphalt evaluation and aggregate adhesion used in asphalt mixtures.

The European standard prEN 12697-11 [7] belongs to this test group. Standard measures evaluate the compatibility between the aggregate and bitumen, expressed by visual observation of the loss of adhesion in uncompacted bitumen-coated aggregate mixtures in the presence of the water. Test specimen is also affected by mechanical load with the presence of water.

From the second group of tests that evaluates adhesion by the mechanical test is Vialit test. The test methodology is the base for European standard *EN 12272-3 Determination of Binder Aggregate Adhesivity by the Vialit Plate Shock Test Method* [8]. This standard specifies test methods for determining the binder – aggregates adhesion as two main components of surfacing.

The standard applies to the measurement of binder – aggregate adhesion and the influence of adhesion agents on adhesion characteristics as the aid to design binder – aggregate systems for surface dressing. This methods allows to evaluate adhesion of:
- hydrocarbon binders used for surface dressings,
- paving grade and modified bitumens,
- cut-back bitumens,
- asphalt emulsions,
- to all aggregate types (with size 6–8, 8–11, 11–16 and 4–6, 6–10, 10–14).

The principle is the measurement of the binder – aggregate adhesion after mechanical exposure. European standard specifies the test method for determining:
- mechanical adhesion of the binder to the aggregate – Vm (property to bond dry aggregate chippings with their natural dust and fine particles)
- active adhesion – Va (the property to bond dump aggregate chippings in their natural state in which they occur in the dumping sites)
- improvement of mechanical and active adhesion using some adhesive agents to the binder or to binder – aggregate interface.

In terms of the standard European requirements prEN 12271-5 [9], the value of mechanical adhesion and active adhesion has to be minimum 95 % res. 90 % to reach value 2 res. 1 (for value 0 there is no adhesion requirement).
The standard has three basic divisions:
- active adhesion and mechanical adhesion,
- wetting temperature,
- fragility temperature.

In the first part, the test procedure is defined according to the known test method Vialit and determining the active adhesion. In the second part, the treatment for the determinng wetting temperature at the lowest binder temperature before the spreading aggregate is described when the grinding of the aggregate is possible with minimum 90 % adhesion (90 of 100 grains of aggregate remain adherent to the experimental plate). And the other treatment to determine fragility temperature at the temperature at which minimum 90 % aggregate chippings remain bonded to the plate is carried out at Vialit premises.

The binder – aggregate adhesion is expressed by the total number of aggregate chippings bonded to the plate and the aggregate with the binder fallen off after test. The advantage of this test method is that it allows measuring and evaluating the adhesion with different types of binders and aggregates. At the same time, it is possible to verify adhesion agents efficiency. Test results are influenced by binder – aggregate adhesion and also by binder cohesion, especially at low temperatures.

### 3.1 Experimental measuring - materials

For experimental measurements of bitumen and aggregate adhesion by the above presented test procedures, we used aggregates from different local sources, especially from the northern

The aggregate composition Tab. 2

| Aggregate content [%] | Varín | Šuja | Biely Potok | Dubná Skala | Malužiná | Hanišberg | Kamenec p. Vtáčnikom |
|---|---|---|---|---|---|---|---|
| $SiO_2$ | 1.04 | 0.30 | 0.30 | 70.74 | 56.77 | 56.5 | 59.27 |
| $Al_2O_3$ | 0.21 | 0.20 | 0.07 | 17.31 | 12.96 | 19.5 | 19.72 |
| $Fe_2O_3$ | 0.20 | 0.10 | 0.25 | 5.65 | 4.77 | 6.50 | 5.82 |
| CaO | 47.02 | 30.90 | 31.60 | 3.49 | 9.06 | 7.50 | 5.81 |
| MgO | 6.86 | 21.40 | 20.70 | 0.63 | 2.68 | 5.00 | 2.17 |

Slovakia, representing these rocks: limestone from the locality Varín, dolomite from two localities (Šuja, Biely Potok), granodiorite from the locality Dubná Skala, melaphyre from the locality Malužiná and andesite from two the localities (Hanišberg, Kamenec pod Vtáč-nikom), and bitumen binders from by-products in Slovnaft oil refinery, both paving grade and modified (with the SBS rubber) [10].

Measured bitumen properties Tab. 3

| Binder | Penetration at 25 °C in 0.1 mm | Softening point R&B v °C. minimum | Ductility at 25 °C in cm. minimum |
|---|---|---|---|
| bitumen 70/100 | 83.7 | 53 | 114.9 |
| modified Apollobit MCA-S | 93.9 | 75 | 62.2 |

### 3.2 Comparison of laboratory results

Experimental measurements of adhesion was performed by two test methods, according to the standard STN 65 7089 and Vialit test [11].

After bitumen and aggregate having been mixed, the process of interaction between aggregate and bitumen begins. These processes are determined by chemical and physical-technical properties of aggregate. The aggregate composition is evaluated from both chemical or mineralogical point of view. The chemical structure has only indirect effect on the aggregate used. From mineral point of view, the aggregate contains mostly one dominant component and some minor mineral components. For example, the limestone rock consists of dominant component limestone, and silica, clay, micaous minerals as minor components. In term of adhesion, the content of $SiO_2$ in aggregate is the most important. The bitumen – aggregate adhesion results by method of STN 65 7089 (tab. 4) and Vialit test (fig. 2) show that the content of $SiO_2$ in aggregate has negative influence on the adhesion of bitumen. The basic aggregate with minor content of $SiO_2$ has good adhesion of bitumens. The adhesion of acid aggregate and bitumens has mostly poor adhesion level.

The worst adhesion results obtained by the Vialit method show the aggregate with high content of $SiO_2$ 70.74 % granodiorite form Dubná Skala locality. On the contrary, the adhesion results with

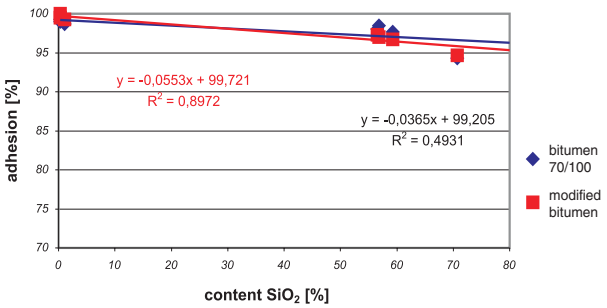


*Fig. 2 The results of bitumens and aggregates adhesion*

limestnones and dolomites with low content of $SiO_2$ showed the best results of adhesion with all used bitumens by Vialit test 98.7 to 100 % adhesion. These results were confirmed by both test methods, adhesion measuring of specimens aggregate with their natural dust and fines and specimens tempering in water. Neutral aggregate (andesites and melaphyre) had average adhesion values 96 to 100 %.

Regression analysis of relation to content of $SiO_2$ in aggregate shows that there is a linear dependence between adhesion results and aggregate content of $SiO_2$. This dependence obtained from the measurements with all used bitumens and aggregates and also with measuring dry aggregate and aggregate with their natural dust and fines, and also adhesion measuring of specimens tempered in water. From the analysis of these dependencies, we can conclude that the adhesion decreases in dependence on the content of $SiO_2$. With the increase of $SiO_2$ in aggregate about 1 %, the adhesion value decreases about 0.037 % (paving grade bitumen) eventually with 0.055 % modified bitumen.

From other mineral ingredients which can be found in the aggregate, some minor minerals that show an increased content of $Al_2O_3$ are important. These minerals with $SiO_2$ have an apparent hydrophilic character in contrast with hydrophobic character of limestone. These minerals show very different reactions toward the bitumen binder and the water.

From these data it is evident that thickness of bitumen coat around the limestone chipping is essentially higher than around silica (quartz) chipping. On the surface of limestone chipping contents adsorption we can find centers in the form of limestone cations (CaO), magnesia (MgO) and ferrate ($Fe_2O_3$), with the intense positive potential. The anion exchange of bitumen binder conducts to the strong binder film bonds.

The adhesion results of bitumens and aggregates by STN 65 7089 Tab. 4

| **Binder** | **Adhesion** | | | | | | |
|---|---|---|---|---|---|---|---|
| bitumen 70/100 | good – suitable | | | suitable – poor | | | poor |
| modified | good | | | good – suitable | | | poor |
| **Aggregate** | dolomite 2 | dolomite 1 | limestone | andesite 1 | melaphyre | andesite 2 | granodiorite |
| | **basic** | | | **neutral** | | | **acid** |

Adhesion results comparison in dependence on the content of limestone (CaO) and magnesia (MgO) show that rocks with high content of these minerals have good adhesion (fig. 3 and fig. 4). The dependence is expressed in regression function. Parameters A and k depend on the type of binder and also the system of measuring (measurement with washed and dry aggregate, aggregate with their natural dust and fines, measurement of experimental samples tempered in water).

Positive effect of CaO and MgO content in the aggregate on the bitumen binder adhesion was confirmed by the adhesion results tested by standard STN 65 7089.

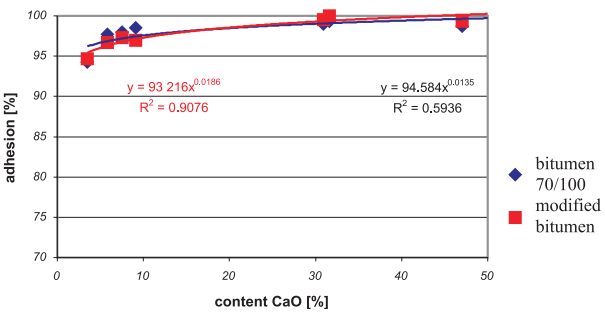


*Fig. 3 The adhesion results of bitumen binder to aggregate in dependence on content CaO in aggregate*

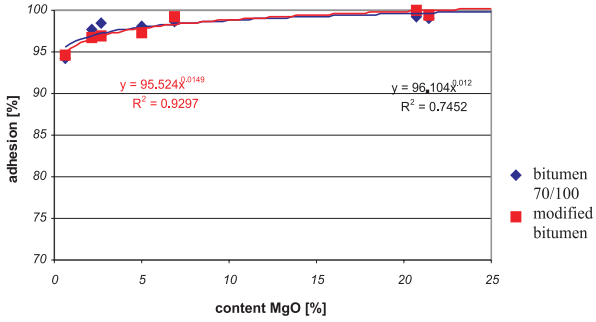


*Fig. 4 The adhesion results of bitumen binder to aggregate in dependence of content MgO in aggregate*

From the measurement results based on the comparison of the observed specimens we can conclude that the best level of adhesion was exibited with basic aggregates with the high of CaO content and MgO, then with neutral aggregates, and from the adhesion point of view the acid aggregate with the high content of $SiO_2$ and $Al_2O_3$ had the worst results with all used binders. The modified bitumen adhesion to aggregate had better results than paving grade bitumen adhesion. Regarding to a limited space of the paper, detailed adhesion results of binders to aggregates at different conditions (wet aggregate, aggregate with dust on the surface, different temperatures, specimens tempering in water, etc.) are not presented in paper.

## 4. Conclusions

Most workplaces in other countries have developed their own laboratory test methods measuring the adhesion, and their own specific criteria of evaluation of bitumen adhesion to aggregate. At our workplace we evaluated the possibility of using the new adhesion test and evaluation method Vialit. Test results and their comparison with the results obtained from measuremets by STN 65 7089 show the suitability of this method to determine adhesion of different binders and aggregates. The test method enables to determine the adhesion and at the same time to study different factors effecting the adhesion: the type of aggregate and binder, surface characteristics of aggregate, temperature sensitivity of binder-aggregate bond, resistance to water, etc. Considering the simplicity of the test equipment servicing, this test method can be included among the general tests of road building materials.

The adhesion results of bitumens and aggregates by STN 65 7089 Tab. 5

| Binder | Adhesion | | | | | |
|---|---|---|---|---|---|---|
| bitumen 70/100 | poor | suitable | suitable | poor | poor | suitable |
| modified | poor | good | good | suitable | good | good |
| content | granodiorite | andesite 2 | andesite 1 | melaphyre | dolomite 1 | dolomite 2 |
| **CaO** | 3.49 % | 5.81 % | 7.50 % | 9.06 % | 30.90 % | 47.02 % |

The adhesion results of bitumens and aggregates by STN 65 7089 Tab. 6

| Binder | Adhesion | | | | | |
|---|---|---|---|---|---|---|
| bitumen 70/100 | poor | suitable | poor | suitable | suitable | suitable |
| modified | poor | good | suitable | good | good | good |
| content | granodiorite | andesite 2 | melaphyre | andesite 1 | limestone | dolomite 2 |
| **MgO** | 0.63 % | 2.17 % | 2.68 % | 5.00 % | 6.86 % | 21.40 % |

**References**

[1] BENEŠ, V.: *Asphalts, production and application,* Praha SNTL, 1961
[2] SCHULZE, W., TISCHER, W., ETTEL, W., LACH, V.: *Non-cement mortars and concretes,* 1990
[3] BAREŠ, R.: *Composite materials,* Praha SNTL, 1988
[4] MOORE, W. J.: *Physical chemistry,* SNTL Praha, 1981
[5] KELLO, V., TKÁČ, A.: *Physical chemistry,* Alfa Bratislava, 1969
[6] STN 65 7089: *Determination of adhesion of asphaltic products to aggregates,* 1982
[7] PREN 12697-11 *Determination of the compatibility between aggregate and bitumen*
[8] EN 12272-3: *Determination of binder aggregate adhesivity by the Vialit plate shock test method 2003*
[9] PREN 12271-5: *Binder – aggregates adhesivity*
[10] SLOVAK GEOLOGICAL INSTITUTE: *Geological exploration,* Final reports and calculation resources, Slovak geological institute Bratislava
[11] REMIŠOVÁ, E.: *Theoretical aspects of bitumen binders' adhesion to aggregates,* dissertation work, Univerzity of Žilina 2000

https://doi.org/10.26552/com.C.2004.1.64-67

kamUNikácie
COMMUNICATIONS

Ján Leľak – Dušan Slávik – Martin Mečár *

# STATIC AND DYNAMIC TESTS OF THE RAILWAY SUBGRADE CONSTRUCTION MODEL

*The presented paper deals with the research of railway subgrade construction. The purpose was to compare static and dynamic modulus of deformation namely on two different railway subgrade constructions. The effect of reinforcing geosynthetics was found out as well, when a different type of reinforcing geosynthetics was used.*

## 1. Introduction

In railway engineering the use of reinforcing geosynthetics plays more and more important role. It should either strengthen the whole railway subgrade construction or reduce the thickness of sub – base layer which would otherwise be required. However, the positive or negative response of the construction under the reinforcing has not been shown in the contemporary specifications so far.

Deformation characteristics are the base of the designing of the railway subgrade construction at ŽSR. Our approach consisted in carrying out of static and dynamic loading tests. Their results are the deformation characteristics aiming to verify the effect of two different reinforcing geosynthetic materials in the railway subgrade construction.

## 2. Model measurements

Model measurements took place at the Department of Railway Engineering since the year 2001 up to now. During this time a number of static and dynamic loading tests was carried out.

Two basic types of construction were proposed for making a comparison between type one and type two according to our determined criterions. They are described in section 2.2.

### 2.1 The testing box description

In order to carry out the considered trials there was built a testing box embedded to a concrete base to prevent a damage of its bottom created only by a steel plate in a relatively moderate thickness of 6 mm reinforced by transverse steel ribs. Further, it consists of a thin steel plate web in thickness of 3 mm partly reinforced by vertical angle reinforcement. The box is equipped with a beam serving as a support against the load which is allowed to vary its position namely in three different locations. Under the test the beam is fixed cross – above the box into two columns of the box. Two different places are tested on each position of the beam.

The scheme of the box which is 3400 mm long 1950 mm wide and 1200 mm high is shown in Fig. 1. There is a photo of the box in Fig. 2.

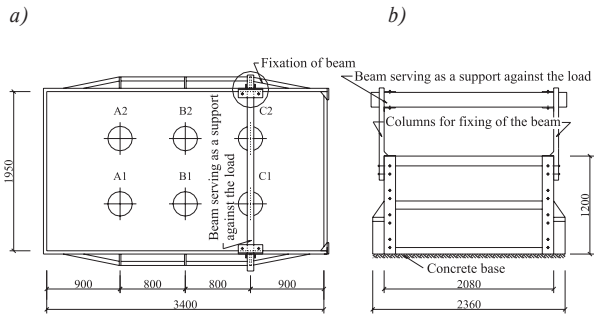


*Fig.1 The scheme of the box with the localization of the static plate loading test sites a) the plan view, b) the front - side view*

### 2.2 The testing constructions description

As mentioned above two types of railway subgrade construction (Fig. 3) were tested. The basic part of construction consisted of the soft soil subgrade where this cohesive soil was classified in accordance with USCS as clay with intermediate plasticity (CI). In addition to this the main part of the construction was a sub – base layer consisted of crushed rocks determined as soil *GP* = poorly graded gravel within the coarser fractions of 0 – 32 mm. These two basic materials were used for both type one and type two. The subgrade and the sub – base materials are very dissimilar and to not occur mechanism of soil fines pumping into aggregate voids or mechanism of aggregate particles intrusion into soil sub-

* **Ing. Ján Leľak, Ing. Dušan Slávik, Ing. Martin Mečár**
Department of Railway Engineering and Track Management, Faculty of Civil Engineering, University of Žilina, Komenského 52, 010 26 Žilina, Slovak Republic, Tel. +421-41-7634818, Fax: +421-41-7233502, E-mail: jose@fstav.utc.sk, dslavo@fstav.utc.sk, mecar@fstav.utc.sk


*Fig. 2 Photography of the testing box at Department of Railway Engineering and Track Management*

grade there had to be placed a suitable geotextile between those layers to separate them. That is why the integrity and functioning of both materials could remain intact or even be improved. In the case of type one there was used Macrit GTW/100 – 100. It is geocomposit consisting of the nonwoven geotextile and the reinforcing geogrid Arter GT. This member has both a separating effect (geotextile) and a reinforcing effect (geogrid). In the other case (type two) there was used a flexible porous separating textile Tatratex. The construction type two also included use of reinforcing geogrid Tensar SS30 laid down on the separating geotextile and away from the box webs in range of 100 mm to activate its function.

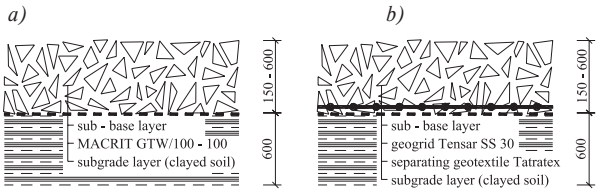


*Fig. 3 The figure presents two types of railway subgrade construction the "type one", b) the "type two"*

## 2.3 The procedures of the model construction building

The proper works were started by a constructing of the subgrade layer in completely thickness of 600 mm, which was after finishing covered with Macrit or with the separating geotextile. Then there was gradually built the sub – base layer by parts of 300, 450 and 600 mm[1]) (type one) and of 150, 300, 450, 600 mm[1]) (type two) (Fig. 3). It was determined that the thickness of free bagged loose gravelled material set by 10 mm on each 50 mm by compaction. The maximum value of thickness of the part – layer (150 mm) resulted from a request of the maximum density in the whole sub – base layer. The thickness of every part – layer was controlled by levelling and then compacted with a step – power – rammer Weber mt SRV 70 and a vibrating – plate – compactor ViDo 25/40.

## 2.4 The performance of the loading tests

Based on the results of the researchers considering the effect of reinforcing geosynthetics it is much more effective with lower values of the subgrade bearing capacity than its counterpart. That is why we needed to achieve that subgrade modulus of deformation ranging from 5 to 10 MPa. However, at the beginning we measured more than 10 MPa and thus it was inevitable to adjust it. The clayed soil was mellowed and watered to reach its lower strength.


*Fig. 4 Building of the sub – base layer of thickness of 150 mm*

The static loading tests (Fig. 5) were carried out with a plate in 300 mm diameter and evaluated in accordance with a railway guide of the subgrade S4 ŽSR [1]. There were performed 6 static loading tests on every part – layer (see 2.3) including the subgrade surface. They were performed after bagging and compaction in those places as marked in Fig. 1. Two loading cycles were generally realized during the test. The final value of modulus of defor-


*Fig. 5 Static plate loading test in the testing box*

mation was calculated from the maximum load 0.20 MPa on the contact area (plate/soil) and from difference of plate deflections calculated from the maximum load of the second loading cycle and from the zero load taken off the end of the first loading cycle. The example of the static loading test record is presented in Fig. 6.

There were also performed 15 dynamic loading tests for a comparison between the static and the dynamic loading tests. The dynamic loading tests were carried out in accordance with the following method [4]: the measurement set was turned on after first impulse, which served for touch down of the plate (300 mm diameter); then three impulses were applied and deflections of the plate were recorded. The maximum applied impulse force was 7.07 kN and the impulse period was 18 ms.

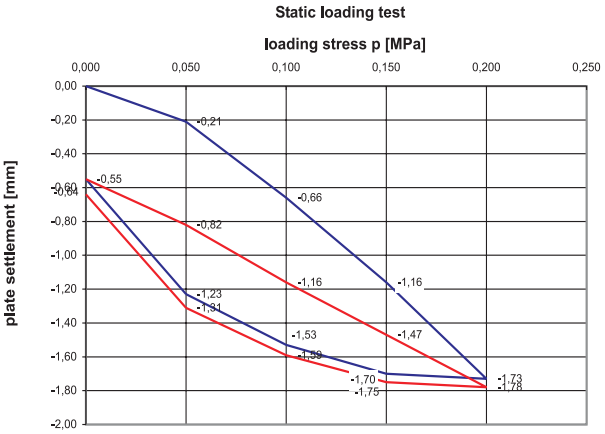


*Fig. 6 The example of the static loading test record*

## 2.5 Evaluation of the measuring results

After testing it was possible to calculate the numeric values of static modulus of deformation due to the equation (1).

$$E = \frac{1.5 \cdot r \cdot \Delta p}{\Delta y} \text{ [MPa]} \qquad (1)$$

where $E$ – static modulus of deformation [MPa],
$r$ – loading plate radius [0,15 m],
$\Delta p$ – loading stress [MPa],
$\Delta y$ – deflection related to loading stress [m],

and the numeric values of dynamic modulus of deformation due to the equation (2)

$$E_{vd} = \frac{F}{d \cdot y_{el}} \cdot (1 - \mu^2) \text{ [MPa]} \qquad (2)$$

where $E_{vd}$ – dynamic modulus of deformation [MPa],
$y_{el}$ – elastic deflection in the middle of the loading plate [mm],
$\mu$ – Poisson's number,
$F$ – loading force [N],
$d$ – plate diameter [mm].

We calculated average values from the measured static and dynamic modulus of deformation which were arranged into the relation with thickness of sub – base layer by a simple function of $E = f(h)$. This relation is shown in graph no. 1 where are 4 curves representing both types of construction:

a) curve no. 1 shows this relation in the case of Macrit with the values of static modulus of deformation E,
b) curve no. 2 shows similar relation with the difference of reinforcement, in this case by Tensar,

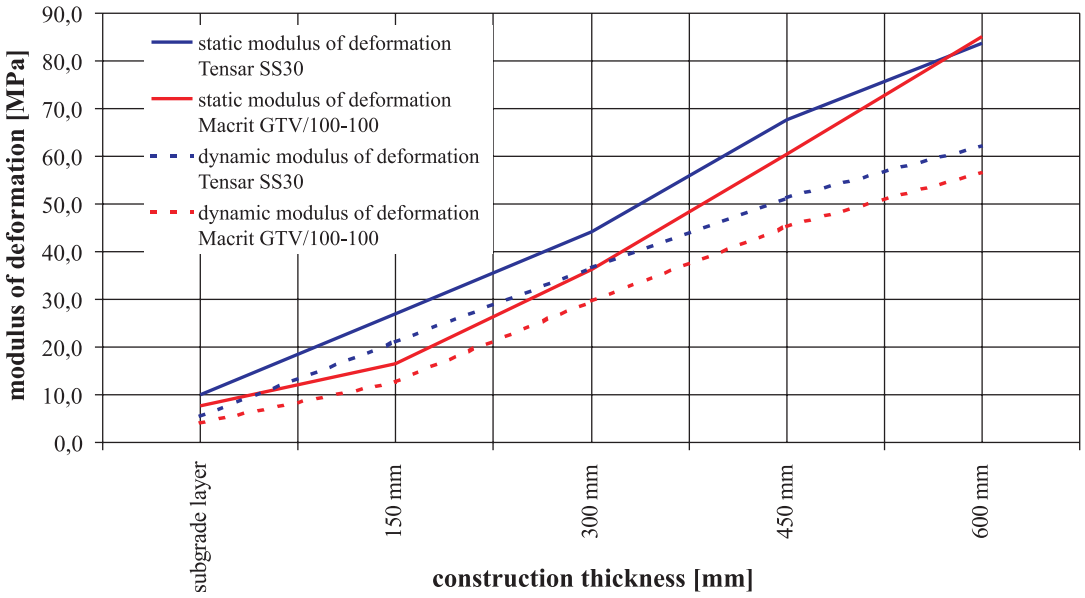


*Graph 1 Relation between the values of static and dynamic modulus of deformation and the thickness of the sub – base layer*

c) curve no. 3 shows the relation with the dynamic modulus of deformation Evd in the case of Macrit,
d) and finally curve no. 4 includes the same relation in the case of the use of Tensar.

Owing to the results we could consider these following statements:

i) crushed rock material of fractions of 0 – 32 mm is suitable enough for sub – base layers in a railway subgrade construction [3],
ii) with the low bearing capacity of the subgrade there was observed substantially enormous increase of the bearing capacity after bagging and compaction of crushed rock material in the case of both Macrit and Tensar,
iii) the subgrade was still more and more compacted due to the building of the sub – base layer and thus it increased its bearing capacity (there was noticed two – times increase of its bearing capacity after excavation of the sub – base material unlike the initial measuring),
iv) a ratio between static and dynamic modulus of deformation had a falling tendency on the sub – base layers except the subgrade layer in both type one and type two,
v) a ratio between values of modulus of deformation (both static and dynamic)

Tensar/ Macrit gradually decreases with the increase of the layer thickness.

## 3. Conclusions

The present way of the checking of the railway subgrade construction increasingly tends mainly to applying of dynamic loading tests which are much faster than static loading tests and which represent greatly better the real behaviour of the construction. That is why we realized a set of the measurements of the static and the dynamic modulus of deformation with the aim of their mutual comparison but the current results do not allow generalization.

We suggest continuing in the model tests but with a better fraction (0 – 63 mm) of aggregates with a fluent particle size distribution than up to now. At the same time there would be needful to regard the moisture, Atterberg limits and particle size changes of both subgrade and sub – base material.

The research, which is presented in this paper, has been conducted under the project VE0GA 1/0341/03.

## References

[1] Guide S4 ŽSR Railway subgrade, Nakladelství dopravy a spojů, Praha 1988
[2] LEĽAK, J.: *Navrhovanie a posudzovanie konštrukcie podvalového podložia,* Projekt dizertačnej práce, Žilina, 2002
[3] LEĽAK, J., SLÁVIK, D., MEČÁR, M.: *The model measurements of the bearing capacity of the railway subgrade construction,* 5-th European Conference of Young Research and Science workers in Transport and Telecommunications TRANSCOM 2003, Žilina, Slovak Republic, 23 - 25 June 2003
[4] The guide for service and use of light dynamic plate LDD 100

https://doi.org/10.26552/com.C.2004.1.68-71

kamUNikácie
COMMUNICATIONS

Slávka Tkáčová *

# THE EIGENVALUE APPROXIMATIONS OF THE LAPLACE OPERATOR DEFINED ON A DOMAIN WITH STRONGLY DEFORMED BOUNDARY

*In this paper the eigenvalue approximations of the Laplace operator defined on a domain with strongly deformed boundary are presented. Because the exact eigenfunctions exhibit complicated behaviour in the vicinity of singular points of the used conformal mapping, the B-spline trial functions are used in order to improve the quality of the eigenfunction approximations near the singular points.*

## 1. Introduction

The eigenvalue problem for the two-dimensional Laplace operator defined on domains with complicated boundary shape arises in many practical situations, for example in mechanical engineering, microwave theory and techniques and biomechanics [3, 6]. The complicated shape form of domains is of interest in practice when the Laplace operator defined on the standard domains as a circle and square does not offer the optimum eigenvalue distribution needed for meeting the design requirements. Standard methods and their combinations with various special techniques have achieved the solution of such problems. The author of this paper [5] has recently presented the eigenvalue computations using this technique based on the sine trial functions. However, because of the presence of geometrical singularities of the exact eigenfunctions, the convergence of the Ritz eigenvalue approximations for the large deformation of domain under consideration is very slow. On the other hand, these singularities are of local character and in this case more precise approximations can be obtained using a local approximation, for example the spline approximation and finite element method.

In this paper the eigenvalue approximations of the Laplace operator defined on a domain with strongly deformed boundary are presented. Because of the presence of shape singularities of the exact eigenfunctions the *B*-spline trial functions are used in order to improve the quality of the eigenfunction approximations near the singular points.

## 2. Formulation of the problem

The eigenvalue problem for the Laplace operator, known also as the homogeneous Helmholtz equation, is given by

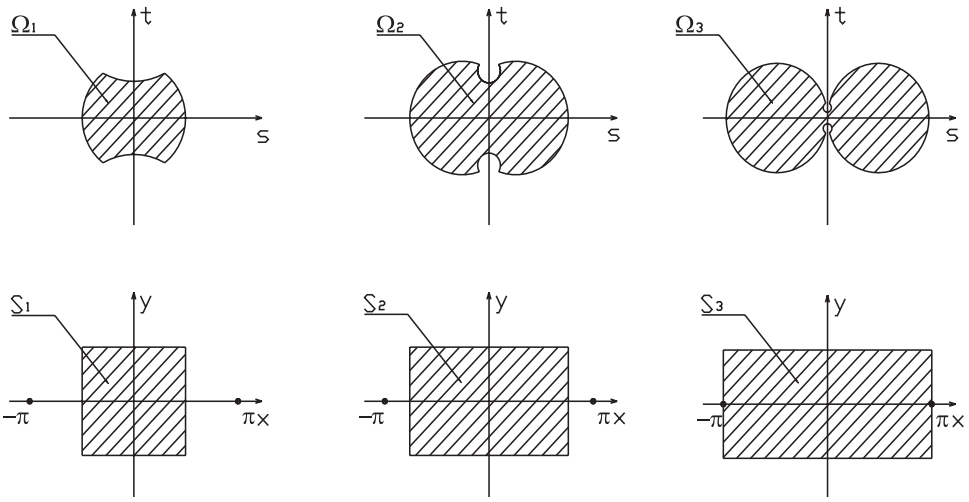


*Fig. 1 Conformal mapping $w = tg(z/2)$ maps the region $S_i$ onto the region $\Omega_i$.*

* **Ing. Slávka Tkáčová**
Department of Mathematic Analysis and Applied Mathematics, Faculty of Science, University of Žilina, Hurbanova 15, 010 26 Žilina, Slovak Republic, Tel. +421-41-5625982, E-mail: tkacova@fpv.utc.sk

$$-\frac{\partial^2\psi}{\partial s^2}-\frac{\partial^2\psi}{\partial t^2}=\lambda\psi \qquad \text{in } \Omega \tag{1}$$

with the Dirichlet boundary condition

$$\psi = 0 \qquad \text{on } \partial\Omega, \tag{2}$$

where $\Omega$ is a bounded two-dimensional domain with a piecewise smooth boundary.

We deal with the problem in which the domain $\Omega$ in the $w$ – plane ($w = s+it$) is generated by conformal mapping $w = f(z)$ of a rectangle in the $z$ – plane ($z = x + iy$). The conformal mapping $w = tg(z/2)$ maps the region $S_i$ in the $z$ – plane onto the region $\Omega_i$ in the $w$ – plane bounded by arcs of the unit circle and a pair of orthogonal circles, see Fig. 1.

Using the conformal mapping $w = f(z)$ the eigenvalue problem (1), (2) is transformed to the equation

$$-\Delta U(x, y) = \sigma(x, y)\,\lambda U(x, y) \quad \text{in} \tag{3}$$

with the Dirichlet boundary condition

$$U = 0 \qquad \text{on } \partial S. \tag{4}$$

Here the function $\sigma(x, y) = \left|\frac{df(z)}{dz}\right|$ is defined as follows

$$\sigma(x, y) = \frac{1}{(\cos x + \cosh y)^2}, \tag{5}$$

The nearest singular points of conformal mapping $w = tg(z/2)$ to the regions $S_i$ are $T_1 = [-\pi, 0]$, $T_2 = [\pi, 0]$. The shapes of the function $\sigma(x, y)$ corresponding to the weakly deformed domain $\Omega_1$ and to the strongly deformed domains $\Omega_3$ are plotted in the left and right in Figure 2, respectively.

The domains $\Omega_1$ and $\Omega_3$ are created by the conformal mapping $w = tg(z/2)$ of the square $S_1 = \langle -\pi/2, \pi/2\rangle \times \langle -\pi/2, \pi/2\rangle$ and the rectangle $S_3 = \langle -1.9\pi/2, 1.9\pi/2\rangle \times \langle -\pi/2, \pi/2\rangle$, respectively.

## 3. Spline approximation

*Definition 1.* Let $t_i$, $i = 1, 2. ..., n$ be an increasing sequence of points of the real axis. The function $B_i^k(t)$ with $i + k \le n$ is called $i$-th algebraic $B$-spline of order $k$ (see Fig. 3), if the following properties are satisfied:

(a) $B_i^k(t) \neq 0$ only for $t \in (t_i, t_{i+k})$,

(b) $B_i^k(t)$ is algebraic polynomial of order $(k - 1)$ on the each interval $\langle t_i, t_{l+1}\rangle$ $i \le l \le i + k - 1$,

(c) $B_i^k(t)$ is continuous function with continuous derivatives up to the order $(k - 2)$ on the whole real axis.

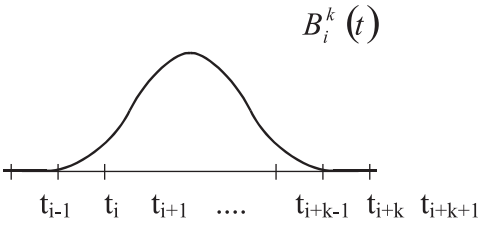


*Fig. 3 Shape of the i-th algebraic B-spline of order*

For the calculation of the $B$-splines and their derivatives the following numerically stable recurrence relations [2] are used

$$B_i^k(t) = t - t_i \backslash t_{i+k-1} - t_i\, B_i^{k-1}(t) + \frac{t_{i+k} - t}{t_{i+k} - t_{i+1}} B_{i+1}^{k-1}(t) \tag{6}$$

$$\text{if } B_i^1(t) = \begin{cases} 1 & t \in \langle t_i, t_{l+1}\rangle \\ 0 & t \notin \langle t_i, t_{l+1}\rangle \end{cases} \tag{7}$$

$$\text{and } B_i^k(t)^{(m)} = (k-1)\left[\frac{B_i^{k-1}(t)^{(m-1)}}{t_{i+k-1} - t_i} - \frac{B_{i+1}^{k-1}(t)^{(m-1)}}{t_{i+k} - t_{i+1}}\right]. \tag{8}$$

## 4. Numerical experiments

The numerical experiments presented in this article are based on the Rayleigh - Ritz method applied on the equation (3) using the $B$-spline trial functions of the form

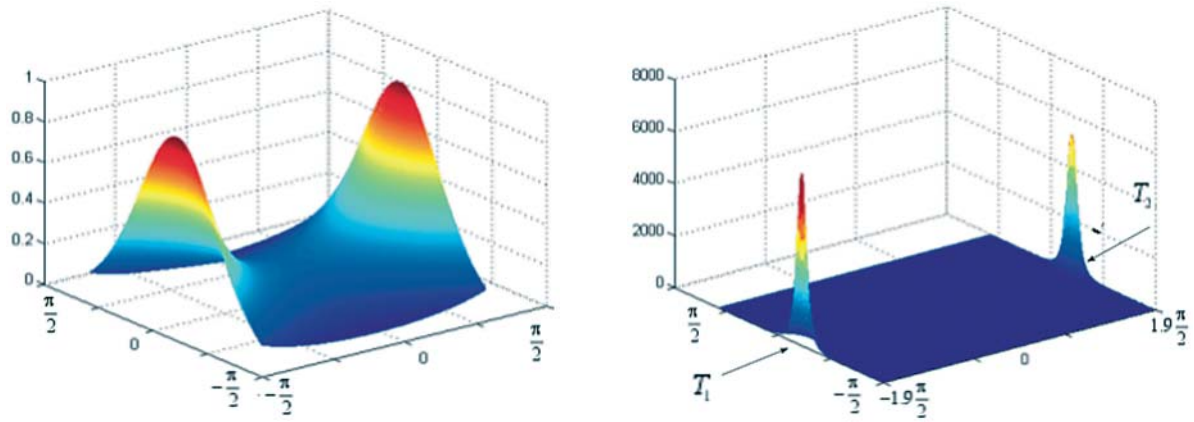


*Fig. 2 Shapes of the function $\sigma(x, y)$ corresponding to the domain $\Omega_1$ (left) and $\Omega_3$ (right)*

$$\psi_{k,l}(x, y) = (\cos x + \cosh y)\ \tilde{\psi}_{k,l}(x, y), \tag{9}$$

where

$$\tilde{\psi}_{k,l}(x, y) = (x - a)(b - x)\left(y + \frac{\pi}{2}\right)\left(\frac{\pi}{2} - y\right) B_k^r(x)\ B_l^r(y) \tag{10}$$

for $r = 8$, $k = 1, 2, ..., n_x$, $l = 1, 2, ..., n_y$ and $a = -b = -\pi/2$ in the case of the weakly deformed domain $\Omega_1$ and $a = -b = -1.9\pi/2$ in the case of the strongly deformed domain $\Omega_3$. The function in (9) is used in order to allow the computations of the scalar products $(\sigma(x, y)\psi_{k,l}(x, y), \psi_{m,n}(x, y))$ as the Cartesian product of one dimensional integrals. These integrals have been computed separately for the variable $x$ and variable $y$ by using the Gauss quadrature formula of order 20 used on each subinterval $\langle x_i, x_{i+1}\rangle$, where $x_i$ are the *B*-spline knots in the interval $\langle a, b\rangle$ in the case of the variable $x$. The resulting matrix eigenvalue problems of order $n (n = n_x \cdot n_y, n_x = n_y)$ have been solved by the subroutine NGHOUD from the FORTRAN package NICER [1]. The convergence of the computed eigenvalue approximations to exact eigenvalues of the equation (3) is prooved in [4].

The Rayleigh-Ritz eigenvalue approximations of the selected eigenvalues using $n$ trial functions are presented in Table 1 – 4. For the sake of convergence comparisons the eigenvalue approximations shown in Table 1 and Table 2 are taken from the author's previous article [5] and correspond to the sine trial functions. The eigenvalue approximations shown in Table 3 and Table 4 are computed using the *B*-spline trial functions (9). The results reported in Table 1 and Table 3 correspond to the case of weakly deformed domain $\Omega_1$, while the results reported in Table 2 and Table 4 correspond to the case of strongly deformed domain $\Omega_3$.

Eigenvalue approximations for the weakly deformed domain $\Omega_1$ using n = 400, 900, 1600 and 2500 sine trial functions. Tab. 1

| n | $\lambda_1$ | $\lambda_2$ | $\lambda_3$ | $\lambda_5$ | $\lambda_7$ | $\lambda_{10}$ |
|---|---|---|---|---|---|---|
| 400 | 7.5705280 | 15.221970 | 22.197600 | 29.167270 | 46.127290 | 66.425740 |
| 900 | 7.5698450 | 15.220040 | 22.196280 | 29.164740 | 46.120670 | 66.413520 |
| 1600 | 7.5696870 | 15.219590 | 22.195970 | 29.164170 | 46.119410 | 66.411250 |
| 2500 | 7.5696330 | 15.219440 | 22.195870 | 29.163970 | 46.119000 | 66.410529 |

Eigenvalue approximations for the strongly deformed domain $\Omega_3$ using n = 400, 900, 1600 and 2500 sine trial functions. Tab. 2

| n | $\lambda_1$ | $\lambda_2$ | $\lambda_3$ | $\lambda_5$ | $\lambda_7$ | $\lambda_{10}$ |
|---|---|---|---|---|---|---|
| 400 | 53.829210 | 56.155410 | 141.61980 | 206.07930 | 311.82790 | 370.58720 |
| 900 | 37.753730 | 38.556880 | 98.792580 | 132.33440 | 207.75130 | 236.73640 |
| 1600 | 31.175410 | 31.522150 | 80.903980 | 101.72670 | 164.54580 | 182.51010 |
| 2500 | 27.901250 | 28.062540 | 71.828140 | 85.913150 | 142.56580 | 154.51040 |

Eigenvalue approximations for the weakly deformed domain $\Omega_1$ using n = 400, 900, 1600 and 2500 B-spline trial functions (9) of order 8. Tab. 3

| n | $\lambda_1$ | $\lambda_2$ | $\lambda_3$ | $\lambda_5$ | $\lambda_7$ | $\lambda_{10}$ |
|---|---|---|---|---|---|---|
| 400 | 7.5695770 | 15.21928 | 22.195761 | 29.163773 | 46.118610 | 66.409851 |
| 900 | 7.5695770 | 15.21928 | 22.195761 | 29.163773 | 46.118610 | 66.409843 |
| 1600 | 7.5695770 | 15.21928 | 22.195761 | 29.163773 | 46.118610 | 66.409843 |
| 2500 | 7.5695770 | 15.21928 | 22.195761 | 29.163773 | 46.118610 | 66.409843 |

Eigenvalue approximations for the strongly deformed domain $\Omega_3$ using n = 400, 900, 1600 and 2500 B-spline trial functions (9) of order 8. Tab. 4

| n | $\lambda_1$ | $\lambda_2$ | $\lambda_3$ | $\lambda_5$ | $\lambda_7$ | $\lambda_{10}$ |
|---|---|---|---|---|---|---|
| 400 | 26.851726 | 26.925258 | 78.485629 | 81.974518 | 164.708914 | 192.756097 |
| 900 | 23.345010 | 23.392738 | 60.415130 | 63.837916 | 124.972830 | 127.908500 |
| 1600 | 23.029351 | 23.074449 | 58.217327 | 59.586448 | 108.096674 | 115.765853 |
| 2500 | 23.007218 | 23.052105 | 58.047942 | 58.841866 | 104.813595 | 107.866751 |

## 5. Concluding remarks

The presented numerical results indicate that the *B*-spline trial functions offer more precise eigenvalue approximations than the sine trial functions. This difference in the eigenvalue convergence is caused by the presence of shape singularities of the exact eigenfunctions which are the consequence of very steep gradient of the function $\sigma(x, y)$ in the vicinity of the points $[-\pi, 0][\pi, 0]$ as seen in Figure 2 (on the right). This case corresponds to the strongly deformed domain $\Omega_3$. Because the *B*-spline trial functions are able to match singular behaviour of functions more precisely than approximations based on the sine trial functions, the corresponding eigenvalue approximations exhibit essentially better convergence. Finally the *B*-spline trial functions are recommended for use at least in the cases when the domain with complicated boundary shape is generated by a conformal mapping of square or rectangle.

## References

[1] BEPPU, Y., NINOMIYA, I.: *NICER – Fast Eigenvalues Routines,* Comput. Phys. Commun., Vol. 23, 1981, pp. 123 – 126.
[2] DE BOOR, C.: *A Practical Guide to Splines*, Springer – Verlag, New York, 1978.
[3] KUTTLER, J. R., SIGILLITO, V. G.: *Eigenvalues of the Laplacian in Two Dimension,* SIAM Review 26, No. 2 (1984), pp. 163 – 193.
[4] REKTORYS, K.: *Variational methods in engineering and in problems of mathematical physic,* SNTL, Praha, 1974.
[5] TKÁČOVÁ, S.: *Computation of Eigenvalues for Domains with Complicated Boundary Shape,* Journal of Electrical Engineering, No. 12/s, Vol. 53 (2002), pp. 24 – 26.
[6] WILLIAMS, K. R., LESSER, T. H. J.: *Natural Frequencies of Vibration of Fibre Supported Human Tympanic Membrane Analysed by the Finite Element Method,* Clin. Oraloryngol., No. 18 (1993), pp. 375 – 386.

https://doi.org/10.26552/com.C.2004.1.72-76

kamUNikácie
COMMUNICATIONS

Andrzej Surowiecki – Edward Hutnik *

# TESTS OF DEFORMATION AND TENSIONS IN REINFORCED NON-COHESIVE SOIL LAYER

*The paper describes the results of laboratory testing of vertical deformations, horizontal pressure and vertical tensions on the close contact between reinforced non-cohesive soil layer and single-parameter subsoil. In particular, the diagrams of deformations and vertical tensions have been presented in the function of static load and reinforcement parameters. The following parameters have been also formulated: pattern to the calculation of coefficient of vertical tensions remittance and condition of equilibrium tensions in the reinforced soil model.*

## 1. Introduction

The subject under analysis is the work of statically loaded soil layer reinforced with horizontal plates, on the basis of carried out testing [5–9]. The models considered constitute an analogue of pavement or road foundation, in relation to which they include non-cohesive soil layer (river sand of medium-size graining, valley gravel 5/10, basalt grit 8/16 and basalt breakstone). The problem of the connection between horizontal and vertical deformations has been discussed, and the attention was focused on the distribution and values of vertical pressures of the models considered on the single-parameter Winkler-type subsoil.

The scope of considerations comprises the following issues:
- horizontal and vertical deformations, and vertical tensions on the contact between soil layer (reinforcement with unwoven fabric) and subsoil;
- deformation of soil layer reinforced with geogrids;
- formulation of the tension equilibrium condition, expressing the relation between vertical pressures of loaded soil layer and horizontal deformations, in conditions of a laboratory model.

## 2. Remarks to the testing method

The modelled soil layer (soil sample) is placed in a test container, whose parameters were characterised in publications [5–9]. Assuming the unidirectional work of the plates, e.g. as strings stretched along the axis, it is enough to accept the reinforcement in the form of flat bars arranged in the direction of the occurrence of tensile forces. The task of the reinforcement consists in partial taking over of horizontal forces of lateral pressure caused by tension from soil vertical load [1, 3, 4]. Due to this, the horizontally placed reinforcement was accepted, i.e. perpendicular to the plane of loading. The soil sample (model) considered is in the spatial state of tension and deformation. Therefore, for the reason of the directions of horizontal forces action, a suitable form of reinforcement may be: mat, grate or grid. Reinforcement of this type can be moulded out of flat bars or rods in the geometrical arrangement of a grid with rectangular or square meshes. The structure of the container enables axial symmetry of load and deformation of the examined soil sample. Taking into account the orthogonal character of the directions of main tensions, reinforcement in the form of grids with straight weave was used in principle, in directions corresponding to the directions of the main axes in the ratio to the container horizontal projection. Generally, the following components were used as reinforcement: steel grids; ordinary plastic grids; plastic grids with tensile strength comparable to steel (the so-called geogrids); geotextile mats (unwoven fabric of Polish and Czech manufacturing) [5–9].

## 3. Protective layer of soil reinforced with unwoven fabrics

The laboratory testing project and the scheme of sand samples reinforced with unwoven fabrics: Polish WD-EB and Czech Terratex 600 are included in publication [7].

Figure 1 presents charts of horizontal pressures of sand samples with triple unwoven fabric reinforcement, in the function of its location. The figures presented above concern sample load $q = 0{,}19$ Mpa. The value of total pressure for the standard (sample with no reinforcement) was accepted as $P_y = 100$ %. Total lateral pressure in proportional relation in the standard ratio was calculated identically as in case of samples reinforced with openwork plates.

As a result of its structure, the unwoven fabric (geotextile mat), totally delaminates soil, therefore the conditions of its work are different than of a grid, i.e. an openrork plane. Moreover, the unwoven fabric is a significantly deformable material. Soil co-operation with this type of plate is possible in the form of friction. The soil mass movement caused by deformations as an effect of load

* **Andrzej Surowiecki[1], Edward Hutnik[2]**
[1]Technical University of Wrocław, Institute of Civil Engineering; Agricultural University in Wrocław, Institute of Building and Landscape Architecture.
[2]Agricultural University in Wrocław, Institute of Building and Landscape Architecture.

is possible only along the mat surface. As for vertical relocations of soil grains situated on the contact with the mat, they are possible as a result of vertical deformations of the unwoven fabric, i.e. local deflections after the formation of a central trough or as a consequence of total settlement of the geosynthetic plane. As an effect of loading, the mat mainly considerably deforms and settles together with the soil overlay. The value of settlement depends, among others, on the plate location in the soil sample.

One can draw a conclusion from the experimental tests as to the functioning of two phases of geo-unwoven fabric, in the mechanical sense:

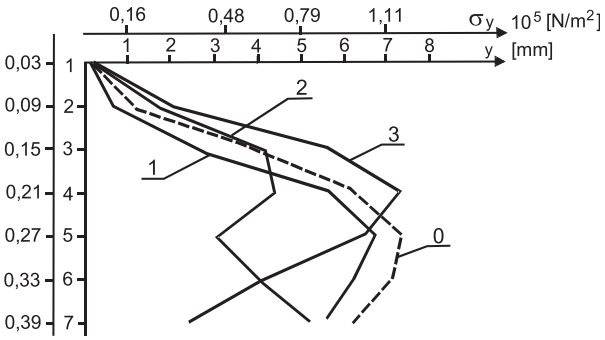


*Phase I – mat settlement (vertical relocation) with loaded soil overlay. Phase II – partial transmission of tensile forces from the soil layer, in the form of friction.*

*Fig. 1 Lateral pressure of sand samples reinforced with triple unwoven Terratex 600 in the function of changeable location [5]: a – cycle I of load; b – cycle IX; 0 – standard; 1 – unwoven fabric Terratex 600 on the level $z_2$; 2 – on the level $z_4$; 3 – on the level $z_6$.*

In this phase, the unwoven fabric undergoes purposeful deformation in the form of a central trough. Moreover, the expected vertical deformation of the mat takes place, consisting in the collapse (pressing) of the mat plane under the influence of vertical constituent tensions. The unwoven fabric stretching was observed. The increase of $\Delta L$ length (L is the length and width of the square surface of the mat used for reported tests) is accompanied by the decrease of the cross-section (width) of the mat:

$$\Delta g = g - g' = g - \upsilon \epsilon \qquad (1)$$

where: $g$ – original mat width; $g'$ – width after deformation; $\epsilon = \Delta L/L$ is a unitary longitudinal deformation; $\upsilon$ – transverse expansion coefficient.

Tearing horizontal forces, originating from tensions of horizontal pressure in the loaded soil, may have certain influence on the change of element $\Delta g$. These forces are partially taken over by the unwoven fabric in the form of friction. The change of $\Delta g$ depends, among others, on the following elements:

- settlement caused by durable changes in the soil layer (sealing of layer);
- settlement, as a result of elastic deformations of soil grain arrangement.

The value of $\Delta g$ may be a durable deformation, partially or totally elastic. The degree of the mat "pressing" $\Delta g$ depends, among others, on the quantity and distribution of the plates. The influence of unwoven fabric on the lateral pressure reduction and on the change of pressure graph course was observed, depending on the quantity and distribution of these plates. Yet, the effects of unwoven fabric (in the quantative sense) are less considerable than, for example, of a steel grid, for which the pressure reduction was achieved by approx. 50 %. Only the triple layer of unwoven fabric secures the lateral pressure reduction by approx. 31 %. The qualitative phenomena proceed similarly as for the effect of steel grids or geo-grids, because the zonal reduction of pressure ordinates also occurs. However, most frequently the maximum reduction of the pressure ordinate takes place below the level of mat location, since the unwoven fabric settled by this value in the first phase of work under the load from the soil overlay (see Fig. 1).

The vertical pressures of soil samples (sand) on the modelled subsoil (vertical tensions on the container bottom from the soil layer weight and external load) were measured in central axes $x$, $y$ of the container bottom. The value and distribution of these pressures is a function of many variables, thus it depends, among others, on:

- type of soil layer (i.e. on graining from which the value of the interior pressure angle results),
- level of soil layer consolidation (which determines the value of the interior pressure angle),
- type of external load (static, dynamic) and load geometry and load history,
- reinforcement parameters (e.g. material, number of plates, distribution).

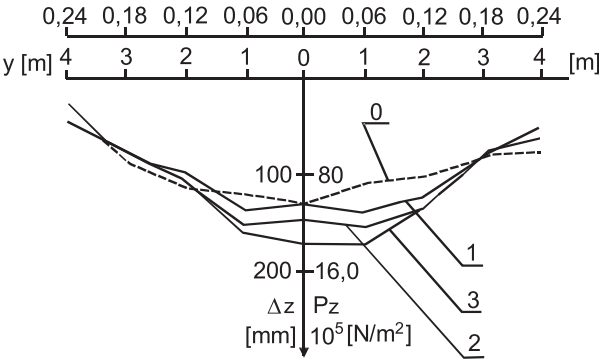


*Fig. 2 Chart of vertical pressures on the soil. Sand reinforced with triple unwoven fabric Terratex 600 at changeable depth [6, 7]. Load 0,19 MPa, cycle I of load. Symbols: 0 – no reinforcement; 1 – reinforcement at the depth of $z_2$ = 0,09 m; 2 – reinforcement at the depth of $z_4$ = 0,21 m; 3 – reinforcement at the level of $z_6$ = 0,33 m.*

The changeability of pressures on the soil is closely connected with a global (spatial) level of soil sample tension, i.e. with the variability of lateral pressure. The chart of vertical pressures on

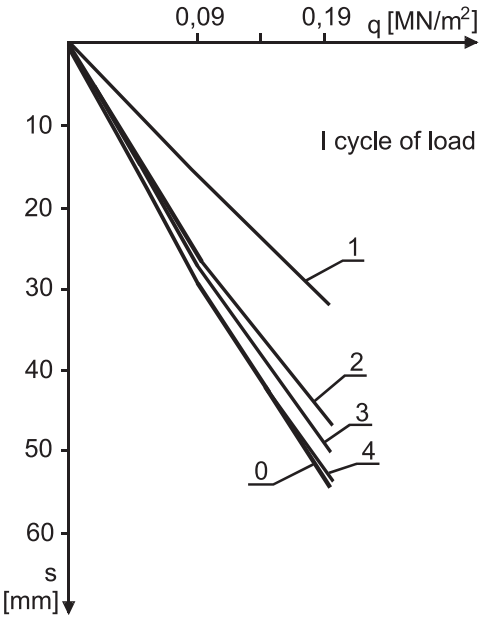


*Fig. 3 Vertical deformations of sand samples reinforced with unwoven fabrics [6, 7]. Symbols in the text.*

the soil for sand reinforced with triple unwoven fabric Terratex 600 situated on the changeable depth is presented in Fig. 2. Fig. 3 illustrates vertical deformations for models with identical reinforcement (at load of 0,19 Mpa). The mean from vertical relocations was accepted as a measure of vertical deformations; the vertical relocations were measured in four corners of a loading plate with dimensions in the plan 0,315 × 0,315 m.

## 4. Soil layer reinforced with geo-grids

Mean pressures on the modelled soil (expressed by mean vertical relocation $\Delta z_{śr}$ of sensors of the container bottom with a soil sample) in the function of load is presented in Fig. 4. The charts have been worked out for selected cases of reinforcement and comparatively for the standard.

As we can see in the drawing, the pressures increase linearly in reinforced and not reinforced sand, together with the increase of load up to the value which is accompanied by active boundary level of pressure. Fig. 5 shows the distribution of vertical pressures on the bottom (measured in one of main central axes of bottom surface) for selected cases of reinforced and not reinforced soil.

Table 1 presents the results of measurements of mean pressures on the soil for selected cases of sample reinforcement and comparatively for the standard. The comparison was conducted with stable load $q_{max}$.

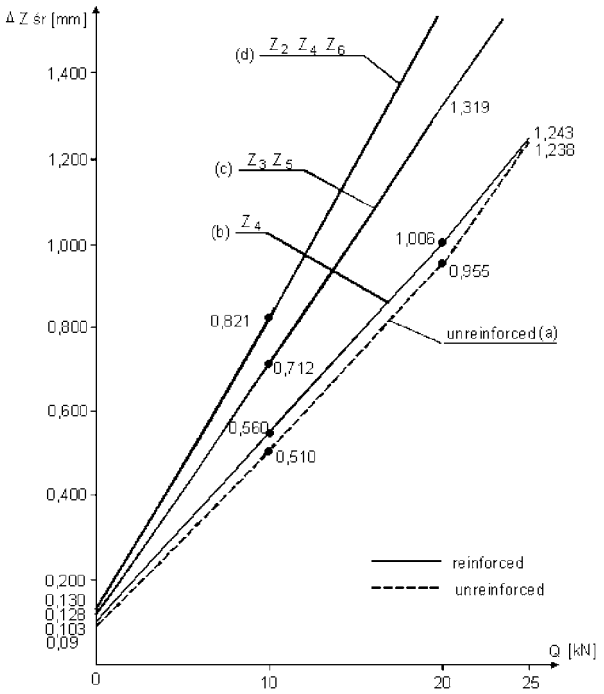


*Fig. 4 Chart of vertical pressures on the soil in the function of load [6, 7]: a – standard; b – single reinforcement at level 4; c – reinforcement with two plates at levels 3 and 5 d – reinforcement with three plates 2, 4 i 5.*

## 5. Condition of tension equilibrium in reinforced soil model and coefficient of pressure transmission to the soil

The variability of pressures $\sigma_z$ on the soil is closely connected with the variability of lateral pressure (i.e. horizontal deformability controlled directly with reinforcement):

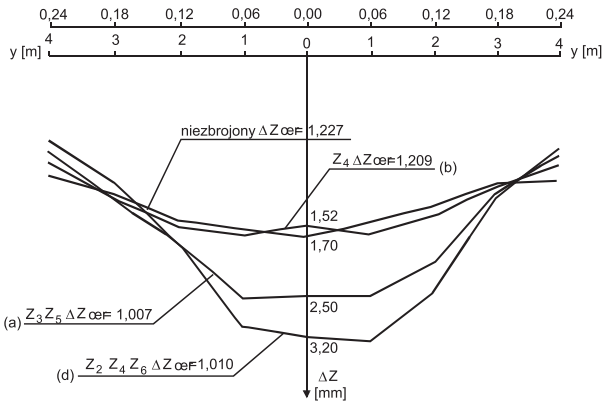


*Fig. 5 Distribution of vertical pressures of the layer on the subsoil along axis y [6, 7]. a – not reinforced (standard); b – reinforcement with single grid; c – reinforcement with two grids; d – reinforcement with three grids.*

Mean pressures on the subsoil for selected cases of soil sample reinforcement, with maximum load $q_{max} = 0.24$ Mpa — Table 1.

| Reinforcement distribution | Total lateral pressure [%] | Maximum pressures on subsoil $\Delta x_{max}$ [mm] | Medium pressures on subsoil $\Delta z_{med}$ [mm] |
|---|---|---|---|
| pattern | 100 | 1.700 | 1.238 |
| $Z_4$ | 54.1 | 1.520 | 1.243 |
| $Z_3$ - $Z_6$ | 33.6 | 2.580 | 1.614 |
| $Z_2$ - $Z_4$ - $Z_6$ | 23.6 | 3.200 | 1.805 |

$$\sigma_z^* = f(\sigma_x^*, \sigma_y^*) \tag{2}$$

where: ($\sigma_x^*$, $\sigma_y^*$ – unitary lateral pressure in the directions of main axes of a co-ordinate system of base *x*, *y*.

The mean value of pressures $\sigma_z$ can be calculated using the elementary method from the equation of equilibrium of forces acting on the soil sample (Fig. 6) considering the technical conditions of the testing facility. This equation acquires the following form for the standard sample:

$$q\,F_{pl} - \sigma z_{śr}\,F_d - s_{śr}\,4\,F_s = 0 \tag{3}$$

where:
q[kPa] – unitary vertical load,
$F_{pl}$ [m$^2$] – loading plate surface,
$\sigma z_{śr}$ [kPa] – mean pressure of soil sample on the modelled single-parameter subsoil,
$F_d$ [m$^2$] – surface of container bottom with soil,
$s_{śr} = fs\ \sigma z_{śr}$ [kPa] – mean unitary friction force between the soil and inner areas of container walls,
*fs* – coefficient of friction between the soil layer and inner area of container walls (as it is provided in a chapter concerning a test stand, the layer-wall contact is indirect: through two layers of PCV foil separated with bearing grease in order to decrease the value of *fs* coefficient),
$\sigma z_{śr}$ [kPa] – mean lateral pressure of the layer in the direction of horizontal axes,
$F_s$ [m$^2$] – surface of container wall.

Equation (3) for soil sample with reinforcement has the following form:

$$q\,F_{pl} - \sigma z_{śr}^*\,F_d - f_s\,\sigma z_{śr}^*\,(4\,F_s) = 0 \tag{4}$$

As it is known from experiments, in the reinforced soil:

$$\sigma z_{śr}^* < \sigma z_{śr} \tag{5}$$

and

$$\sigma z_{śr}^* > \sigma z_{śr} \tag{6}$$

The inequality (6) results from considerations over equation (4) after accepting condition (5). Because of the above, the following functional dependence for reinforced soil can be formulated:

$$\sigma z_{śr}^* = f(\alpha, \beta, \gamma) = f(\lambda) \tag{7}$$

where: $\alpha$ – reinforcement rigidity, $\beta$ – number of plates (quantity of reinforcement), $\gamma$ – reinforcement distribution. The vertical range of anisotropic cohesion, which the soil sample receives as a result of reinforcement, is connected with these three parameters.

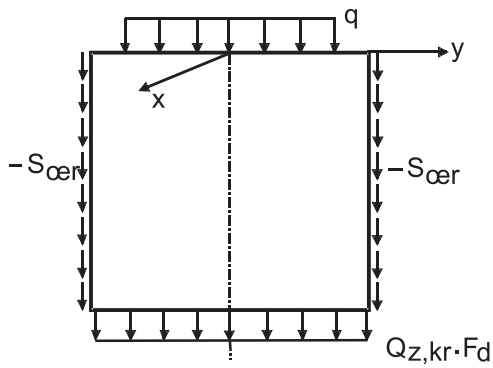


*Fig. 6. Scheme for the static analysis of the soil sample work [6,7].*

One of the parameters, characterising the work of loaded non-cohesive soil layer, is the coefficient of pressure transfer to the subsoil. It was introduced by S. Mazur [2] on the basis of test results of vertical tensions transmitted through a layer 0.10 m thick; 0.20 and 0.30 m of basalt breakstone 20/60. It is specified as a ratio of observed value of pressure on the subsoil to mean values of pressures transmitted to the soil layer:

$$W_p = \sigma_{z,max}\,(\sigma_0)^{-1} \tag{8}$$

where: $\sigma_{z,max}$ – the highest pressure on the subsoil,
$\sigma_0$ – unitary pressure of a panel loading the soil layer.

Coefficient $W_p$ is approximately a stable value for a given type of a soil layer and a specified area transferring the load, in case of a layer 0.30 m thick.

## 6. Conclusion

The dependence of mean values of horizontal pressures of a soil layer from elastic flexibility of a modelled subsoil was observed (in specified conditions of laboratory representation). The highest pressure value is achieved at rigid subsoil. The differences of flexibility of the order of 50 $10^{-6}$ N/m$^3$ do not influence the value of horizontal pressures in an unquestionable way. The subsoil hardening ($Cp = \infty$) causes the increased displacement of the layer from under the panel, and in consequence also influences the increase of vertical deformations (settlement).

The following parameters result from the analysis of the vertical pressure values of the layer:
- the values and distribution of the sample pressure on the subsoil are in given soil a function of load, number and distribution of reinforcement;
- a change of the pressure values at stable loading but variable parameters related to reinforcement (number of plates and distribution) takes place together with the change of the shape of a curve of their distribution on the surface of the container bottom;
- the variability of pressure values of the layer is closely connected with the variability of horizontal pressure, and in tested models it results from technical conditions of the test stand.

The reinforcement placed horizontally influences the increase of the load-carrying ability of the soil layer loaded vertically, through the reduction of vertical and horizontal deformations. The reduction of deformability denotes the improvement of strength parameters.

Less significant vertical deformations of the loaded soil are connected with the reduction of the horizontal pressure value. Horizontally located reinforcement partially takes over the forces of soil horizontal pressure.

Laboratory tests of lateral pressure of the loaded reinforced soil, carried out at an original stand, enabled the control of variable factors operation, concerning the soil layer and reinforcement as well as establishing general regularities related to the behaviour of two-component composites (consisting of materials with extremely different mechanical properties: soil layer – reinforcement plates) at static loading.

## References

[1] LONG N.T.: *Badania gruntów zbrojonych [Tests of reinforced soils].* W: Wybrane zagadnienia geotechniki [Selected issues of geotechnics], PAN-IBW, Ossolineum, Wrocław 1978, s. 185–210.
[2] MAZUR S.: *Wybrane zagadnienia nośności nawierzchni kolejowej [Selected issues of load-carrying ability of track structure],* Prace Nauk. Instytutu Inżynierii Lądowej P.Wr. [Scientific Papers of the Institute of Civil Engineering], Nr 27, Seria: Monografie, Wrocław 1983
[3] SAWICKI A.: *Statyka konstrukcji z gruntu zbrojonego [Statics of structures made of reinforced soil].* IBW-PAN, Gdańsk 1999.
[4] SCHLOSSER F.: JACOBSON H. M., JURAN J., *Soil reinforcenment.* Second Int. Conf. on geotextiles, Las Vegas 1982, s. 1158–1180.
[5] SUROWIECKI A.: *Arbeit der bewehrten Sandschicht unter Dauerbelastung.* Tiefbau Ingenieurbau Strassenbau, Nr 3, 1988, s. 130–135.
[6] SUROWIECKI A.: *Laborversuche zum Einfluss ausgewaehlter Parameter auf die Wirkung der Bewehrung in lockeren Boeden.* Bauingenieur, Nr 5, 1989, s. 215–217.
[7] SUROWIECKI A.: *Laboruntersuchungen von mechanischen Eigenschaften bewehrter lockerer Bodenschichten.* Bautechnik, 71, Heft 11, 1994, s. 707–711.
[8] SUROWIECKI A.: *Badania modelowe sypkiego gruntu zbrojonego [Model testing of non-cohesive reinforced soil].* Drogownictwo [Highway engineering], Nr 7, 1994, s. 155–158.
[9] SUROWIECKI A.: *Warunki współdziałania elementów gruntu zbrojonego [Conditions of co-operation of reinforced soil elements],* Drogownictwo [Highway engineering], Nr 12, 1997, s.383–387.

**Názov doktorandskej dizertacnej práce:** **Oscilatorické vlastnosti diferenciálnych rovníc s posunutým argumentom a ich aplikácie**

**Autor:** **RNDr. Beatrix Bacová**
**Vedný odbor:** **11-14-09 Aplikovaná matematika**
**Školiace pracovisko:** **Katedra matematickej analýzy a aplikovanej matematiky Fakulty prírodných vied Žilinskej univerzity v Žiline**
**Školitel:** **Doc. RNDr. Rudolf Olach, CSc.**

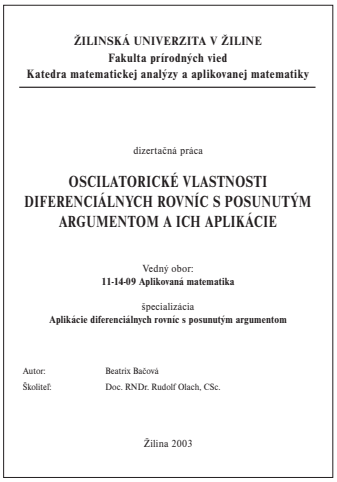
ŽILINSKÁ UNIVERZITA V ŽILINE
Fakulta prírodných vied
Katedra matematickej analýzy a aplikovanej matematiky

dizertačná práca

OSCILATORICKÉ VLASTNOSTI DIFERENCIÁLNYCH ROVNÍC S POSUNUTÝM ARGUMENTOM A ICH APLIKÁCIE

Vedný obor:
11-14-09 Aplikovaná matematika

špecializácia
Aplikácie diferenciálnych rovnic s posunutým argumentom

Autor: Beatrix Bačová
Školiteľ: Doc. RNDr. Rudolf Olach, CSc.

Žilina 2003

*Resumé:*

*Dizertačná práca sa zaoberá vyšetrovaním oscilatorických vlastností riešení lineárnych diferenciálnych rovníc tretieho rádu neutrálneho typu nasledujúceho tvaru:*

$$\frac{d^3}{dt^3}\,[x(t) - p(t)x((t))] + q(t)x(\tau(t)) = 0\,, \qquad t \geq t_0$$

*s týmito predpokladmi:*

*(a)* $p \in C\,[[t_0, \infty)\,;(0, \infty)]$;

*(b)* $\sigma, q, \tau \in C\,[[t_0, \infty)\,; R]$ $\sigma$, $\tau$, *sú rastúce* $\lim_{t\to\infty} \sigma(t) = \infty$, $\lim_{t\to\infty} \tau(t) = \infty$, $q(t) \neq 0$; *na žiadnom podintervale intervalu* $[t_0, \infty)$

*Výsledky sú sformulované do 5 viet, ktoré dávajú nové postačujúce podmienky, aby každé riešenie uvedenej diferenciálnej rovnice bolo oscilatorické.*

*Práca sa ďalej zaoberá oscilatorickými vlastnosťami nelineárnych diferenciálnych systémov s posunutým argumentom. Systémy diferenciálnych rovníc s posunutým argumentom, podobne ako aj diferenciálne rovnice takéhoto typu, majú uplatnenie najmä v aplikáciách. Rieši sa tu oscilácia nelineárnych diferenciálnych systémov s oneskoreným argumentom nasledujúceho tvaru:*

$$y_i'(t) - p_i(t)y_{i+1}(t) = 0, \qquad i = 1, 2, \ldots, n-2,$$
$$y_{n-1}'(t) - p_{n-1}(t)\,|y_n(h_n(t)|^{\alpha}\, sgn\,[y_n(h_n(t))] = 0,$$
$$y_n'(t) sgn\,[y_1(h_1(t))] + p_n(t)\,|y_1(h_1(t)|^{\beta} \leq 0,$$

*pričom sa predpokladá splnenie nasledujúcich podmienok:* $n \geq 3$, *n je nepárne číslo,* $\alpha > 0$, $\beta > 0$ *sú konštanty,* $p_i : [a, \infty) \to [0, \infty)$, $a \in R$, $i = 1, 2, \ldots, n$, *sú spojité funkcie, ktoré nie sú identicky rovné nule na žiadnom podintervale intervalu* $[a, \infty)$,

$$\int_a^{\infty} p_i(t)\,dt = \infty, \qquad i = 1, 2, \ldots, n-1,$$

$h_1 : [a, \infty) \to R$, $h_n : [a, \infty) \to R$ *sú spojité neklesajúce funkcie a* $h_1(t) < t$, $h_n(t) < t$ *na intervale* $[a, \infty)$, $\lim_{t\to\infty} h_1(t) = \infty$, $\lim_{t\to\infty} h_n(t) = \infty$.

*Výsledok práce je tu sformulovaný do 6 liem a 4 viet, ktoré rozširujú už existujúce podmienky. Tieto nové podmienky zaručia, že všetky riešenia, ktoré im budú vyhovovať, budú oscilatorické.*

*Posledná časť práce, vzhľadom na nezastupiteľné miesto diferenciálnych rovníc s posunutým argumentom v aplikačných úlohách, je venovaná osciláciám v epidemickom modeli. Tieto modely sú vhodné všade tam, kde riešenia rovnice sú závislé od neznámej funkcie. Vychádza sa tu z funkcionálnej diferenciálnej rovnice tvaru:* $\dot{x}(t) = a\,x(t - h(t, x(t)))$, *ktorá reprezentuje epidemický model. Neznáma funkcia* $x(t)$ *predstavuje počet jedincov, pri ktorých sa predpokladá, že v čase t môže u nich vzniknúť infekcia. Argument* $(t - h(t, x(t)))$ *predstavuje spätný mechanizmus, ktorý je ovplyvnený počtom jedincov, ktorí následkom infekcie uhynuli. Samotný vznik nákazy závisí od viacerých faktorov. V prípade zmeny životných podmienok sa môžu začať objavovať jedinci, ktorí sú náchylní k infekcii a následkom toho môže prepuknúť epidémia. Tieto zmeny sú vyjadrené deriváciou neznámej funkcie* $x(t)$. *Opätovná zmena podmienok má za následok, že počet nakazených jedincov sa môže zvýšiť, ale môže sa aj znížiť, resp. vznik epidémie sa môže zopakovať po určitom časovom období.*

*Sú tu sformulované 4 vety, ktorých podmienky zaručujú, že každé riešenie uvedenej rovnice je oscilatorické alebo bude existovať jej neoscilatorické riešenie. Uvažuje sa tu rovnica tvaru:* $\dot{x}(t) + a(t)x(t - h(t, x(t))) = 0$, $t \geq t_0$, *kde* $a(t)$, $h(t, x(t))$ *sú spojité funkcie. Uvedená rovnica reprezentuje epidemický model. V uvažovanom modeli z dôkazov dvoch viet taktiež vyplýva, že počet jedincov reprezentujúcich funkciou* $x(t)$ *časom klesá, bude dokonca menší ako 1, čo z praktického hladiska znamená, že epidémia sa prestane šíriť.*

## COMMUNICATIONS – Scientific Letters of the University of Žilina
## Writer's Guidelines

1. Submissions for publication must be unpublished and not be a multiple submission.
2. Manuscripts written **in English language** must include abstract also written in English. The submission should not exceed 7 pages (format A4, Times Roman size 12). The **abstract** should not exceed 10 lines.
3. Submissions should be sent: **by e-mail** (as attachment in system Microsoft WORD) to one of the following addresses: *holesa@nic.utc.sk* or *vrablova@nic.utc.sk* or *polednak@fsi.utc.sk* **with a hard copy** (to be assessed by the editorial board) **or on a 3.5″ diskette** with a hard copy to the following address: Zilinska univerzita, OVaV, Moyzesova 20, SK-10 26 Zilina, Slovakia.
4. Abbreviations, which are not common, must be used in full when mentioned for the first time.
5. Figures, graphs and diagrams, if not processed by Microsoft WORD, must be sent in electronic form (as GIF, JPG, TIFF, BMP files) or drawn in contrast on white paper, one copy enclosed. Photographs for publication must be either contrastive or on a slide.
6. References are to be marked either in the text or as footnotes numbered respectively. Numbers must be in square brackets. The list of references should follow the paper (according to **ISO 690**).
7. The author's exact **mailing address of the organisation where the author works, full names, e-mail address or fax event. telephone number,** must be enclosed.
8. The editorial board will assess the submission in its following session. In the case that the article is accepted for future volumes, the board submits the manuscript to the editors for review and language correction. After reviewing and incorporating the editor's remarks, the final draft (before printing) will be sent to authors for final review and adjustment.
9. The deadlines for submissions are as follows: September 30, December 31, March 31 and Juny 30.
10. In the year 2004 each issue will be dedicated to one of the following topics: Material engineering, Transport building, Telecommunications and information networks.

## POKYNY PRE AUTOROV PRÍSPEVKOV DO ČASOPISU KOMUNIKÁCIE – vedecké listy Žilinskej univerzity

1. Redakcia prijíma iba príspevky doteraz nepublikované alebo inde nezaslané na uverejnenie.
2. Rukopis musí byť **v jazyku anglickom**. Príspevok by nemal prekročiť 7 strán (formát A4, písmo Times Roman 12 bodové). K článku dodá autor **resumé** v rozsahu maximálne 10 riadkov (v anglickom jazyku).
3. Príspevok prosíme poslať: **e-mailom**, ako prílohu spracovanú v aplikácii Microsoft WORD, na adresu: *holesa@nic.utc.sk* alebo *polednak@fsi.utc.sk* príp. *vrablova@nic.utc.sk* (alebo doručiť na diskete 3,5″) **a jeden výtlačok** článku na adresu Žilinská univerzita, OVaV, Moyzesova 20, 010 26 Žilina.
4. Skratky, ktoré nie sú bežné, je nutné pri ich prvom použití rozpísať v plnom znení.
5. Obrázky, grafy a schémy, pokiaľ nie sú spracované v Microsoft WORD, je potrebné doručiť buď v digitálnej forme (ako GIF, JPG, TIFF, BMP súbory), prípadne nakresliť kontrastne na bielom papieri a predložiť v jednom exemplári. Pri požiadavke na uverejnenie fotografie priložiť ako podklad kontrastnú fotografiu alebo diapozitív.
6. Odvolania na literatúru sa označujú v texte alebo v poznámkach pod čiarou príslušným poradovým číslom v hranatej zátvorke. **Zoznam použitej literatúry** je uvedený za príspevkom. Citovanie literatúry musí byť **podľa STN 01 0197 (ISO 690)** „Bibliografické odkazy".
7. K rukopisu treba pripojiť **plné meno a priezvisko autora a adresu inštitúcie v ktorej pracuje, e-mail adresu** alebo číslo telefónu event. faxu.
8. Príspevok posúdi redakčná rada na svojom najbližšom zasadnutí a v prípade jeho zaradenia do niektorého z budúcich čísiel podrobí rukopis recenziám a jazykovej korektúre. Pred tlačou bude poslaný autorovi na definitívnu kontrolu.
9. Termíny na dodanie príspevkov do čísiel v roku sú: 30. september, 31. december, 31. marec a 30. jún.
10. V roku 2004 budú tieto nosné témy jednotlivých čísiel: Materiálové inžinierstvo, Dopravné staviteľstvo, Telekomunikačné a informačné siete.

KOMUNIKÁCIE
COMMUNICATIONS

VEDECKÉ LISTY ŽILINSKEJ UNIVERZITY
SCIENTIFIC LETTERS OF THE UNIVERSITY OF ŽILINA
5. ROČNÍK – VOLUME 5



**Adresa redakcie:**
**Address of the editorial office:**
Žilinská univerzita
Oddelenie pre vedu a výskum
Office for Science and Research
Moyzesova 20, Slovakia
SK 010 26 Žilina
Tel.: +421/41/5620 392
Fax: +421/41/7247 702
E-mail: polednak@fsi.utc.sk, holesa@nic.utc.sk

Každý článok bol oponovaný dvoma oponentmi.
Each paper was reviewed by two reviewers.

Časopis je excerpovaný v Compendexe
Journal is excerpted in Compendex

Vydáva Žilinská univerzita
v EDIS – vydavateľstve ŽU
J. M. Hurbana 15, 010 26 Žilina
pod registračným číslom 1989/98
ISSN 1335-4205

It is published by the University of Žilina in
EDIS - Publishing Institution of Žilina University
Registered No: 1989/98
ISSN 1335-4205

Objednávky na predplatné prijíma redakcia
Vychádza štvrťročne
Ročné predplatné na rok 2004 je 500,– Sk

Order forms should be returned to the editorial office
Published quarterly
The subscription rate for year 2004 is 500 SKK

Jednotlivé čísla časopisu sú uverejnené tiež na:
http://www.utc.sk/komunikacie
Single issues of the journal can be found on:
http://www.utc.sk/komunikacie